TECHNISCHE UNIVERSITÄT WIEN

DIPLOMARBEIT

Characterization of anionic polystyrene-divinylbenzene ion exchange material by mass spectrometric and particle sizing techniques

Ausgeführt am

Institut für Chemische Technologien und Analytik

der Technischen Universität Wien

unter der Anleitung von

Univ.Prof. Mag.pharm. Dr.rer.nat.Günter Allmaier
und Assistant Prof. Mag.rer.nat. Dr.rer.nat.Victor Weiss

durch

Teresa Schlögl, BSc.

Helenenstraße 83/3/3, 2500 Baden

_____ _____

Ort, Datum Teresa Schlögl, BSc

DANKSAGUNG

Ich möchte mich zu allererst bei meinem Betreuer Prof. Günter Allmaier für die Möglichkeit, die Arbeit in seiner Arbeitsgruppe durchzuführen, sowie seine Hilfe und seinen Rat bedanken.

Gleichermaßen gilt mein Dank auch Prof. Marchetti-Deschmann, für ihre freundliche Hilfe und Unterstützung.

Außerdem gilt mein besonderer Dank auch Prof. Victor Weiss, der mir jederzeit bei Problemen und Unklarheiten geduldig zur Seite gestanden ist.

Des Weiteren möchte ich mich auch bei Dr. Ernst Pittenauer für seine hilfreiche Unterstützung bedanken, sowie bei der gesamten weiteren Arbeitsgruppe für die liebe Aufnahme, die Hilfe, die Essensbestelllisten und den Humor!

Ein herzliches Dankeschön gilt auch der Boehringer Ingelheim RCV GmbH AG Co KG für die konstruktive Kooperation, das wertvolle Feedback und die Finanzierung der Arbeit. Besonders möchte ich Dr. Moritz Imendörffer für die unkomplizierte und freundschaftliche Zusammenarbeit danken.

Zusätzlich möchte ich mich auch noch bei Elisabeth Eitenberger, Prof. Thomas Konegger, DI Lukas Voggler und Dr. Valentina Pintus bedanken, die mir den Zugang zu Messgeräten ihrer Arbeitgruppen ermöglicht haben und mir bei der Messdurchführung und Auswertung eine große Untersützung waren.

Ein ganz persönlicher und besonderer Dank gebührt auch meinen Eltern, Birgitta und Günter Gmeiner, die mich von Geburt an immer tatkräftigt unterstützt und liebevoll gefördert haben und ohne die ich in meinem Leben nie so weit gekommen wäre. Zusätzlich möchte ich mich auch bei meinen Geschwistern, Magdalena, Johannes und Klara, bedanken, die stets ein offenes Ohr, eine tröstliche Umarmung und einen aufmunternden „Schmäh“ parat gehabt haben!

Zuallerletzt möchte ich mich bei meinem unglaublichen Mann, Klemens Schlögl, bedanken, der in Allem zu 100 % hinter mir steht und mich aufbaut, ermuntert, anspornt und auch, wenn nötig, am Boden hält.

ABSTRACT

Anionic polystyrene-divinylbenzene cross-linked ion exchange material is frequently used in various fields of application for extraction, purification and separation purposes. Even though mainly particles in the few hundred micrometer size-range are used nowadays, smaller particles in the sub micrometer range might influence the chemical processes or exhibit biological impact. Thus, in order to estimate the fraction of ion exchange material in the nanometer range, a fast and reliable method has to be available.

In this thesis several mass spectrometric techniques were applied to characterize six polystyrene-divinylbenzene based ionic exchange material samples (called resins in the following) of different type and different degree of milling (and therefore, of different expected particle sizes as well as distributions). The applicability of these techniques for resin detection in aqueous solution as well as in cell extract samples was tested. For verification of the results polystyrene-based size standards as well as soluble polystyrenes of different M_n/M_w values were analyzed alongside the resins.

Characteristic resin fragment ion spectra could be recorded utilizing Laser Desorption Ionization Mass Spectrometry (LDI-MS), Secondary Ion Mass Spectrometry (SIMS) and pyrolysis Gas Chromatography Electron Impact-Mass Spectrometry (GC EI-MS). Furthermore, SIMS, LDI-MS and pyrolysis GC EI-MS allowed the detection of resin particles (partly even within a cell extract sample). Using Matrix Assisted Laser Desorption Ionization Mass Spectrometry (MALDI-MS) no useful mass spectra of the resin samples could be recorded, probably due to the method inherent small energy transfer rate.

Furthermore, different particle sizing techniques were applied to characterize the particle size as well as size distribution of the six resin samples and to examine the effect of higher milling energy application on the size distribution. In this case polystyrene-based particle size standards were used as reference material.

It was shown, utilizing Gas Phase Electrophoretic Mobility Molecular Analysis (GEMMA) that the resin particles exhibit a size distribution maximum around 60 nm (surface dry particle diameter) independent of the applied milling energy. The GEMMA method has turned out to be a suitable technique for sizing similar particles and by application of an advanced differential mobility analyzer the size range can be increased up to 800 nm. Laser Diffraction (LD) analysis failed to yield data below approx. 100 nm hydrodynamic particle diameter. Nevertheless, it showed a second and third maximum at higher particle diameters for samples with low milling energy application.

In the future, more detailed method development is necessary to check for resin detectability in for example biological fluids utilizing LDI-MS, SIMS and pyrolysis GC EI-MS.

ZUSAMMENFASSUNG

Anionisches, polystyrol-divinylbenzolquervernetztes Ionenaustauschermaterial wird häufig in verschiedenen Anwendungsgebieten für Extraktions-, Aufreinigungs- und Trennungsschritte eingesetzt. Obwohl hierfür meist Partikel von einigen hundert Mikrometer Durchmesser verwendet werden, können kleinere Partikel im Submikrometerbereich chemische Prozesse oder biologische Systeme beeinflussen. Um die Menge an Ionenaustauschermaterial im Nanometerbereich abschätzen zu können, ist das Vorhandensein einer schnellen und zuverlässigen Detektionsmethode essentiell.

Mehrere massenspektrometrische Methoden wurden in dieser Arbeit angewendet, um sechs polystyrol-divinylbenzolbasierte Ionenaustauschermaterialien (im Folgenden kurz Harze genannt), die sich in Art und Mahlenergieeintrag (und somit in den zu erwartenden Partikelgrößen und -verteilungen) unterschieden, zu charakterisieren. Ihre Anwendbarkeit zur Detektion der Harze, sowohl in wässriger Lösung, als auch in Zellextraktproben wurde untersucht und verglichen. Um die erhaltenen Ergebnisse zu überprüfen, wurden ebenfalls Messungen mit polystyrolbasierten Größenstandards und löslichen Polystyrolen mit unterschiedlichen M_n/M_w Werten durchgeführt.

Charakteristische massenspektrometrische Fragmentionenspektren der Harze konnten mit Laser Desorptions/Ionisations Massenspektrometrie (LDI-MS), Sekundärionen-Massenspektrometrie (SIMS) und Pyrolyse Gas Chromatographie gekoppelt mit Elektronenstoß-Massenspektrometrie (GC EI-MS) erhalten werden. Damit konnten mittels SIMS, LDI-MS und Pyrolyse GC EI-MS die Harzpartikel auch eindeutig detektiert werden (teilweise sogar in Zellextraktproben). Matrix-Assistierte Laser Desorptions/Ionisations Massenspektrometrie (MALDI-MS) führte nicht zu brauchbaren Massenspektren der Harzproben, was durch die methodeninherente, niedrige Energietransferrate erklärbar ist.

Des Weiteren wurden verschiedene Partikelgrößenmessmethoden angewandt, um die Partikelgrößen, sowie die Partikelgrößenverteilung der sechs Harzproben zu bestimmen und den Effekt höherer Mahlenergieeinträge auf die Verteilung zu analysieren. Hier wurden polystyrolbasierte Größenstandards als Referenzmaterial eingesetzt.

Es konnte mit Gas Phase Electrophoretic Mobility Molecular Analysis (GEMMA) gezeigt werden, dass die Partikel in den Harzproben ein Maximum der Größenverteilung bei 60 nm (Trockendurchmesser) aufwiesen, welches unabhängig von dem Mahlenergieeintrag war. GEMMA erwies sich als eine geeignete Methode, um den Durchmesser und die Größenverteilung ähnlicher Partikel zu messen. Durch Einsatz eines erweiterten differentiellen Mobilitätsanalysators, kann man den messbaren Bereich auf bis zu 800 nm ausdehnen. Mittels Laser-Beugungs Messungen konnten Partikel kleiner als ca. 100 nm hydrodynamischer Durchmesser nicht gemessen werden. Dafür konnte gezeigt werden, dass bei geringerem Mahlenergieeintrag ein zweites und drittes höheres Maximum zusätzlich auftritt.

Zukünftig ist eine noch detailiertere Methodenentwicklung für die Techniken LDI-MS, SIMS und Pyrolyse GC EI-MS anzustreben, um die Harzpartikel in z.B. Zellextraktproben detektieren zu können.

TABLE OF CONTENT

ABBREVIATIONS

AgTFA	Silver trifluoroacetate
AIEX	Anion exchange
approx	Approximately
au	Arbitrary units
CE	Cell extract
CPC	Condensation particle counter
CW-laser	Continuous wave laser
Da	Dalton
DCTB	Trans-2-[3-(4-tert-Butylphenyl)-2-methyl-2-propenylidene]malononitrile
DHB	2,5-Dihydroxybenzoic acid
DI	Dithranol
DVB	Divinylbenzene
EI	Electron ionization
EMD	Electrophoretic mobility diameter
ES-DMA	Electrospray differential mobility analyzer
ESI	Electrospray ionization
ES-SMPS	Electrospray - scanning mobility particle sizer
FTICR	Fourier-transform ion cyclotron resonance
GEMMA	Gas phase electrophoretic mobility molecular analysis
HABA	2-(4-Hydroxyphenylazo)benzoic acid
Hz	Hertz
IAA	3-Indolacrylic acid
LD	Laser diffraction
LDI	Laser desorption ionization
LOD	Limit of detection
Lp	Laser power
lpm	Liter per minute
m/z	Mass to charge ratio
MALDI	Matrix-assisted laser desorption ionization
MCP	Multichannel plate
M_n	Number-averaged molecular weight
MQ	Milli-Q water
MTBE	Methyl-tert-butyl-ether
M_w	Weight-averaged molecular weight
M_z	Centrifugal-averaged molecular weight
nES	Nano electrospray
NIST	National Institute for Standards and Technology
PDI	Polydispersity index
PEG	Polyethylene glycol

PS	Polystyrene
Pyrolysis GC-MS	Pyrolysis gas chromatography mass spectrometry
rf	Radio frequency
RI	Refractive index
SEC	Size exclusion chromatography
SEM	Scanning electron microscopy
SIMS	Secondary ion mass spectrometry
THF	Tetrahydrofurane
TOF	Time-of-flight
Tol	Toluene
VLP	Virus like particle

1. INTRODUCTION

1.1 AIM OF THIS WORK

It was the aim of this work to characterize material originating from AIEX resin after milling (i) according to polymer composition, utilizing various mass spectrometric techniques, as well as (ii) according to particle size distribution, utilizing different particle analysis techniques. As control, polystyrene-based NIST particle standards and different 'soluble' polystyrenes of lower molecular weight were analyzed.
Subsequently, LOD values of some of the used techniques were determined. Likewise, the applicability of several methods to assess resin residues in cell culture samples was determined.

1.2 RELEVANCE/BACKGROUND

1.2.1 ANIONIC EXCHANGE MATERIALS (AIEX)[1]

The main function of ionic exchange materials is to extract analyte ions of a given charge in solution and to exchange these analyte ions with another type of ions of the same charge. This can be used in many ways: In the environmental field sewage water is cleaned of heavy metal atoms. Similarly, very pure water can be generated for pharmaceutical or micro electronical purposes. In agriculture, anionic exchange materials can be used to transmit essential elements to plants over time and in the mining industry they are used to enrich precious metals from ore bodies. In chemical analysis they are increasingly used in the field of chromatography as column material.

To fulfill their purpose ionic exchange materials consist of an inert core, which allows diffusion of hydrated ions, and carry a fixed charge, called the fixed ion. It interacts with ions of the opposite charge which can move freely and are called counter ions. The inert core can be of inorganic or organic nature, with ion exchange resins being a special form of the organic type.

In this work anionic exchange material was investigated. It is characterized by its ability to exchange anions (negatively charged ions). Therefore, its fixed charge consists of cations. One can distinguish weak and strong anionic exchangers with weak ones usually carrying a weak base like a secondary or tertiary amine and strong ones carrying strong bases like quaternary amines.

The resin characterized in this work consists of a polystyrene backbone, crosslinked with divinyl-benzene and functionalized with trimethylamine to receive benzyltrimethyl-ammonium chloride as a fixed charge. The chemical structure is shown in Figure 1.

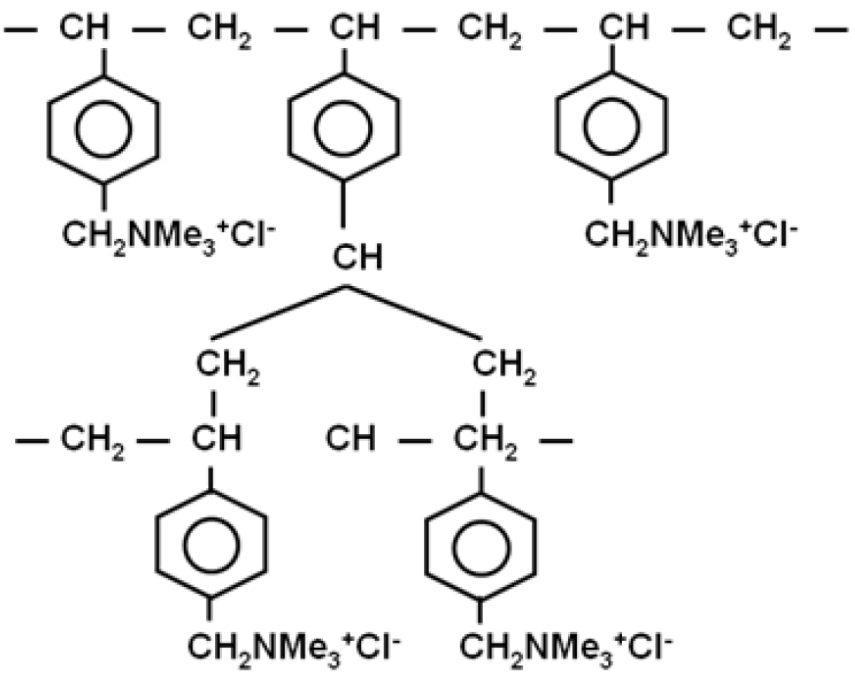

FIGURE 1: CHEMICAL STRUCTURE OF A POLYSTYRENE BASED ANIONIC EXCHANGE MATERIAL FUNCTIONALIZED WITH TERTIARY AMINO GROUPS AS USED IN THIS THESIS[2]

1.2.2 NANOMATERIALS

Due to their many unique properties nanomaterials and nanoparticles as such have recently found increasing interest in science and technology. Since new materials always pose a risk, with some time lag, also extended discussions on safety and health hazard have been led.

A big difficulty in nanomaterial characterization is that no proper general screening or detection method for nanoparticles was developed so far. Most conventional methods are either only usable for bigger particle sizes (e.g. laser diffraction) or way smaller particles or macro molecules (e.g. mass spectrometric techniques). When using different analysis techniques, they often give very different, even contrary, results due to method inherent limitations and drawbacks. This problem increases with increasing polydispersity of the sample. Since most industrially produced nanomaterials are extensively polydisperse, this poses a real problem. Another difficult factor is the sheer endless variety of chemically different particles and surfaces. Even though all nanoparticles seem to have some similar features, their specific properties depend on their three-dimensional extensions, their chemical composition, whether they carry fixed surface charges or are of lipophilic nature, their coverage of functional groups, their stability and their biological activeness. How reliably a nanomaterial can be characterized as such has been discussed by Babick et al. in 2016.[3]

The European Commission defines nanomaterials as "*a natural, incidental or manufactured material containing particles, in an unbound state or as an aggregate or as an agglomerate and where, for 50 % or more of the particles in the number size distribution, one or more external dimensions is in the size range 1 nm - 100 nm.*"[4] This gives a further reason to develop suitable techniques for reliable and consistent nanomaterial detection and number size distribution based classification.

Due to above mentioned reasons it is of big interest if and at which amount there are nanoparticles present in the investigated milled resins. Therefore, their existence and their distribution as well as the possibility to remove them by filtration was tested.

1.3 MASS SPECTROMETRIC TECHNIQUES

1.3.1 GENERAL INTRODUCTION[5–7]

In the early 1900s Sir Joseph John Thomson built the first mass spectrometric device based on a magnetic sector analyzer for isotope analysis at the Cavendish laboratories in Cambridge. Technical improvements since then have led to many different mass spectrometer types being commercially available nowadays. Their main function is to separate ionized elements, molecules and complexes (in vacuum) according to their mass-to-charge ratio (m/z). To achieve separation, a mass spectrometer consists of three functional entities. An ion source, a mass analyzer and a detector. Furthermore, a sample inlet system and a data processing system (nowadays mainly a computer) are needed. A wide selection of different ion sources, mass analyzers and detectors have been developed in the last decades and are commercially available in different combinations. While some ion sources can be operated at low vacuum or even ambient pressure, high vacuum is needed for the analyzer and detector. An overview of the mass spectrometric set-up is given in Figure 2. In the following a more detailed description of the function of those three entities is given, with focus on those types used in this work.

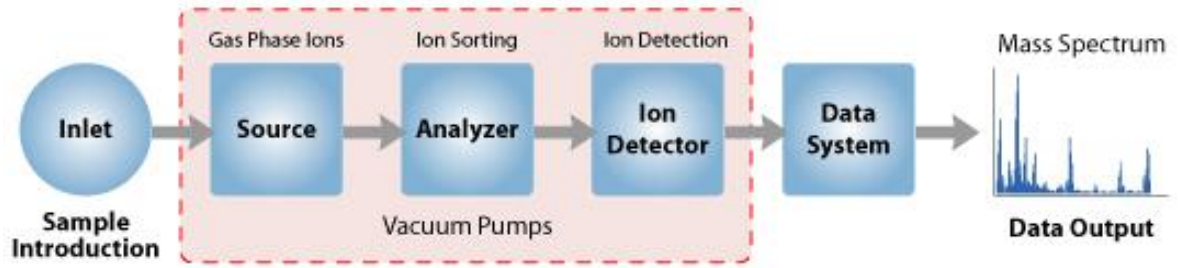

FIGURE 2 GENERAL SET-UP OF A MASS SPECTROMETER[8]

The ion source's main function is to produce charged particles (ionization) which can be separated in the next step. Ionization can take place by electron bombardment (e.g. EI), by applying a high electric field combined with a spraying process (ESI), by depositing energy by means of a pulsed laser (LDI) or an ion beam (SIMS). The so produced ions in the vapor phase are then transmitted (or accelerated by an electric field) to the mass analyzer. One can distinguish two main classes of ion sources, soft ionization and hard ionization techniques. Soft ionization like electrospray ionization (ESI) produces singly or higher charged molecular ions (which are formed by adding or subtracting a proton or ion to the neutral molecule) but little to no fragment ions. On the other hand, hard ionization techniques, like electron ionization (EI), produce mainly (radical) molecular ions and fragment ions and no higher charged molecules. The ionization takes place by attaching a proton, charged molecule or small ion to the analyte (soft ionization techniques) or by transfer of enough energy to the molecule to either abstract an electron or remove an electron and lead to fragmentation (hard ionization).

The mass analyzer separates the generated ions according to their mass-to-charge ratio in space or time. It either measures a mass selection of ions simultaneously (FTICR or orbitrap) or trans-

mits a narrow mass range to the detector at a given time (Quadrupole or TOF). Transmitted ions can be separated in space (Quadrupole) or in time (TOF). Important mass analyzer features are its upper mass limit, transmission, resolving power, mass accuracy, dynamic range and operating pressure since the quality of the recorded mass spectra and possibility to detect certain features of the analyte strongly depends on those values.

Some mass analyzers are intrinsic detectors (FTICR or orbitrap) by measuring the image current produced by the moving ions (and subsequent Fourier transformation of the signal). Others transmit the separated ions to a detector which generates a current signal proportional to the transmitted ion load. Mainly secondary electron multipliers are used. In this case a voltage is applied to a dynode which is for example curved in a specific way. Each transmitted ion leads to a release of electrons at the entrance of the dynode which in turn releases many electrons through a cascade of collisions to the dynode wall. This leads to a signal amplification of 10^5 to 10^8.

In polymer analysis mass spectrometry was established as a powerful tool over the last few years. Its main advantage compared to the traditionally used techniques (like size exclusion chromatography or light scattering) is its possibility to look at single individual oligomers instead of only measuring mean values. Molar mass and its distribution, sequence of repeat units, end groups and purity have a big influence on polymer properties, and can all be determined by mass spectrometric techniques. Furthermore, it is possible to characterize the molecular weight as an absolute value unlike the traditional methods where it was always determined compared to a (more or less) defined standard. Another advantage of mass spectrometry is its necessity of small amounts of sample and the possibility to elucidate molecular structure by fragmentation or, even more powerful, tandem mass spectrometry. Finally, mixtures can also be analyzed and distinguished by either hyphenation with chromatographic techniques or using soft desorption and ionization methods.

The main limit of the usability of mass spectrometry for polymer characterization is its limited working range in terms of molecular mass. Mass spectrometric techniques can detect particles up to 1 MDa but many polymer samples and most particle samples have a higher molecular weight. In addition, heavier analytes are often less well desorbed and ionized, and the detected distribution therefore overestimates the analytes with smaller molecular mass. Also, the shape of a particle cannot be determined, and the analytes should be soluble to a certain extent for most techniques which is not always the case. Finally, also particle heterogeneity leads to problems due to an obtained broad m/z distribution.

In the following, the mass spectrometric techniques used in this thesis are elaborated and their advantages and disadvantages discussed.

1.3.2 MATRIX ASSISTED LASER DESORPTION IONIZATION[7,9]

The concept of MALDI MS was first introduced by Karas et al. in 1985[10]. It is a soft ionization technique in which the analyte is mixed with a matrix which is absorptive in the UV range. Next, the mixture is irradiated by a short laser pulse which leads to an energy deposition and subsequent desorption of matrix-analyte clusters. To achieve a good signal-to-noise ratio many laser pulses and according mass spectra are recorded and superimposed.

In the gas phase the analytes are ionized via various mechanisms which are mostly not fully understood so far. Commonly radical cations, protonated molecules and cationized molecules are formed in the positive mode. It is believed that ions produced in a first ionization step in a

high energy mixture of neutral matrix molecules and clusters can undergo collisions and thereby lead to secondary ionization leading to protonated and cationized analyte species. The desorption and ionization process is demonstrated in Figure 3.

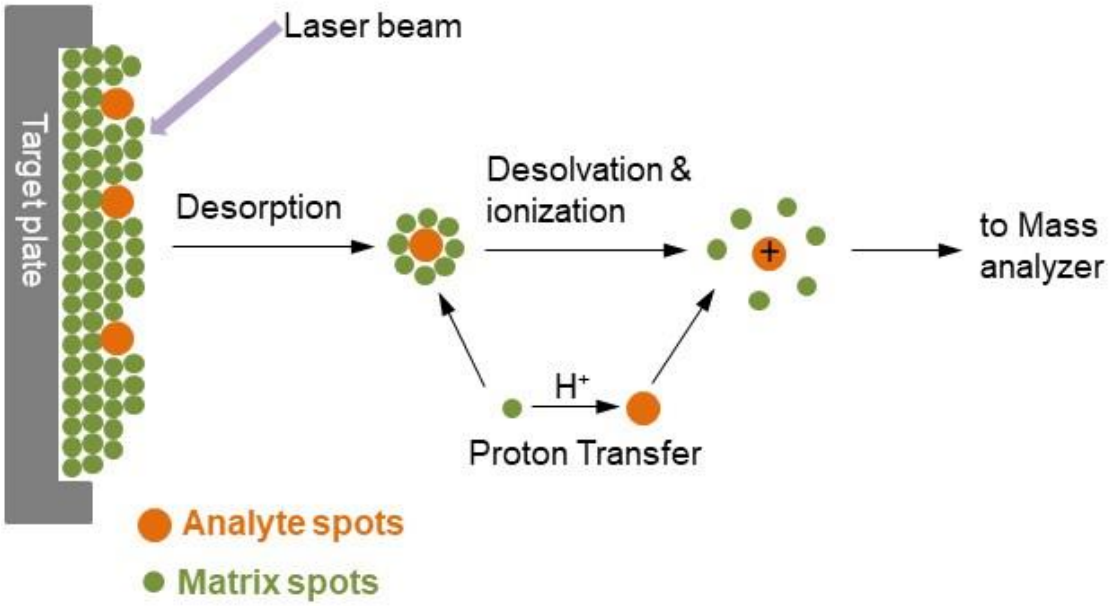

FIGURE 3: MALDI PROCESS OF DESORPTION AND IONIZATION[11]

Many different MALDI matrices have been described in literature. Their main purpose is to mediate the energy transfer by the laser to avoid excessive energy and thereby fragmentation of the analyte. Even though the choice of matrix may be crucial for the detectability of certain analytes, due to their empirical understanding many different matrices and preparation techniques might have to be tested to find an optimal set-up for a given analyte. Still some mechanisms are understood and can help to facilitate the choice of proper matrix.

It is crucial to use substances as a matrix which can absorb the used laser wavelength for desorption. Therefore, most matrices contain aromatic moieties which absorb UV light in the range emitted by typically used lasers (e.g. nitrogen at 337.1 nm).

The pulsed energy transfer of the laser leads to a plume formation of matrix clusters and analyte. Within this plume proton or cation transfer can take place. Therefore, a matrix with a proton affinity or gas phase basicity fitting for the analyte should be chosen. Also, the pH of the sample/matrix solution has an influence on the ionization process and should be adjusted likewise.

Other than the matrix, the sample preparation has a big influence on the quality of the measured spectrum. Mainly it is optimized to achieve co-crystallization with an excess of matrix to avoid analyte cluster formation. The sample preparation most commonly used is the so called “dried droplet” method shown in Figure 4. In this case analyte and matrix are mixed in a molar ratio of 1:100 to 1:1000 and if necessary, an about 0.1 molar solution of cationizing agent is additionally added. Typically, a matrix solution of about 20 mg/L and an analyte solution of 1 to 10 mg/L are prepared. This strongly depends on the used solvent and thereby the crystallization behavior of the matrix. In general, small, homogeneously distributed matrix crystals are desired to assure reproducibility of subsequent measurements. Figure 6 shows a microscope picture of homo-

genously distributed MALDI matrix crystals after application of a 5 mg/mL DCTB solution in THF to a Ni-coated MALDI target plate. Other commonly used matrix preparation techniques include the so called "sandwich" technique shown in Figure 5 where first the matrix is deposited and dried for crystallization and then the analyte solution is added on top of the dried matrix crystals in a second step. This is an especially helpful technique if the matrix's solvent and the analyte's solvent are not miscible. Also, air-spray deposition, spin coating[12], sublimation[13] and electrospray deposition[14] are often used and described in literature.

Other than the matrix, addition of a cationizer can have a big influence on the recorded mass spectra quality. An addition of cationizer can lead to a better ionization of the analyte which might be necessary to see its signal at all. On the other hand, it also leads to an increased signal-to-noise ratio and can suppress signals caused by other salts present in the sample. For polymers with a π-electron system (e.g. phenyl ring) silver salts are the cationizer of choice since their d-orbitals interact with the π-electrons which leads to a firm attachment of the cations.

Also, the used laser power has an influence on the mass spectrum quality. A certain laser power is necessary to achieve desorption and ionization but if it is too high the resolution of the mass spectra will decrease. Also, there might be (more) fragmentation at higher laser power.

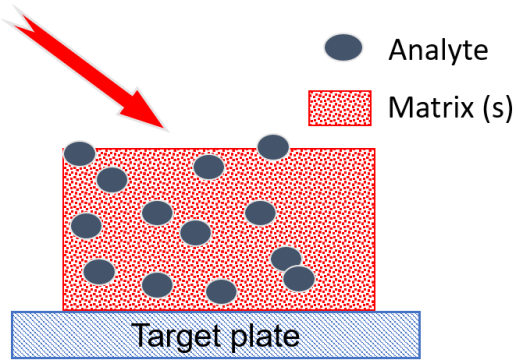

FIGURE 4: DRIED DROPLET SAMPLE PREPARATION

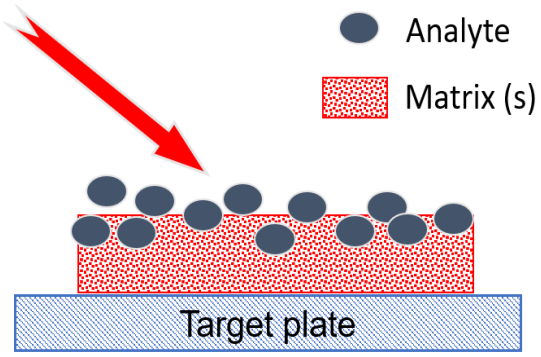

FIGURE 5: SANDWICH SAMPLE PREPARATION

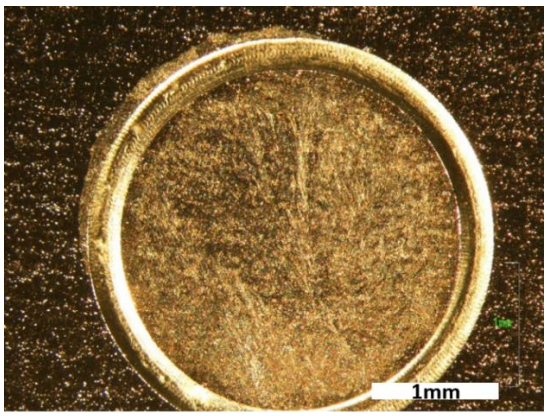

FIGURE 6: HOMOGENOUS CRYSTAL FORMATION OF DCTB DISSOLVED IN THF AFTER APPLICATION TO A NI-COATED MALDI TARGET

In this work the MALDI MS instrument used consists of a time-of-flight (TOF) analyzer. This type of analyzer is often used in combination with pulsed ion sources. It is an analyzer resolving the produced ions according to their mass-to-charge ratio in the time domain. It thereby utilizes the equality of kinetic energy and electrostatic force in uniform linear motion (Newton's first law of motion) as seen in equation 1. By rearranging this equation (compare equation 2), it can be seen

that the velocity of charged particles is equal to the reciprocal square root of its mass-to-charge ratio (given a constant acceleration voltage). This physical principle is used in a linear TOF analyzer by accelerating the produced ions to a fixed kinetic energy and subsequently passing them on into a field free drift tube, where they can move freely, thereby separating them according to their velocity (which is proportional to their mass-to-charge ratio).

EQUATION 1

$$\frac{\boldsymbol{mv^2}}{\boldsymbol{2}} = \boldsymbol{zeU}$$

$m \ldots\ldots\ldots mass\ of\ charged\ particle\ [u]$

$v \ldots\ldots\ldots velocity\ of\ charged\ particle\ \left[\frac{m}{s}\right]$

$z \ldots\ldots\ldots charge\ number\ of\ charged\ particle$

$e \ldots\ldots\ldots elementary\ charge\ [C]$

$U \ldots\ldots\ldots accelerating\ voltage\ [V]$

EQUATION 2

$$\boldsymbol{v} = \left(\frac{\boldsymbol{2zeU}}{\boldsymbol{m}}\right)^{\boldsymbol{1/2}}$$

In this case lighter ions travel faster than heavier ones. Their resolution is theoretically solely dependent on the length of the drift region. Due to internal delays in electronics and other uncertainties the measured flight time may be different than the one calculated (by replacing the velocity in equation one by the tube length and the travel time) therefore, a calibration of the instrument is necessary. Some reasons for non-uniform flight times of the same ions (identical molecular mass) may be them being formed at slightly different times, them being formed at different locations (especially when the on-target preparation of the analyte/matrix mix exhibits a rough surface) and therefore, starting their flight from different points, them being formed with different kinetic energy or them being formed with opposite velocity vectors. To decrease the initial energy spread of the ions produced two important techniques are often used.

The first technique is the reflectron system. A typical reflectron TOF set-up is shown in Figure 7. In this case the ions are reflected by an electrostatic mirror of opposite direction to the acceleration field at the end of the drift tube. Faster ions (with same molecular mass) can penetrate into the mirror further than slower ones and thereby travel a longer distance. In this way all ions of the same mass-to-charge ratio show the same velocity at the exit of the mirror. Afterwards they hit the detector. Often systems with a built-in reflector mirror can both be operated in linear mode (reflector not used) and reflectron mode. The advantage of the linear mode is that high molecular mass analytes (which would lose too much of their kinetic energy and would not be seen in the reflectron mode) can be detected. On the other hand, the reflectron mode leads to a much higher resolution. The optimal operation mode must be chosen according to the given analytical problem.

The second technique is the so-called time-lag focusing. A delay is introduced between the desorption/ionization of the analyte and the acceleration of the formed ions. During this time the ions spread according to their initial velocities. When the accelerating voltage then is applied,

ions with velocity components in the forward direction are accelerated to a lesser extent than those with opposite velocity components. This leads to a focusing of the ion package. This technique can be used both in linear and reflectron mode. Ideally reflectron mode and time-lag focusing should be combined since this leads to the highest possible mass spectrometric resolution.

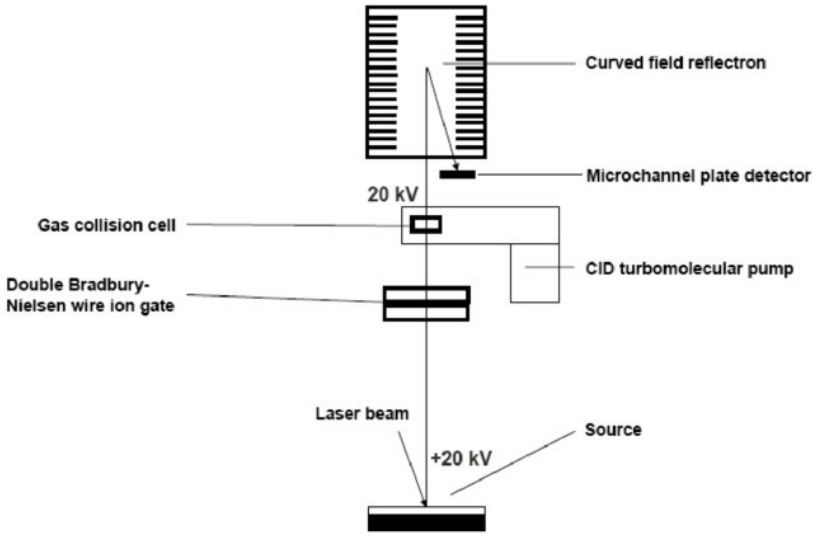

FIGURE 7: TYPICAL SET-UP OF A REFLECTRON TOF MASS ANALYZER[15]

Two different forms of detectors are utilized in the instrument used in this work. For the linear mode a secondary electron multiplier as described in section 1.3.1 is used. For the reflectron mode a multichannel plate detector (MCP) is used. It consists of many micro channels of a highly resistive material arranged in parallel to which a strong electric field is applied. Thereby, each microchannel becomes a single dynode and one impinging ion sets free a cloud of electrons in a cascade way propagating along the channel. The organization of the multichannel plate allows spatial resolution of the signals and the impact of separated ions should not be very focused but on the other hand it has a longer recovery time than a secondary electron multiplier.

MALDI MS is a powerful tool in the field of polymer analytics due to its ability to measure absolute molecular mass, single oligomers, end groups, impurities and even mixtures of different oligomers, i.e. polydispersity of samples. It is therefore more and more used and many papers are published in this field.

Matrices most often used in polymer analytics are dithranol, HABA, DHB and IAA.[9] Their chemical structures are shown in Figure 8Figure 11. As with other analytes mass spectral quality and detectability strongly depends on the chosen matrix and sample preparation. But also, the laser power and the cationizing agent influence the recorded mass spectra. Care must be taken with highly polydisperse polymers since higher mass oligomers might be ionized or detected to a lesser extent leading to a distortion of the “true” mass spectrum and false interpretation. Those types of influence on the recorded mass spectra as well as the influence of mixtures of samples have been extensively discussed in literature.[16–19]

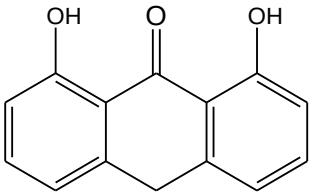

FIGURE 8: CHEMICAL STRUCTURE OF DITHRANOL

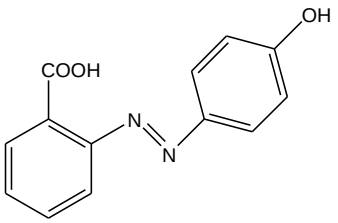

FIGURE 9: CHEMICAL STRUCTURE OF HABA

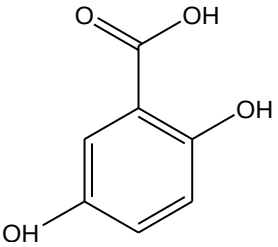

FIGURE 10: CHEMICAL STRUCTURE OF DHB

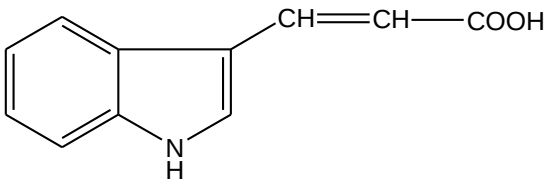

FIGURE 11: CHEMICAL STRUCTURE OF IAA

1.3.3 LASER DESORPTION IONIZATION[7,9]

In laser desorption ionization mass spectrometry, the sample is desorbed and ionized by a pulsed laser similar to MALDI MS. The only difference is the absence of matrix in this case. This leads to a higher energy input as well as a thermal desorption/ionization process and consequently to a higher fragmentation in LDI compared to MALDI. LDI is the older technique of the two but has been widely replaced by MALDI MS since adding a matrix enhances the signal intensity in most cases and fragmentation is most often undesired.

In this work the same instrument was used for MALDI and LDI experiments and consequently the same instrument parts using a TOF analyzer and a secondary electron multiplier and multi-channel plate as detectors.

In polymer analysis, some papers have been published mainly dealing with low molecular weight polymers up to a few thousand Da by LDI[20,21]. For higher mass polymers and more detailed investigations mainly MALDI MS is used as an alternative.

1.3.4 SECONDARY ION MASS SPECTROMETRY

SIMS is in many ways similar to LDI. In this method a beam of (primary) ions leads to energy transfer and subsequently to a thermal desorption and ionization of the sample. Thereby, both positive and negative ions are produced but about 90 % of the material is desorbed as neutral particles and thereby lost for analysis. The ionized particles can be produced by abstraction or addition of an electron, gain or loss of a proton or ion attachment. The latter two are the most common ionization methods taking place. In general, several ion formation mechanisms may occur simultaneously in competition with each other.

The mass spectrum quality depends on the primary ions used (e.g. Ar^+, Ga^+, Bi_3^+), the substrate, if the sample was prepared in a thin film or thick film and of course the physico-chemical nature and molecular mass of the analyte. SIMS can be operated in dynamic mode, where a high primary current is used. This leads to multiple sputtering events at the same site on the surface and often a generation of very small fragments. The dynamic mode can also be used to record depth profiles of the samples up to several micrometer thickness. This is often used in the

microelectronic industry. Another way a SIMS instrument can be operated is in the static mode. There, the primary ion dose is kept low decreasing the probability of multiple sputtering events from the same site. This also leads to ions with higher m/z values (can be either larger fragment ions or even molecular ions of different types).

In this work a SIMS utilizing a TOF analyzer was used (compare 1.3.2)

Much information about polymers can be gained by SIMS for example on polymer repeat units, functional groups present and in favorable cases number/weight-average molecular weights. For this reason, SIMS has been applied frequently to analyze polymers in the past. Static mode is more often used, since it leads to bigger fragments (or even oligomer distributions) which are most often wanted in polymer analysis.

1.3.5 Pyrolysis gas chromatography mass spectrometry[22–25]

The general set-up of a pyrolysis GC MS instrument is shown in Figure 12. The sample is introduced in a heating chamber and heated, up to 600-1000 °C under a flow of an inert carrier gas. Three different thermal systems are commonly used: isothermal furnace, inductive heating or resistive heating using platinum wires. The heating can be done in a so-called single shot approach where the sample is introduced into the chamber at the highest temperature. At that temperature pyrolysis of the sample takes place instantaneously with the molecule's weakest bonds breaking and other bonds being rearranged. Thereby, the generally solid sample is transferred into the gas phase. Another way is the so-called double shot approach where the sample is inserted in the chamber at a lower temperature which is subsequently slowly increased to a first plateau. At this point a first gas chromatographic separation is done. In a second step the sample is quickly heated to the maximum temperature and a second chromatographic separation is done. Thereby, two mass spectra per sample are recorded. This method allows to get rid of volatile impurities.

After pyrolysis the sample is transferred into a capillary gas chromatograph. This instrument is designed to separate volatile components of a mixture. The device consists of an injection system, a capillary column, a column heater and a detector (in this case the EI mass spectrometer) which is shown in Figure 14. The column most commonly consists of fused silica material covered on the inner surface with different stationary phases to vary the capillary column's separation properties. The sample is "flushed" through the column together with an inert gas which is called the mobile phase. Separation takes place according to the distribution constants of the mixture's components between the stationary and mobile phase. It is mainly influenced by the type of stationary phase, the temperature of the column and the flow velocity of the mobile phase.

After separation in the gas chromatograph the sample is transferred into the mass spectrometer where it is ionized and separated according to mass-to-charge ratio (compare 1.3.1) which is shown in Figure 13. In this case an EI ion source was used. The sample is ionized by collision with an electron beam of typically 70 eV produced by a hot wire. It is a hard ionization technique and typically many fragment ions are produced besides molecular ions. The degree of fragmentation can be controlled by changing the energy of the electron beam.

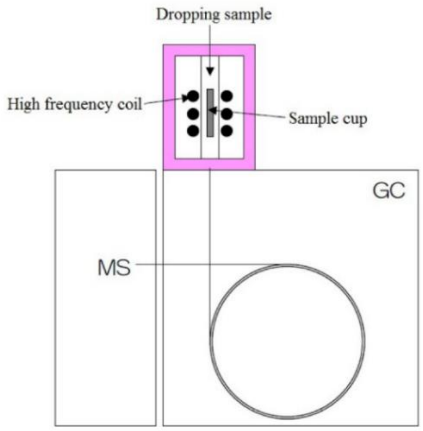

FIGURE 12: GENERAL SET-UP OF A PYROLYSIS GC MS INSTRUMENT[26]

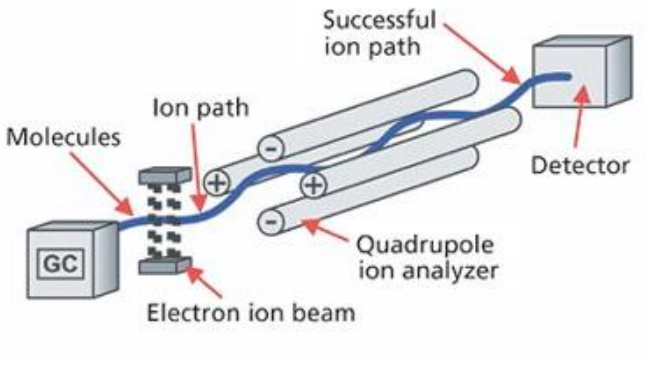

FIGURE 13: SCHEMATIC SET-UP OF THE MASS SPECTROMETRIC SYSTEM USED IN PYROLYSIS GC MS[27]

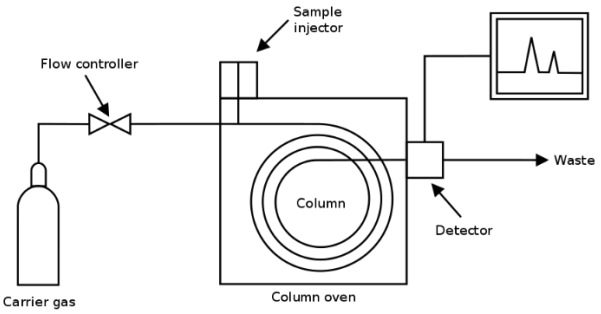

FIGURE 14: GENERAL SET-UP OF A GAS CHROMATOGRAPHY SYSTEM[28]

As a mass analyzer, a quadrupole analyzer was used. It consists of four parallel circular or hyperbolic rods. A constant and an rf electric field are applied to the rods with the two opposite rods having the same potential. The ions are pushed on certain trajectories by the alternating field with only one distinct m/z being on a stable trajectory and leaving the quadrupole analyzer at a given time. All other ions collide with one of the rods at a certain point which leads to a discharge. The quadrupole scans for all m/z ratios by subsequently changing the electric field components which leads to a separation of present ions of different m/z ratio. As a detector a secondary electron multiplier was used in this work as described in 1.3.1.

Pyrolysis GC MS provides a simple but powerful tool in the field of polymer characterization. It is simple, rapid and extremely sensitive (especially when combined with an MS as a detector) particularly for intractable cured polymers with three-dimensional networks. A big advantage is the fact that the sample is being pyrolyzed quantitatively and therefore, the information gained is very reproducible.

On the other hand, due to the pyrolysis the information about analyte molecular mass and distribution gets lost. Also, mixtures cannot be distinguished, and the thermal decomposition might lead to decaying processes which are similar for different compounds and therefore, two such compounds might not be distinguishable anymore.

1.4 PATRICLE SIZE ANALYSIS TECHNIQUES

1.4.1 GENERAL INTRODUCTION[3,29]

As described in chapter 1.2.2 nanomaterials show a tremendous potential for unique and customized properties. On the other hand, they might pose a not yet fully known and understood health risk. To study and define the risk, reliable analytical methods must be available to determine the nanoparticle size and distribution. This makes it possible to classify a material as a nanomaterial according to European law. Currently used risk values like the PM_{10} or the $PM_{2.5}$ are based on the weight-based size distribution. The official European classification of nanomaterials is referring to a number-based size distribution, making it even more important to develop reliable methods for number-concentration based measurements of nanoparticles.

Problems in measuring the "size" of particles arise due to their three-dimensionality. Very few particles are ideally spherical. Generally, a physical constant like the volume, the surface, the weight, the sedimentation velocity or even an external extension (length) of the particle is measured. From this value an equivalent sphere is calculated which has the same physical property but is ideally spherical to receive a (theoretical) diameter of the analyte.

Another problem is the subjectivity of different measurement techniques due to the physical properties they measure. A technique measuring the volume of a distribution will give a different mean diameter than a technique measuring the sedimentation velocity of the same sample. Therefore, results obtained using two different techniques are in general not directly comparable.

Various particle size analysis techniques have been around for quite a while but since the demand for measuring smaller and smaller particles with higher polydispersity is ever increasing, many of the conventional techniques are at their limits and new techniques have to be developed. Since industrially used properties of nanomaterials include volume- and surface-based properties, most commercially used techniques measure the weight-concentration. In this case especially multimodal or highly polydisperse materials often pose a problem because many techniques, including light scattering based techniques like laser diffraction or dynamic light scattering, lead to an overestimation of larger particles.

In this work three different particle sizing analysis techniques were used. The first two, scanning electron microscopy and laser diffraction, have both been around for quite a while. Gas phase electrophoretic mobility molecular analysis, the third technique discussed, is a comparably new technique and has been successfully applied in the study of biological nanoparticles such as VLPs and others.[30–38]

Those three particle size analysis techniques employ three different measurement principles and therefore give a representative cross section on the field of particle size analysis. SEM as an imaging method is able to not only detect the size of a particle but also its morphology. Laser diffraction is a method which can be easily used routinely for a large number of samples but only for mainly monodisperse particles larger than 100 nm. It measures the volume distribution and therefore overestimates the number of bigger particles. GEMMA provides a good alternative for particles below 300 nm down to a few nm in size. Contrary to laser diffraction it measures the number-based particle concentration.

The AIEX particles were measured using all three methods. NIST size standards were measured as well to verify the results.

1.4.2 SCANNING ELECTRON MICROSCOPY

In electron microscopy, accelerated and focused electrons are utilized to create an image in a very similar way as in light microscopy. Since electrons are accelerated to about 50 % of the speed of light within an electron microscope, they can be considered as electromagnetic waves, which explains the great similarity between electron microscopy and light microscopy. In both techniques a beam of electromagnetic waves is focused on an image plane by an array of lenses and the transmitted or backscattered "light" can be detected. Information about the sample can be transduced by the attenuation and the phase shift of the electromagnetic waves. On top of that "conventional" information, further information is provided by electron spectroscopy due to element characteristic X-rays, Auger electrons and secondary electrons. In a similar way to optical microscopy lens aberrations can be reduced or avoided by special set ups of lenses. Handling electrons has to be done in high vacuum due to collision and beam-widening effects. Instead of optical lenses, electromagnetic lenses are used in electron microscopy and instead of using the human eye or an LCD camera for detection, a secondary electron detector and a backscattered electron detector are used. Figure 15 shows the typical set-up of a SEM.

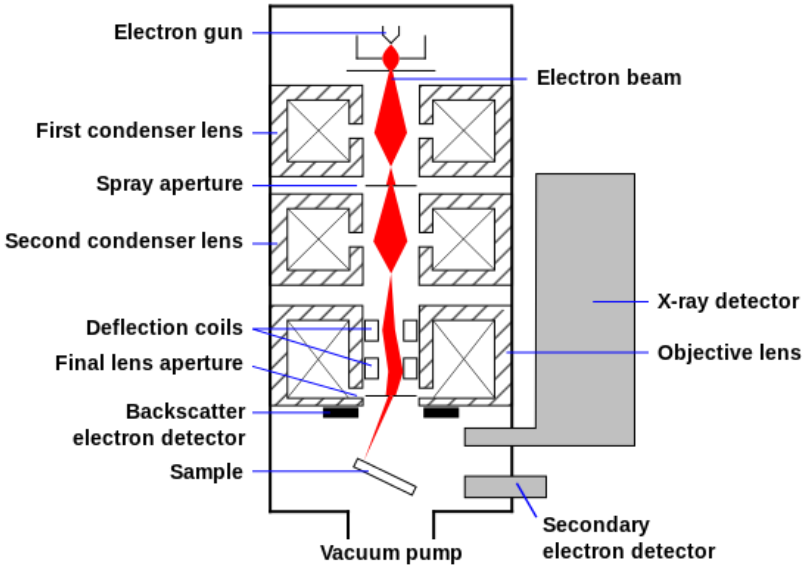

FIGURE 15: SCHEMATIC VIEW OF AN SCANNING ELECTRON MICROSCOPE INTERIOR SET-UP[39].

The electron beam is produced by a heated tungsten filament, accelerated by an applied voltage and focused on a sample by electro-magnetic lenses. Hitting the sample, the electrons can have various effects. An overview of the effects is shown in Figure 16: usable signals in scanning electron microscopy produced by an electron beam hitting a sample surface [40]. At the surface so called Auger electrons are produced when an electron of the outer shell fills an empty space in an inner shell of an atom. This leads to a release in energy which in turn leads to the emission of an outer shell electron. Those electrons give information about the surface atomic composition. A bit deeper within the sample secondary electrons are produced. They are formed by energy transfer of the primary electron beam to the sample atoms and subsequent release of an electron by the latter. They give topographical information about the sample. Some primary electrons are back-scattered and detected by the backscattered electron detector. They give information about atomic number and phase differences. Primary electrons can also lead to the abstraction of an electron in the inner shell of the sample atoms. This leads to a subsequent characteristic X-ray release and gives information about the elemental composition of the sample. For sufficiently

thin samples electrons can also pass through the sample and be attenuated. Also, a phase shift can occur. Those transmitted electrons can also be collected to form an image of the sample (morphological information) which is utilized in transmission electron spectroscopy.

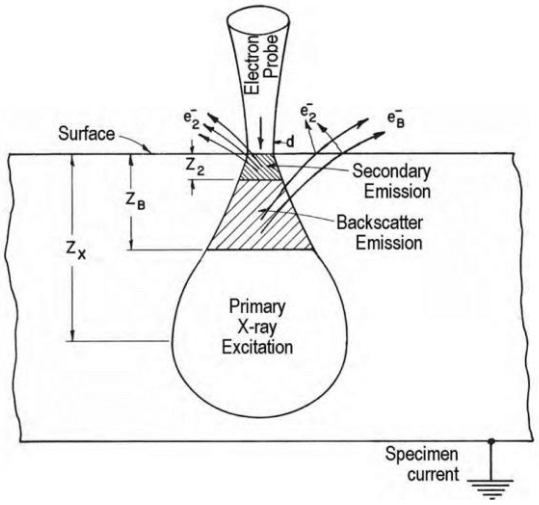

FIGURE 16: USABLE SIGNALS IN SCANNING ELECTRON MICROSCOPY PRODUCED BY AN ELECTRON BEAM HITTING A SAMPLE SURFACE [40].

SEM is often used in nanoparticle analysis since a direct image of the sample can be acquired. Resolution can be as low as 3-6 nm [41]. Therefore, the shape and size of the particles can be determined both for monodisperse as well as polydisperse systems as well as non-uniformly shaped systems. Image analysis also enables the automatic detection and classification of particles to a certain extent.

A disadvantage is the necessity of the sample to be conductive to avoid charging effects. Also, the measurements have to be done under high vacuum which can lead to a modification of the analyte if it is usually present in aqueous media (e.g. proteins). Also, the preparation of the sample might be laborious and qualified staff is needed to operate the instrument. On top of that only a small section of the sample can be viewed at a time which makes taking a representative image very subjective and a large number of images is necessary to obtain statistically significant numbers.

Nonetheless, SEM is a useful tool to get an overview of an unknown sample and to analyze non-uniformly shaped nanomaterials.

1.4.3 LASER DIFFRACTION

Laser diffraction, also called low angle laser light scattering, is a very frequently used technique to determine particle size distributions between 0.1 and 2000 µm.

A typical set-up of a laser diffraction instrument is shown in Figure 17. A laser beam (typically a He-Ne CW-laser) is widened to shine a parallel beam path through a suspended sample. Depending on the size of the sample particles the light is scattered at one or even at various points within the sample. The scattered light interacts constructively or destructively with other light rays and is finally focused onto a detector array using an optical lens. Depending on the particle size the scattered light is mainly scattered in the forward direction (particles bigger than laser wavelength) or in all directions (particles smaller than laser wavelength).

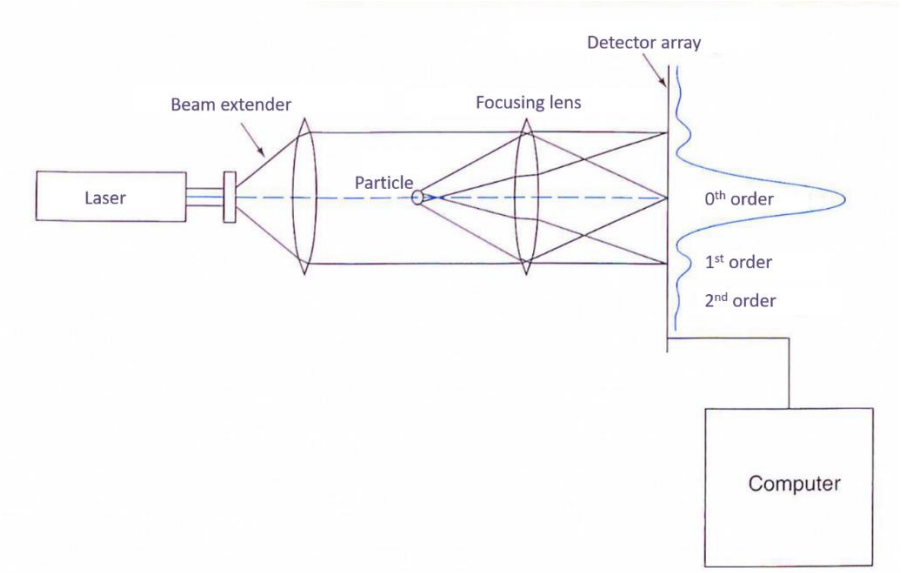

FIGURE 17: SET-UP OF A PARTICLE SIZE ANALYZER UTILIZING LASER DIFFRACTION[42]

The sample can be either suspended in air or in a liquid which does not dissolve the particles. The suspended particles are then transported into an optical unit (for measurements in water this consists of a cuvette with defined length) where the laser beam is shone through the sample.

A certain percentage of extinction in the beam path which correlates with a certain particle concentration is needed for a sufficient measurement. To observe this, an extinction detector which is located in the focal point of the lens is used.

The recorded scattering pattern is then calculated into a size distribution using various mathematical models. Two widely used models are the Mie scattering theory and the Fraunhofer diffraction model.

The Mie scattering model can be used to calculate the size of spherical, isotropic particles with a smooth surface, taking their absorption and the light passing through into account. It is very accurate but some particle parameters such as absorption index must be known. The particles are considered as extended objects with many scattering points within. At each of this points light can be scattered and the differently scattered beams can thereafter interact with each other. This leads to complex intensity distributions at the detector array which can be back calculated to find the original particle size distribution. This model cannot be used for mixtures of different components.

On the other hand, the Fraunhofer diffraction model is a simplified model dealing with particles way bigger than the laser wavelength. It does not take the scattering of light at different positions within one object into account and subsequently neglects the interference of such beams. The model considers the particles as hollow disks (aperture) which lead to diffraction patterns known as Airy pattern. The detected intensity pattern can be considered as the sum of all the Airy patterns of all individual particles and the size distribution can be back calculated using the Airy function.

A big advantage of laser scattering measurements is its wide dynamic range and the ease of use. Furthermore, it is very accurate and can be used for samples with different shapes. It is often used in polymer analysis especially if material properties like refraction index are known.

Disadvantages are its lower limit of nanoparticle detection of about 100 nm, the fact that a few bigger particles dominate the (volume) distribution and that there always are results given but the trueness of the measurement cannot be determined easily. Furthermore, the chemical nature of the analyte cannot be analyzed, only its size distribution.

1.4.4 NANO-ELECTROSPRAY GAS PHASE ELECTROPHORETIC MOBILITY MOLECULAR ANALYSIS

The nES GEMMA also known as ES-SMPS, ES-DMA or macroIMS™ Macroion Mobility Spectrometer separates singly charged analytes in the gas phase according to their electrophoretic mobility diameter at ambient pressure.

The nES GEMMA instrument consists of three parts shown in Figure 18 and Figure 20; a nano-electrospray aerosol generator with a charge reduction chamber, an electrostatic classifier based on a nano differential mobility analyzer (DMA) and an ultrafine condensation particle counter (CPC).

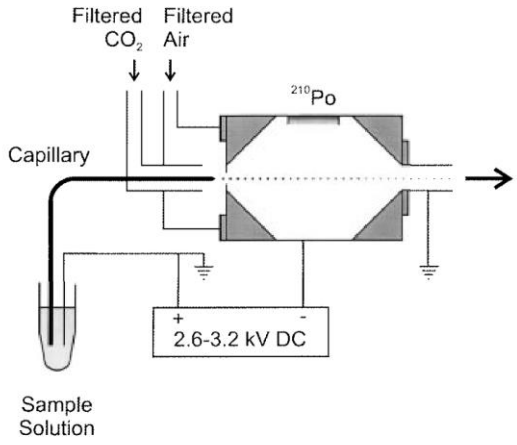

FIGURE 18: NANO-ELECTROSPRAY AEROSOL GENERATOR WITH A CHARGE REDUCTION CHAMBER[43]

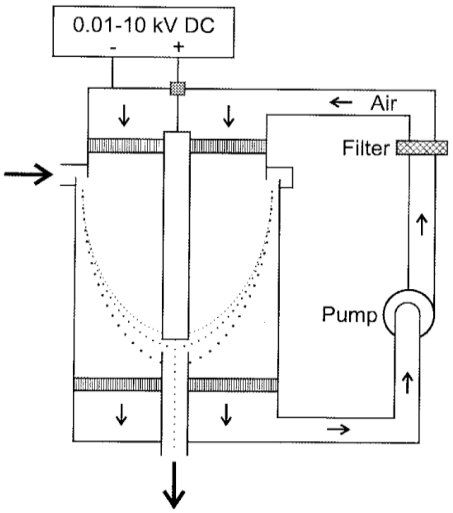

FIGURE 19: ELECTROSTATIC CLASSIFIER BASED ON A NANO DIFFERENTIAL MOBILITY ANALYZER[43]

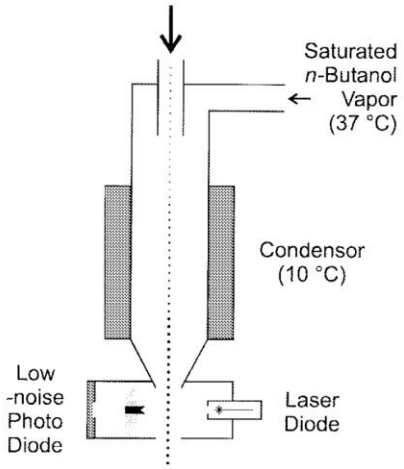

FIGURE 20: ULTRAFINE CONDENSATION PARTICLE COUNTER[43]

The nano-electrospray aerosol generator is used to generate multiply-charged analytes in the gas phase. The sample is dissolved in a volatile electrolyte prior to the measurement and the solution is placed within a sample holder. By applying over pressure, the sample is pushed through a fine capillary (e.g. a fused silica capillary). A voltage of a few kV is applied leading to the formation of a so-called Taylor cone and subsequent liquid aerosol droplet formation. The volatile electrolyte evaporates which leaves multiply charged analyte particles in the gas phase. To enhance the spray process and to move the particles to the next compartment filtered CO_2 and filtered particle-free air are applied as shown in Figure 18. They next enter a ^{210}Po chamber in which a mixture of many different radical species is kept up (bipolar atmosphere). This leads to a charge reduction leaving mostly neutral and a certain percentage of singly charged analyte particles.

The singly charged analyte particles next enter the DMA. Here, air with a defined high sheath flow (up to 15 Lpm) is flushed through, moving the particles in the direction of the flow. Orthogonally an electric field is applied moving the charged particles in an orthogonal direction due to electrostatic forces. This leads to a separation of particles according to electrophoretic mobility, i.e. size in case of spherical analyte particles. The electric field is subsequently tuned (10 V-10 kV) within a certain range to allow only one size of particles to exit the DMA into the CPC at a given time. The other particles leave the DMA with the exhaust air or are neutralized on the inner electrode.

The now monodisperse singly charged analyte particles next enter the ultrafine condensation particle counter in which there is a saturated n-butanol or water atmosphere. The singly charged particles serve as condensation nuclei forming larger, µm-sized droplets during entering the cooling part of the CPC kept at lower temperature. Finally, those droplets enter a laser chamber and are detected by scattering of a laser beam. This detection is independent of the chemical nature of the analyte particles.

The nES GEMMA system has previously been used for the detection of biomolecules such as proteins or glycoproteins[35,43] virus-like particles[32,33], colloidal nano particles[34] and others. Its feasible size range is between 1.9 nm and up to 300 nm. It therefore covers a size range in between mass spectrometric techniques and laser scattering but similar to SEM. Furthermore, the particle number concentration is directly measured leading to a more representative result than with techniques where it is back calculated from surface or volume measurements. Consequently, it is also usable for polydisperse systems. In contrast to SEM a much higher particle number (usually several thousands) is analyzed giving a more representative and statistically solid picture.

On the down side the technique assumes the particles to be spherical and highly non-spherical particles might not be represented correctly. Also, the chemical nature of the analyte cannot be analyzed directly. The handling of the instrument needs qualified staff similar to SEM and is not as straight forward as with laser diffraction. A close control of the nES process is required for reproducible measurements.

2 EXPERIMENTAL

2.1 RECEIVED SAMPLES

Table 1 gives an overview of the investigated analyte classes specifying the number of received and selected samples, the methods which can be used for characterization and whether all samples were analyzed or only one representative. The analytes and methods shown in Table 1 are described in more detail in the following.

TABLE 1: OVERVIEW OF THE USED SAMPLE TYPES AND THE METHODS USED TO CHARACTERIZE THEM. GREEN CELLS INDICATE THAT ALL SAMPLES WERE MEASURED USING THE ACCORDING METHOD, YELLOW CELLS INDICATE THAT ONE REPRESENTATIVE OF THE SAMPLE CATEGORY WAS MEASURED AND RED CELLS INDICATE THAT NO MEASUREMENTS WERE DONE. WHITE CELLS INDICATE THAT THE METHOD CANNOT BE UTILIZED FOR THE ACCORDING SAMPLE TYPE.

Sample	*Number of samples*	*MALDI MS*	*LDI MS*	*SIMS*	*Pyrolysis GC MS*	*SEM*	*LD*	*GEMMA*
Soluble polystyrenes	6							
Particle size standards	5							
Resin samples	6							
Cell extracts	5							

6 anionic exchange resin samples of different degree of milling (expressed as milling energy content) and therefore, putative different particle content were received from Boehringer Ingelheim for analysis. They were obtained using two different base products both from comercial resin sources. Both resins (A400 and A600) were carrying a type I quaternary ammonium functional group and a Cl- counter ion. An overview of the received samples is given in Table 2. All resins were milled in a device with bigger sized grinding bodies in a first step (called pre-milling). Subsequently the mixtures were transferred to a milling device containing smaller milling bodies to receive finer particle sizes. The milling energy content given in Table 2 only refers to the transferred energy of the second milling step (since there was no difference in milling in the first step). In the following, the abbreviations Axxx_y is used to describe the resin type utilized for the according experiments. Where xxx is the number of the according resin type and y the milling energy content. Four different milling energies were used described as high (y=h), medium (y=m), low (y=l) and extra low (y=el). An exception is given for the resin t34_0 (as shown in Table 2) since it did not undergo the second milling step and therefore represents the samples after the first milling step. The milled resins were suspended in an aqueous solution containing a weight concentration of about 10 %. It can be assumed that for higher milling energy content, a higher fraction of smaller particles within the resin sample is to be expected.

Furthermore, cell extract samples were received to test the detectability of resin particles in cell extracts. An overview of the received cell extract samples is given in Table 3.

TABLE 2: RECEIVED RESIN SAMPLES AND CORRESPONDING SUBSEQUENTLY USED ABBREVIATIONS

Sample ID	Milling energy	Resin type	Abbreviation
t08_3	high	A400	A400_h
t08_2	low	A400	A400_l
t01_8	high	A600	A600_h
t01_6	medium	A600	A600_m
t08_1	extra low	A400	A400_el
t34_0	after premilling	A400	A400_0

TABLE 3: RECEIVED CELL EXTRACT SAMPLES AND RESIN ADDED

Sample	Test protein	Resin added
AIEX pool (cell extract after AIEX column cleaning)	mCardinal	A400_l
AIEX load (cell extract after AIEX column cleaning)	mCardinal	A400_l
Positive control	GFP	A400_h
Negative control (equal to AIEX load)	GFP	None (pure cell extract)
Negative control (equal to AIEX load)	mCardinal	None (pure cell extract)

2.2 CHEMICALS AND REAGENTS

For validation of the results obtained for resin samples, polystyrene particle size standards of different mean diameter were used. An overview of the used standards, the company of which they were purchased, and the used size determination method according to their certificate is given in Table 4.

Additionally, soluble polystyrene standards of different average molecular weight were used and are listed in Table 5.

Other chemicals used are also listed in Table 5 in alphabetical order showing the product name, the purchase company, the product number and lot number.

Table 6 gives an overview of the used materials in alphabetical order showing the product name, the purchase company, the product number and lot number if existent. The used instruments are listed in Table 7 in alphabetical order showing the company and the model data.

Used instrument parameters are given in the according experimental section.

TABLE 4: USED POLYSTYRENE PARTICLE SIZE STANDARDS AND USED METHOD FOR DIAMETER DETERMINATION ACCORDING TO CERTIFICATE

Product name	Purchase Company	Certified mean diameter	Size determination method for certification
Nanosphere Size Standards 3020A	Thermo Fisher Scientific Inc. (Waltham, MA, USA)	22 ± 2 nm	Photon correlation microscopy
Nanosphere Size Standards 3040A	Thermo Fisher Scientific Inc.	41 ± 4 nm	Photon correlation microscopy
Nanosphere Size Standards 3060A	Thermo Fisher Scientific Inc.	60 ± 4 nm	Transmission electron microscopy
Nanosphere Size Standards 3080A	Thermo Fisher Scientific Inc.	81 ± 3 nm	Transmission electron microscopy
Microparticle Size Standard based on Monodisperse Polystyrene	Sigma-Aldrich (St. Lois, MO, USA)	102 ± 3 nm	Disc centrifugation
Nanosphere Size Standards 3200A	Thermo Fisher Scientific Inc.	203 ± 5 nm	Transmission electron microscopy

TABLE 5: LIST OF USED CHEMICALS IN ALPHABETICAL ORDER AS WELL AS THEIR PURCHASE COMPANY, PRODUCT NUMBER AND LOT NUMBER

Product name	Company	Product number	Lot number
Acetic acid, ACS reagent ≥ 99.8 %	Honeywell Fluka™ (Buchs, Switzerland)	33209-2.5L	SZBG2450
Acetone, ACS, ISO, Reag. Ph Eur, for analysis	Merck, KGaA (Darmstadt, Germany)	1.000.142.500	K48802114713
Silver trifluoroacetate, ≥ 99.99 %	Sigma-Aldrich (St. Lois, MO, USA)	482307-1G	MKCC6135
Ammonium acetate, ≥ 99.99 % trace metal basis	Honeywell Fluka™ (Buchs, Switzerland)	431311-50G	MKBZ7537V
Hyaluronic acid sodium salt from *Streptococcus equi*, mol wt 15,000-30,000	Sigma-Aldrich (St. Lois, MO, USA)	97616-10MG	
Sodium hydroxide pellets, EMPROVE® ESSENTIAL Ph Eur,BP,FCC,JP,NF,E 524,	Merck, KGaA (Darmstadt, Germany)	1.064.825.000	B561682439
Hexadimethrine bromide (Polybrene), ≥ 94% (titration)	Sigma-Aldrich (St. Lois, MO, USA)	H9268-5G	
trans-2-[3-(4-*tert*-Butylphenyl)-2-methyl-2-propenylidene]malononitrile (DCTB), ≥ 98 %	Sigma-Aldrich (St. Lois, MO, USA)	727881-1G	9499
2,5-Dihydroxybenzoic acid (DHB), 98 %	Sigma-Aldrich (St. Lois, MO, USA)	149357-25G	WXBB7481V
Dithranol, Matrix substance for MALDI-MS, ≥ 98.0%	Honeywell Fluka™ (Buchs, Switzerland)	10608-1G-F	BCBN3098V
Isopropanol, for LC-MS	SERVA Electrophoresis GmbH (Heidelberg, Germany)	45636.02	180499
Potassium Chloride, Puriss. P.A., ≥ 99.5%	Honeywell Fluka™ (Buchs, Switzerland)	60130	80150
Methanol, hypergrade for LC-MS LiChrosolv®, ≥ 99.9 %	Merck, KGaA (Darmstadt, Germany)	1.060.352.500	10908835739
Ultra high quality water (UHQ), was obtained by using a Simplicity system with 18.2 MΩ × cm resistivity at 25 °C	Milipore (Bedford, MA, USA)		

Methyl *tert*-butyl ether, ACS reagent, ≥ 99 %	Sigma-Aldrich (St. Lois, MO, USA)	216-653-1	MU14785LU
Sodium Chloride, for analysis EMSURE® ACS,ISO,Reag. Ph Eur	Merck, KGaA (Darmstadt, Germany)	106.404.100	
Ammonium hydroxide solution, Puriss., > 25 % NH3 in H2O	Honeywell Fluka™ (Buchs, Switzerland)	9857	GA1801
1-Butanol, for analysis EMSURE® ACS,ISO,Reag. Ph Eur	Sigma-Aldrich (St. Lois, MO, USA)	1.019.902.500	K42156890
Sinapic acid, ≥ 98%, powder	Sigma-Aldrich (St. Lois, MO, USA)	D7927-5G	SLBK4211V
Polystyrene standards, low molecular weight kit	Sigma-Aldrich (St. Lois, MO, USA)	48937	
Tetrahydrofuran, anhydrous, ≥ 99.9%, inhibitor-free	Sigma-Aldrich (St. Lois, MO, USA)	401757-100ML	
Toluene, anhydrous, 99.8%	Sigma-Aldrich (St. Lois, MO, USA)	244511-100ML	
Tween® 20, Sigma Ultra	Sigma-Aldrich (St. Lois, MO, USA)	P7949-100ML	087K01981

TABLE 6: LIST OF USED MATERIALS IN ALPHABETICAL ORDER AS WELL AS THE COMPANY AND THEIR PRODUCT NUMBER

Material name	Company	Product number	Lot number
Carbon tape	Local hardware store		
Copperhead BBs, Airgun Shot, Steel BB Cal. (4.5 mm)	Crosman (Bloomfield, NY, USA)		
Eco-cup LF, 80 µL	Frontier Laboratories (Tokyo, Japan)	PY1-EC80F	
Flexible Fused Silica Capillary Tubing, Inner Diameter 40 µm, Outer Diameter 150 µm	Polymicro Technologies (Phoenix, AZ, USA)	1068150014	AZZJ04A
20 mm Injection stopper, 4023/50 Grey	APG (Uithoorn, Netherlands)	2407858	
4 mL Injection vial, Amber Type 1 Tubular glass	APG (Uithoorn, Netherlands)	1011586	
Microcentrifuge tubes, Safe-Lock, Eppendorf®, 0.5 mL, 1.5 mL and 2 mL	VWR (Fontenay-sous-Bois, France)	211-2140, 211-2130, 211-2120	
Minisart® NML Syringe Filter, 0.2 µm Surfactant-free Cellulose Acetate	Sartorius (Göttingen, Germany)	16534-K	81258103
Nanosep® Centrifugal Devices with Omega™ Membrane, 300K, orange	Pall (Dreieich, Germany)	OD300C34	FC9077
2 mL Screw Top Vial Caps, blue	Agilent Technologies (Santa Clara, CA, USA)	5182-0717	AGI201188
2 mL Screw Top Vials	Agilent Technologies (Santa Clara, CA, USA)	5182-0715	838-05-17/001
Silicon wafer	Infineon Technologies Austria (Villach, Austria)		
Shimadzu, Kratos analytical DE2115TA (Ni-coated target plate)	Shimadzu (Kyoto, Japan)	DE2115TA	
Shimadzu, UniMass™_96 (Stainless steel target plate)	Shimadzu (Kyoto, Japan)		

TABLE 7: LIST OF USED INSTRUMENTS IN ALPHABETICAL ORDER AS WELL AS THEIR COMPANY AND THE MODEL USED

Instrument name	Company	Model
Aerosol Generator including ^{210}Po charge equilibration device	TSI Inc (Shoreview, MN, USA)	3480
Analog vortex mixer	VWR (Fontenay-sous-Bois, France)	
Analytic balance	Satorius (Göttingen, Germany)	BP121S
Electrostatic Classifier based nano Differential Mobility Analyzer (nDMA)	TSI Inc (Shoreview, MN, USA)	3080
GC EI MS	Shimadzu (Kyoto, Japan)	QP2010 Plus
In-house-made capillary tip sharpener according to Tycova et al. in 2016[44]	Home built at TU Wien	
MALDI/LDI mass spectrometer	Shimadzu (Kyoto, Japan)	Axima TOF2™
Mastersizer particle sizer	Malver Panalyticals (Kassen, Germany)	2000 hydro
Nanometer aerosol sampler	TSI Inc (Shoreview, MN, USA)	3089
pH meter	Mettler Toledo (Columbus, OH, USA)	FiveEasy standard
Pyrolizer	Frontier Lab (Koriyama, Japan)	PY-2020iD
Refrigerated centrifuge	Sigma Laboratory Centrifuges (Osterode am Harz, Germany)	1-14
SIMS	IONTOF (Münster, Germany)	TOF.SIMS^5
Ultrafine condensation particle counter (CPC)	TSI Inc (Shoreview, MN, USA)	3025A
Ultrasonic cleaner	VWR (Fontenay-sous-Bois, France)	
UNIVAPO Vacuum concentrator centrifuge	Uniequip (Planegg, Germany)	100 H
Zoom stereo microscope	Nikon Instruments Europe (Amstelveen, Netherlands)	SMZ800

2.3 PRECEDING EXPERIMENTS

2.3.1 DISSOLUTION EXPERIMENTS

Dissolution experiments were carried out using resin A400_h and A600_h. They were diluted in a ratio of 1:100, 1:1000 and 1:10000 (v/v) and the aqueous solvent was evaporated off in a vacuum centrifuge. Thereafter, THF, toluene and MTBE were added, the sample vortexed and the obtained solutions / suspensions checked by sight after 30 min. Next, the sample was put in an ultrasonic bath for 30 min and the solutions / suspensions checked by sight again. To check the effect of the organic solvents on the resin particles SEM images of the aqueous suspension and the organic solution were taken (after evaporation of the solvent). Furthermore, a 1:10000 (v/v) aqueous dilution of the resin was filtered using a 0.2 µm syringe filter and SEM images were taken to check for left-over particles (compare section 3.6.1).

2.4 MALDI MS EXPERIMENTS

2.4.1 SAMPLE PREPARATION: VOLUME TECHNIQUE

For preceding crystallization experiments a simplified version of the volume sample preparation technique (also called “dried droplet” technique) was used. Different amounts of matrix were dissolved in different solvents and 1-2 µL of the mixture was applied to the target plate and left to dry at room temperature. DHB, sinapinic acid, DCTB and dithranol were tested at 1 mg/mL, 5 mg/mL, 10 mg/mL and 20 mg/mL concentration in THF, toluene, MTBE and THF:MeOH 3:1 [v:v]. Dithranol at 1 mg/mL and 5 mg/mL and DCTB at 1 mg/mL and 5 mg/mL in both THF and toluene were chosen for further experiments due to their good crystallization properties. Since THF and toluene lead to leaching of polyethylenes from Eppendorf safe-lock tubes and pipette tips (compare section 3.2.3), glass vials and a Hamilton syringe were used for handling of the solvents in general. As target plates a Ni-coated Aluminium target, a stainless-steel target and a stainless steel-coated polymer-based single use targets were used.

As analytes a representative resin sample (A400_h), a representative particle size standard (40 nm) and soluble polystyrenes of three different average molecular weights (2500 Da, 9000 Da and 30 kDa) were chosen. AgTFA was used as cationizer for the particle standards and the soluble polystyrene since it was found to yield good result described in literature[45,46]. It was not used for the resin samples since they already contain covalently bound cationic functional groups.

In the following the general sample preparation procedure is described without giving exact values. Since the concentration of analyte, matrix and cationizer as well as the used solvents and target plate were varied for different experiments, the specifically used values are given in the according result section in detail. For sample preparation the resin suspension was dried in a vacuum centrifuge to remove the water. Next the appropriate amount of analyte, MALDI matrix and cationizer were weighed in separately into Eppendorf tubes in the first experiments. Due to leaching of polymers from the Eppendorf tubes, glass vials were used for later experiments. The according solvent was added, and the mixture was vortexed to dissolve the solid compounds. Next, the solutions were centrifuged to deposit non-dissolved parts. This was not done for the resin samples since it was suspected that they were not soluble and to avoid removal of the analyte particles. The three solutions were mixed in a defined ratio and about 0.5 µL of the

solution was applied to the target plate. Then, it was left to dry at room temperature before measurement.

Since polyethylene impurities could be seen in first recorded mass spectra, contact with polymer-based parts was avoided as much as possible in a next preparation step. Glass vials were used for preparing solutions and a Hamilton syringe for pipetting steps instead of Eppendorf tips.

2.4.2 Sample preparation: thin layer technique

For thin-layer sample preparation the MALDI matrices were dissolved in THF or toluene respectively at the appropriate concentration and about 2 µL applied to a stainless-steel target plate. This one was chosen due to its bigger target rings for sample application. Since a Hamilton syringe was used for the preparation steps to avoid polymer contamination the applied volume had to be larger and therefore, bigger rings were necessary. After evaporation of the solvent 2 µL of an aqueous analyte suspension and dissolved cationizer in water was applied to the matrix crystals. Since DCTB and dithranol are insoluble in water, the crystal structure was not changed during this process. After evaporation of the water the sample could be measured. For the resin samples no cationizer was applied since they already consist of polycations.

Figure 21 shows the appearance of the thin layer sample preparation of 1 mg/mL dithranol in toluene at different resin concentrations.

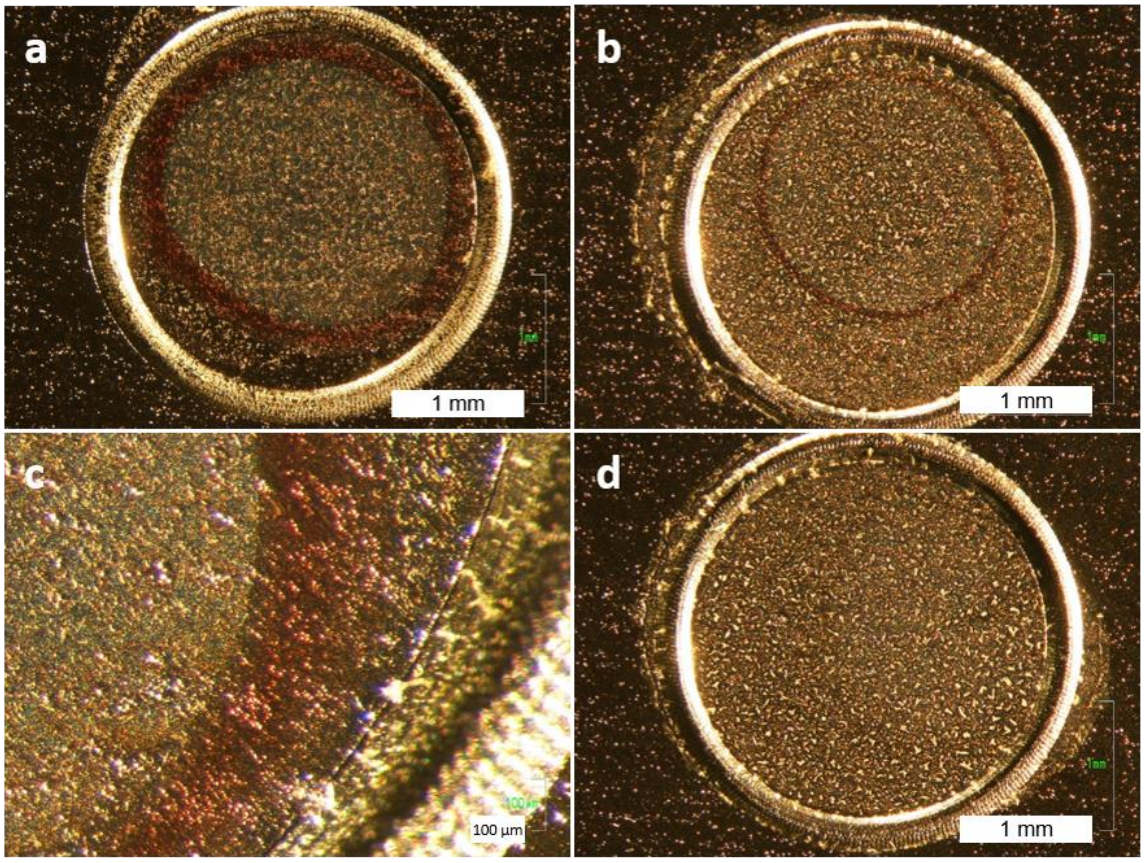

Figure 21: thin layer preparation of 1 mg/mL dithranol in toluene after resin application at different concentrations. a: resin dilution 1:100, b: resin dilution 1:1000, c: resin dilution 1:100 at higher resolution, d: resin dilution of 1:10000. for a, b and d the white box corresponds to 1 mm, for c to 100 µm

2.4.3 Sample preparation: solvent free technique

Since polyethylene oligomers were seen in almost every recorded spectrum a solvent-free matrix preparation technique according to Hanton et al. in 2005[47] was tested to avoid any leachable impurities due to the solvents used. It is schematically shown in Figure 22.

20 mg or 40 mg of matrix were weighed into a 4 mL injection glass vial, 1 mg of analyte and 1 mg of cationizer were added. Next, 3 copper coated metal beads were added, the vial closed and vortexed for 30 s in a way that the beads were moving around in the whole vial and not only at the bottom. Subsequently, the mixture sticking to the side of the vial was pushed down using a spatula and the mixture was vortexed another 30 s. A small amount of the homogenized mixture was applied to the target plate and flattened utilizing a spatula. For the resin samples no cationizer was added since they already consist of polycations.

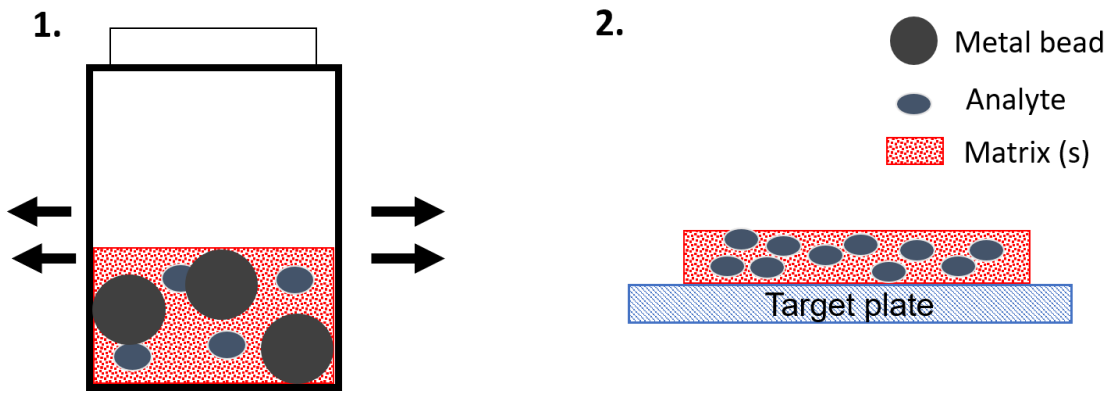

Figure 22: Schematic demonstration of the solvent-free MALDI matrix preparation. 1: Matrix, analyte and metal beads are mixed in a glass vial and vortexed. 2: The mixture (excluding the beads) is applied to a target plate and flattened with a spatula for measurement.

2.4.4 Mass spectrometric instrument parameters

Measurements were done on an Axima TOF^{2}™ from Shimadzu in positive reflectron mode for masses up to 2500 Da and in positive linear mode for higher masses. Laser power was varied between 70 and 170 arbitrary units (maximum 180 arbitrary units, au). The laser repeat rate was set at 20 Hz and pulsed extraction optimized for the expected molecular mass range. Mass spectra were always recorded once in raster mode and once by looking at so-called "sweet-spots". The shown mass spectra in the results section are a sum of about 600 single mass spectra (depending on the covered m/z range).

2.5 LDI MS experiments

2.5.1 Sample preparation

A suspension of soluble polystyrene standard of 50 kDa was prepared by weighing in 1 mg of polymer and adding 1 mL of deionized water. The mixture was vortexed and put in an ultrasonic bath for 30 min.

The polystyrene particles standard of 40 nm as well as the resin A400_h, which were used as representative samples of their group, were already suspended in aqueous solution. The particle

standard was diluted 1:10 (v/v) and pipetted onto the silicon wafer directly. The resin sample was diluted 1:100 previously.

To avoid cross-contamination the sample solutions were pipetted on 1 × 1 cm silicon wafer chips using a Hamilton syringe. About 1-2 µL of the sample solution were pipetted and dried at room temperature. The wafer chip was then glued to an aluminum target using double sided carbon tape. To ensure conductibility a piece of tape was also stuck to the sides of the silicon wafer to connect the top with the aluminum target as shown in Figure 23.

As blank, a clean silicon waver chip was measured and as solvent blank, pure deionized water was pipetted onto a silicon waver chip and left to dry at room temperature.

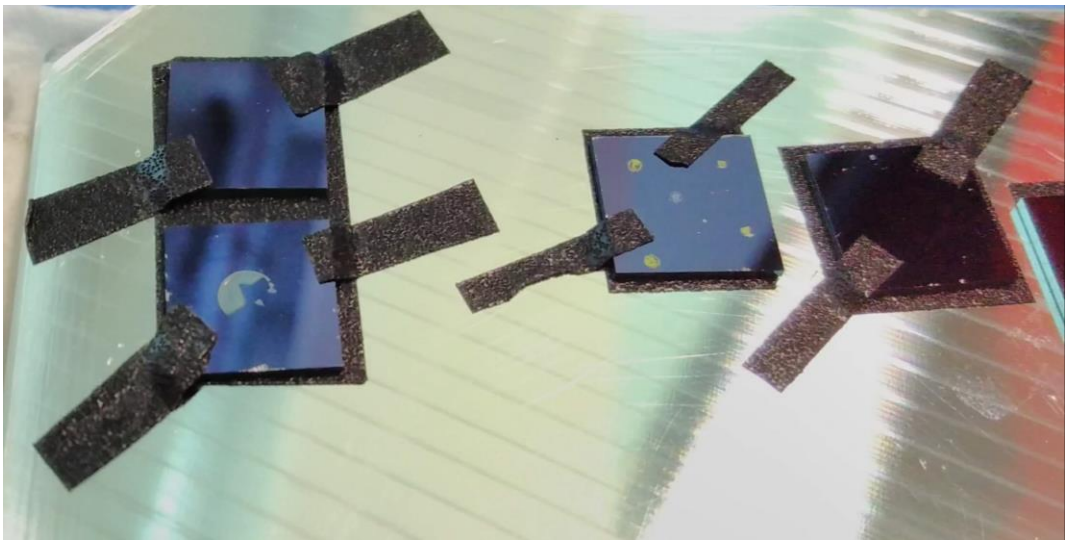

FIGURE 23: SILICON WAFER CHIPS TAPED TO AN ALUMINUM TARGET PLATE USING CARBON TAPE. TO ENSURE CONDUCTIBILITY, TAPE WAS ALSO APPLIED FROM THE WAFER TOP TO THE TARGET PLATE SURFACE

2.5.2 MASS SPECTROMETRIC INSTRUMENT PARAMETERS

Measurements were done on an Axima TOF^{2}™ from Shimadzu in positive reflectron mode. Laser power was varied between 70 and 170 au. The laser repeat rate was set at 20 Hz and pulsed extraction optimized for the expected molecular mass range. Mass spectra were recorded in raster mode were no microscopic difference between different areas was apparent. All samples were measured by looking at so-called “sweet-spots” as well. For unevenly distributed samples (especially for lower concentrations and for the soluble polystyrene) no raster mass spectra were recorded. The shown mass spectra in the results section are a sum of 600 single spectra.

2.6 SIMS EXPERIMENTS

2.6.1 SAMPLE PREPARATION

Sample preparation was carried out as described for LDI MS in section 2.5.1. Two resin samples, resin A400_h and resin A400_el were prepared in this case and the silicon-wafer chip was not fixed by using a carbon tape but by placing it into a sample holder and introduced into the SIMS instrument.

As blank the parts of the silicon waver not containing sample were targeted with the ion beam. When filtering for the total amount of Si in the spectra, the sample boundaries are clearly visible as shown in Figure 24.

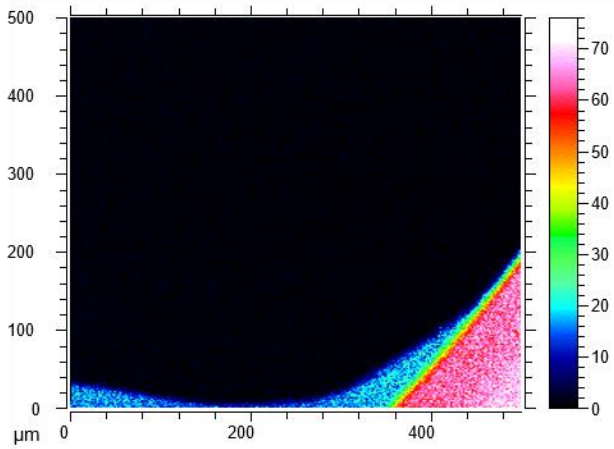

FIGURE 24: RESIN A400_H SAMPLE USING A FILTER FOR THE SI^+ ION. THE COLOR-SCALE TO THE RIGHT SHOWS THE RELATIVE INTENSITY OF THE SI^+ ION SIGNAL. THE BLACK PART IN THE MIDDLE CORRESPONDS TO THE RESIN SAMPLE WHERE THERE IS NO SI^+ DETECTED. AT THE BORDER OF THE RESIN SAMPLE ITS INTENSITY INCREASES AND IN THE CORNER OF THE IMAGE WHERE THERE IS ONLY PURE SILICON LEFT THE IMAGE SHOWS A RED-TO-WHITE COLOR

2.6.2 MASS SPECTROMETRIC INSTRUMENT PARAMETERS

Measurements were done on a TOF.SIMS^5 instrument by IONTOF. Bi_3^+ ions were used as primary ion beam and accelerated with 25 keV toward the sample. A 500 µm × 500 µm field was hit yielding 256 x 256 pixel. The secondary ions were measured at 2kV in a TOF analyzer in reflectron mode in a m/z range of 50 to 365. 80 scans were summed up to receive the shown distributions.

2.7 PYROLYSE GC - MS EXPERIMENTS

2.7.1 SAMPLE PREPARATION

Resin particle suspensions (containing about 10 % resin weight content; compare section 2.1) were used directly without dilution. Prior to introducing them to the sample cup, the cup was heated in a Bunsen burner to remove any remaining organic impurities. Next, 100 µL of sample solution were added and left to dry at room temperature. The metal cup was placed into the auto-sampler of the instrument and heated up.

2.7.2 GC-MS INSTRUMENT PARAMETERS

For analysis the GC-MS unit was equipped with a capillary column of 30 m length x 0.25 mm internal diameter x 0.25 µm film thickness containing bonded and highly cross-linked 5% diphenyl / 95% dimethyl siloxane. The capillary column was connected with a deactivated silica pre-column of 5 m length x 0.32 mm internal diameter.

The pyrolysis temperature was set at 600 °C. The pyrolysis interface and the injector temperature were set at 280 °C and 250 °C, respectively. The sample material was added in a sample cup. For GC analysis the column conditions were adjusted as follows: Initial temperature 40 °C, held for 5 min followed by a temperature increase of 6 °C/min to 280 °C for 40 min and the temperature was held for another 3 min. The helium gas flow was set at 1 mL/min and the electronic pressure control was set to a constant flow of 7.6 mL/min, in split mode at 1:50 ratio. The mass spectra were recorded using EI ionization in positive ion mode at 70 eV and the temperature of the MS interface and the ion source were set to 280 °C and 200 °C, respectively. The mass spectrometer was scanned from m/z 50 to 750. The event time was 0.5 sec and the scan speed 1666.

2.8 SEM EXPERIMENTS

2.8.1 RESINS PREPARATION IN WATER AND THF

The stock solution of resin particles was diluted 1:100, 1:1000 and 1:10000 (v/v) using MQ water. Furthermore, 100 µL of resin solution were pipetted into an Eppendorf tube and the solvent was evaporated in a vacuum centrifuge. 1 mL of THF was added to the dried resin and the solution was vortexed for 30 s. Then it was put in an ultrasonic bath for about 30 min. The solution was next diluted 1:10, 1:100 and 1:1000 (v/v) to achieve the same resin weight content as in the aqueous samples.

10 µL of each solution was pipetted on a silicon wafer and the solvent evaporated at room temperature overnight. The next day the samples were measured by SEM.

2.8.2 SEM INSTRUMENT PARAMETERS

Measurements were done on a FEI Quanta 200 FEG instrument utilizing an acceleration voltage of 10 kV and a magnification of 30 000.

2.9 LASER DIFFRACTION EXPERIMENTS

2.9.1 SAMPLE PREPARATION OF PURE SAMPLES AND POLYSTYRENE BEAD MIXES

All resin samples and all polystyrene particle standard solutions were used undiluted (containing about 10 % resin weight content; compare section 2.1). The according sample was added dropwise to the dispersion unit of the LD instrument until a laser extinction of about 10 % was achieved. After this, the measurement was started.

Three different polystyrene particle standard mixes were prepared by mixing the appropriate amount of standard solutions. The used standards and their concentrations in the three prepared mixtures are shown in Table 8. The mixtures were added dropwise to the dispersion unit of the LD instrument until a laser extinction of about 10 % was achieved. After this, the measurement was started.

TABLE 8: PREPARED PARTICLE STANDARD MIXES FOR LD MEASUREMENTS

Particle mix name	*Added particle standard sizes*	*Comment*
PS mix number conc.	40 nm, 60 nm, 80 nm and 100 nm	All standards added at same particle concentration (40 nm:60 nm:80 nm:100 nm = 1:3.4:8:15.6)
PS mix 1:1	40 nm, 60 nm, 80 nm and 100 nm	All standards added at same mass concentration
PS mix various	40 nm, 60 nm, 80 nm and 100 nm	All standards added at same mass concentration except for the 40 nm standard which was added at half the mass concentration of the others

2.9.2 INSTRUMENT PARAMETERS

For analysis an instrument template SOP for polystyrene latex particles was adapted. The analysis chamber was cleaned twice before sample introduction. Water was used as dispersant with a dispersant RI of 1.330. The analysis model was chosen as "Universal" and the particle RI as 1.590. A size range of 0.020 to 2000 µm was recorded. Five single extinction measurements were carried out for 12000 ms with a 10 s break between measurements and averaged.

2.10 GEMMA EXPERIMENTS

2.10.1 BUFFER PREPARATION

0.77 g Ammonium acetate was dissolved in 50 mL of MQ water. Acetic acid or NH_4OH was added dropwise and the pH of the solution measured until the required pH was achieved. In this way buffer solutions of pH 4, pH 7 and pH 9 of 200 mM ammonium acetate were prepared. The buffer solutions were subsequently filtered using a 0.2 µm syringe filter to remove contaminations which could clog the capillary.

2.10.2 CAPILLARY PREPARATION

A capillary piece of about 20 cm length was cut off the capillary bundle and the tip was prepared using a home-made tip grinding apparatus shown in Figure 25. The quality of the tip was checked under a microscope. Fused silica capillaries with an inner diameter of 25 µm and 40 µm were used.

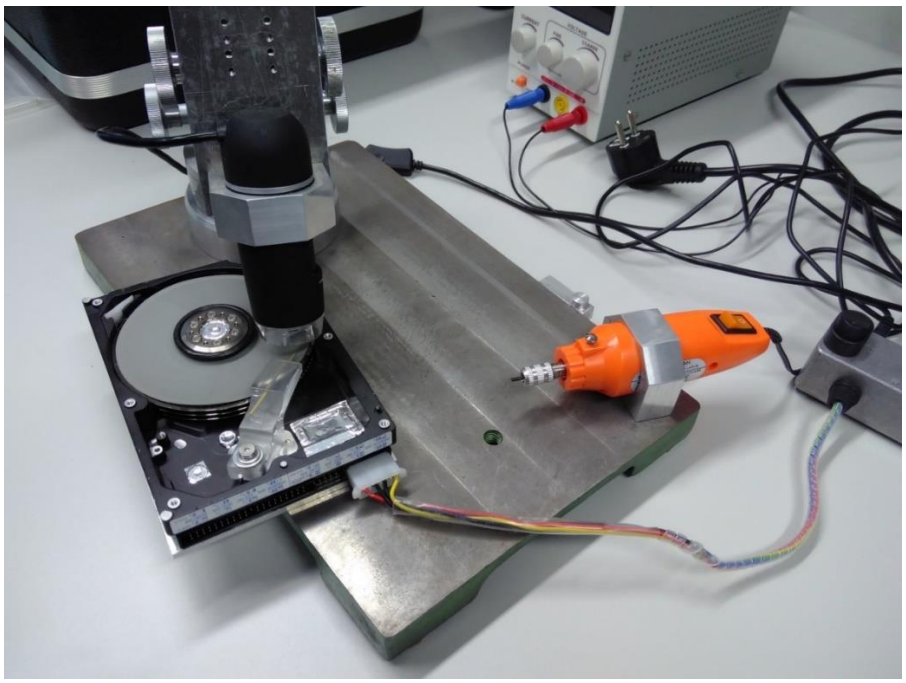

FIGURE 25: HOME-MADE CAPILLARY TIP WHETTING APPARATUS ACCORDING TO[44]

2.10.3 CAPILLARY COATING

The capillary was coated according to an adapted procedure from Pei et al. in 2014[48].

All flushing steps were done using a syringe with an adapter to fit the capillary tightly shown in Figure 26. After preparation of the capillary tip according to section 2.10.2 the capillary was flushed with a 1:1 mixture of MQ water and isopropanol for about 30 s until a big liquid droplet was forming at the tip. Next it was flushed with air, refilling the syringe three times with air in between. Thereafter, the capillary was flushed with a 0.1 M NaOH solution for surface activation and left to react for 10 min. This step was repeated 3 times. Afterwards the capillary was flushed with MQ water and with air. Subsequently, the capillary was flushed with a 10 % polybrene solution and left to react for 10 min for three times as well. The same procedure was thereafter performed using a 1 % hyaluronic acid solution and a 10 % polybrene solution again. Finally, the capillary was flushed with MQ water thoroughly and dried by flushing it repeatedly with air.

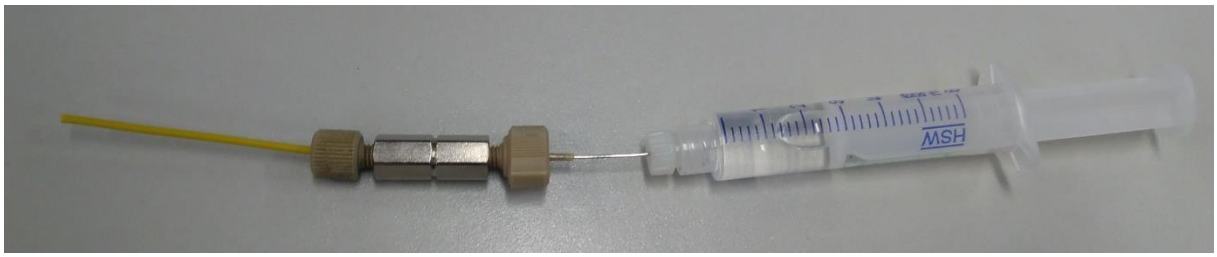

FIGURE 26: SYRINGE ADAPTER TO FIT CAPILLARY TIGHTLY

2.10.4 SAMPLE PREPARATION

Different sample concentrations were tested and therefore, samples were prepared by mixing analyte solutions, buffer and MQ water in a way to receive the desired concentration of analyte in a 50 mM ammonium buffer solution. The exact concentration is given in the results section. For early experiments (measurement of polystyrene particle standards) 0.001 % Tween-20 was

added to avoid capillary clogging. Since this approach only increased the background signal but did not yield better results it was abandoned for further resin measurements.

2.10.5 Filtration experiments

For filtration using a 0.2 µm syringe filter the resin samples were prepared at the appropriate concentration in water and then filled in a syringe and pressed through the syringe filter. Afterwards, the buffer was added.

For filtration using a 300 kDa Nanosep® centrifugal device the resin sample solution was prepared at the according concentration and buffer of pH 4 was added. About 500 µg of the solution were pipetted onto the Eppendorf filter and centrifuged for 2 min at 1000 g. The retendate was transferred into an Eppendorf tube and buffer was added until the original weight of 500 µg was achieved. For the cell extract samples buffer of pH 7 was used to avoid precipitation of dissolved proteins and similar sample components. The cell extract was diluted 1:10 and 0.01 % of resin A400_h was added to one portion of the cell extract. Both solutions were pipetted onto a 300 kDa Nanosep® centrifugal device and centrifuged in a refrigerated centrifuge at 10 000 g for 15 min. The remaining retentate was then transferred to an Eppendorf tube and mixed with 50 mM buffer solution to receive 500 µL of sample solution which was subsequently measured.

2.10.6 Instrument parameters and sample measurement

For analysis a capillary of 25 µm or 40 µm inner diameter and a length of 20-25 cm was inserted into the aerosol generator. A CO_2 flow of 0.1 L/min and an air flow of 1.0 L/min was used. An overpressure of 4.0 psid (approx. 28 kPa) was applied to the sample chamber to press the sample solution through the capillary. A voltage of 1.4 – 1.6 kV was applied between the capillary tip and the orifice until a stable spray was achieved. This led to a current between -200 and -400 nA. The sheath flow rate in the electrostatic classifier was set to 15 L/min (if not stated otherwise in the results section). N-butanol was used as working fluid for the CPC.

A newly inserted capillary was first flushed for about two hours with buffer solution to remove small impurities and reduce the background signal. At least four background measurements were recorded, and the median of the measured particle counts was determined to receive the final distributions shown in the results section. For the sample measurements the capillary was flushed with sample solutions until the recorded distribution was stable (which was the case after about half an hour to two hours sample infusion depending on the sample type). Afterwards, five to ten measurements were recorded, and the median of the measured particle counts was determined to receive the final distributions shown in the results section. For measurement of the polystyrene particle size standards the measurements were started after 10 min of flushing since too long flushing times led to a clogging of the capillary. This in turn led to higher background signals.

3 RESULTS AND DISCUSSION

3.1 PRECEDING EXPERIMENTS

Prior to measuring the analytes some preceding experiments were done to choose the best suited measurement conditions. Firstly, the resin was tested for solubility in different organic solvents according to section 2.3.1. Secondly, the crystallization behavior of different MALDI matrices found in literature was tested for different solvents and at different concentrations. The two most suitable solvents, THF and toluene, and the two most suitable matrices, dithranol and DCTB, were chosen for further experiments.

3.1.1 DISSOLUTION EXPERIMENTS

At a dilution of 1:100 (v/v) of resin A400_h no dissolving effect could be seen in any of the used solvents. At higher dilutions it was not possible to distinguish the particles in solution any longer. Therefore, the samples were investigated with the electron microscope. According results are discussed in section 3.4.1.

No evidence of a dissolution of the particles could be detected in the SEM pictures. This finding corresponds to literature[1] where it is stated that polystyrene resins are not soluble in any conventional solvents. Nonetheless, the polystyrene particle standard of 40 nm and the A400_h resin were chosen as representative samples of their group and analyzed using MALDI MS to exclude any possible characteristic leachable parts.

3.1.2 CRYSTALLIZATION BEHAVIOR OF DIFFERENT MALDI MS MATRICES IN DIFFERENT SOLVENTS FOR POLYMER ANALYSIS

The quality of a recorded MALDI mass spectrum greatly depends on the crystal structure of the matrix and the embedded analyte as discussed in section 1.3.2. Four different MALDI matrices, which are frequently used in literature for polystyrene characterization[19,50–52], were tested for crystal quality in different solvents and at different concentrations. As solvents THF, toluene, MTBE and THF:MeOH = 3:1 [v:v] were chosen, since they were described to dissolve polystyrene in literature. Figure 27 compares the crystallization properties of sinapinic acid (A), dithranol (B), DHB (C) and DCTB (D) at a concentration of 5 mg/mL in THF. Sinapinic acid and DCTB show the most homogenous crystal structure (at the used concentration and with the used solvent).

Figure 28 compares the crystal behavior of two different matrices, dithranol and DCTB, at 5 mg/mL concentration in THF on different target surfaces. A and C show their behavior on a single use polymer target which is nanocoated with stainless steel. B and D show their behavior on a Ni-coated Aluminum target. For dithranol the difference is small even though the crystals are more evenly distributed on the Ni-coated target. For DCTB the difference is severe. This is probably due to a low surface-wetting on the single use target. The effect is most likely caused due to the stainless steel being transferred onto the polymer target by vapor deposition leading to a very smooth surface. On the other hand, the Ni-coated target was used many times before and therefore, exhibits scratches which can initiate crystallization.

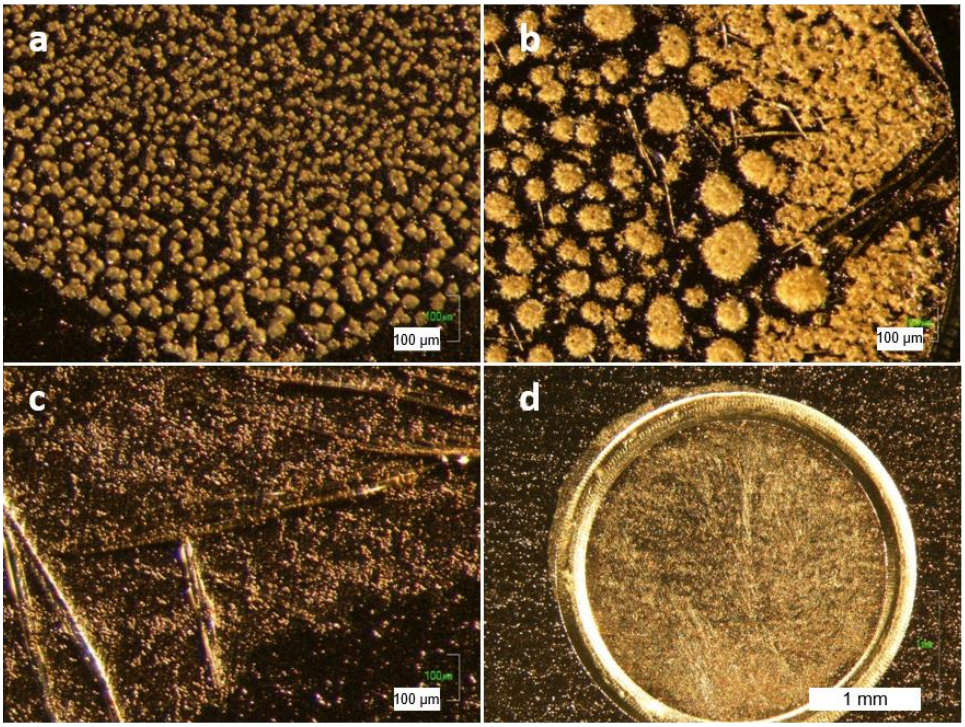

FIGURE 27: COMPARISON OF DIFFERENT CRYSTAL STRUCTURES OF FOUR DIFFERENT MALDI MATRICES AT 5 mg/mL CONCENTRATION IN THF. a SINAPINIC ACID, b: DITHRANOL, c: DHB, d: DCTB. FOR a, b AND c THE WHITE BOX CORRESPONDS TO 100 µm, FOR d TO 1 mm

Figure 29 compares the crystal structure of dithranol dissolved in THF at different concentrations. At higher concentrations the matrix agglomerates during crystallization leading to big, non-uniform crystals. For too small concentrations, on the other hand, the target spot area is no longer entirely covered.

For further experiments dithranol and DCTB were chosen as suitable matrices due to their good crystallization qualities in the solvents THF and toluene. The other solvents were not tested further since their solubility properties were not sufficient and the crystallization properties of the matrices in these solvents were inferior to the chosen ones. For DCTB best crystallization results were obtained at 1 mg/mL and 5 mg/mL and for dithranol at 5 mg/mL and 10 mg/mL. Those two concentrations of both matrices were used for further experiments and the single use target was found to be inappropriate for useful matrix crystallization and not used in the following.

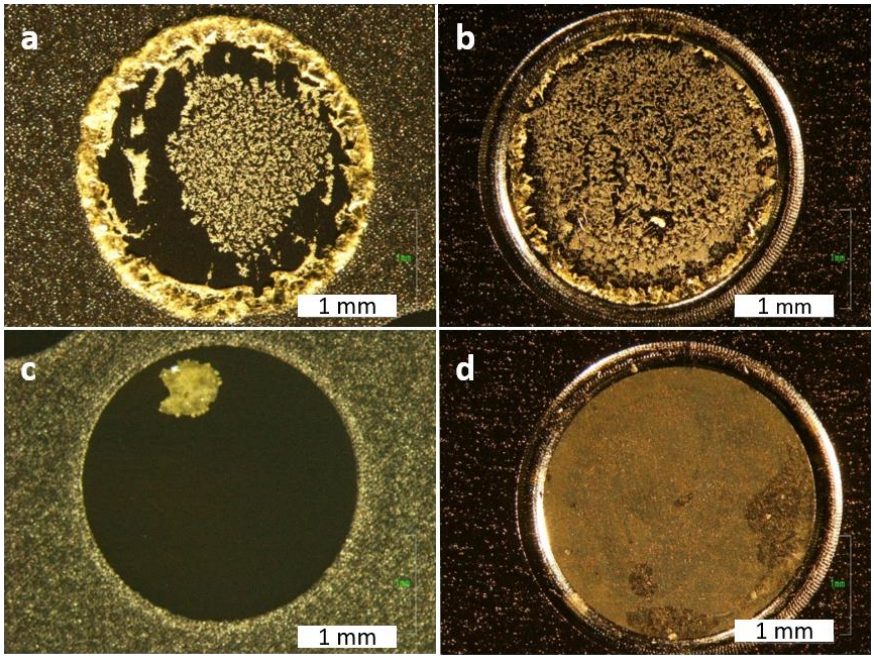

FIGURE 28: COMPARISON OF DIFFERENT CRYSTAL STRUCTURES ON TWO DIFFERENT TARGET PLATE SURFACES FOR TWO DIFFERENT MALDI MATRICES AT 5 mg/mL CONCENTRATION IN THF. a: DITHRANOL ON A SINGLE USE STAINLESS STEEL TARGET, b: DITHRANOL ON A NI-COATED ALUMINUM TARGET, c: DCTB ON A SINGLE USE STAINLESS STEEL TARGET, d: DCTB ON A NI-COATED ALUMINUM TARGET. THE WHITE BOX CORRESPONDS TO 1 mm.

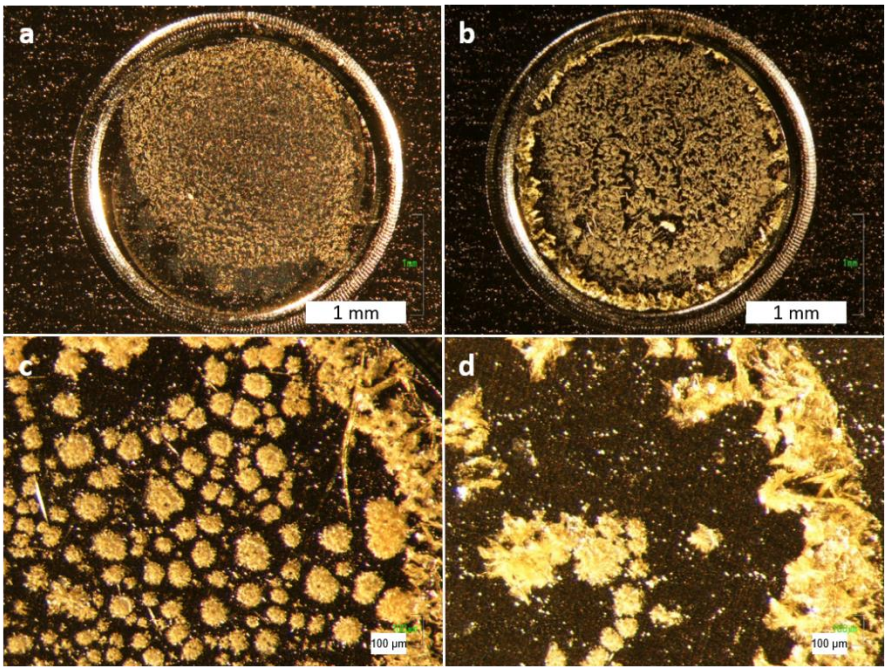

FIGURE 29: COMPARISON OF DIFFERENT CRYSTAL STRUCTURE OF DITHRANOL DISSOLVED IN THF AT DIFFERENT CONCENTRATIONS. a: 1 mg/mL, b: 5 mg/mL, c: 10 mg/mL AND d: 20 mg/mL CONCENTRATION. FOR A AND B WHITE BOX CORRESPONDS TO 1 mm, FOR c AND d TO 100 µm

3.2 MALDI MS EXPERIMENTS

One representative polystyrene particle standard (40 nm diameter) and one representative resin sample, A400_h, were chosen for all experiments to test for their detectability with MALDI MS or the detectability of leachable parts (e.g. small oligomers or fragments). Furthermore, three different soluble polystyrene standards at average molecular weights of 2500 Da, 9000 Da and 30 kDa were used for all experiments to verify the suitability of the used set-up since they are well described in literature.

3.2.1 COMPARISON OF SOLUBLE POLYSTYRENES, POLYSTYRENE BEADS AND RESIN PARTICLES

Soluble polystyrene standards at an average weight of 2500 Da, 9000 Da and 30 kDa as well as the polystyrene particle standard of 40 nm diameter and the resin A400_h particles were first analyzed using the volume technique as sample preparation. Dithranol at 5 mg/mL and 10 mg/mL and DCTB at 1 mg/mL and 5 mg/mL were used as matrices respectively in THF and toluene.

Figure 30 shows a comparison of representative recorded spectra of the polystyrene particle standard and the resin particles at low m/z values. Some signals can be seen at comparatively low intensities. Those can be either attributed to matrix clusters and impurities like keratin or PEGs, which are omnipresent, or might be contaminations from the milling or the synthesis of the resin. Figure 31 shows the according high m/z region. Here the intensities are even lower than in the low m/z region and no difference between the blank and the samples can be seen.

Figure 32 shows the recorded mass spectra of the soluble polystyrenes at different average molecular weight. Table 9 compares the specified average molecular weight with the average molecular weight calculated from the recorded mass spectra.

TABLE 9: COMPARISON OF SPECIFIED AVERAGE MOLECULAR WEIGHT AND DIFFERENT MOLECULAR WEIGHT VALUES CALCULATED FROM MEASURED SPECTRA

Specified weight [Da]	M_N	M_W	M_Z	***Polydispersity index D***
2500	2161	2201	2238	1.018
9000	7414	7438	7462	1.003
30000	32916	32962	33009	1.001

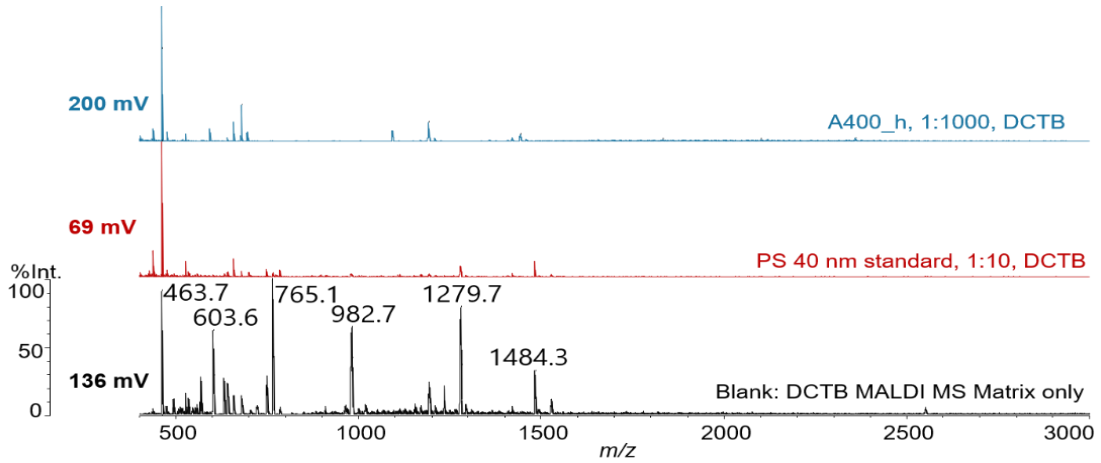

FIGURE 30: COMPARISON OF POLYSTYRENE PARTICLE STANDARD 40 NM (RED) AND A400_H RESIN (BLUE) IN DCTB AT 1 MG/ML IN COMPARISON TO PURE DCTB (BLACK) AT A MASS RANGE OF 500-3000 DA. ALL MASS SPECTRA WERE RECORDED AT A LASER POWER OF 100

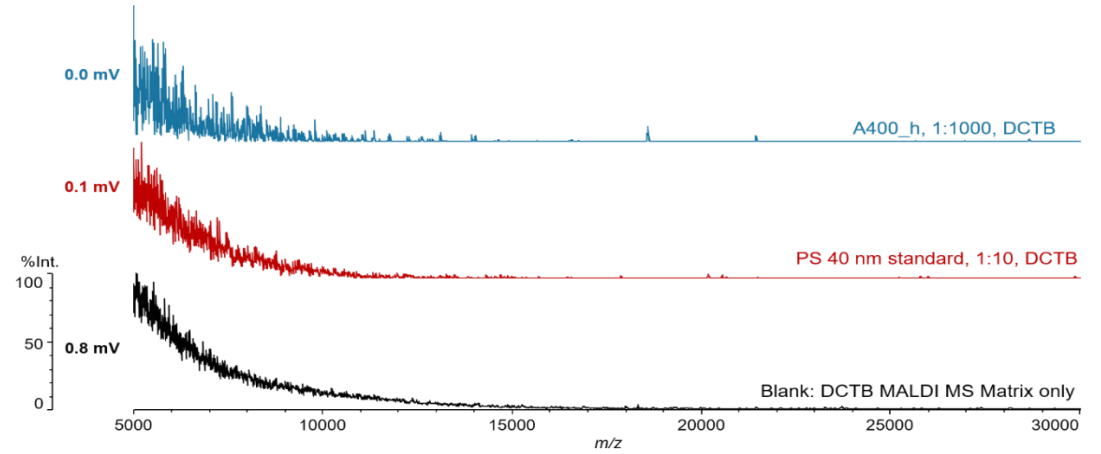

FIGURE 31: COMPARISON OF POLYSTYRENE PARTICLE STANDARD 40 NM (RED) AND A400_H RESIN (BLUE) IN DCTB AT 1 MG/ML IN COMPARISON TO PURE DCTB (BLACK) AT A MASS RANGE OF 5000-30000 DA. ALL MASS SPECTRA WERE RECORDED AT A LASER POWER OF 100

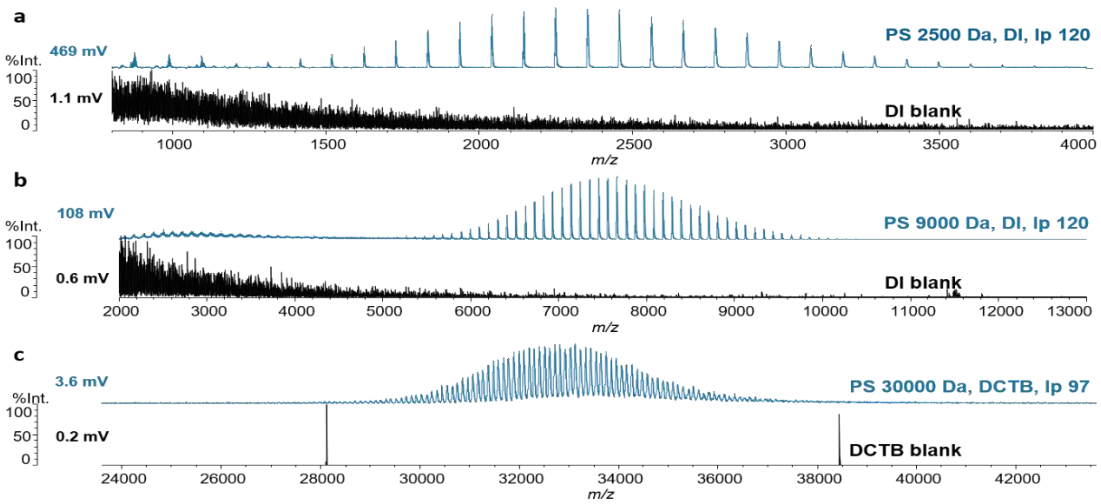

FIGURE 32: COMPARISON OF REPRESENTATIVE MASS SPECTRA OF SOLUBLE POLYSTYRENES WITH DIFFERENT AVERAGE MOLECULAR WEIGHT. A AND B WERE RECORDED USING DITHRANOL AS MATRIX, C WAS RECORDED USING DCTB WHICH LEAD TO A HIGHER ENERGY TRANSFER AND THEREFORE, LESS LASER POWER WAS NEEDED TO ACHIEVE A NICE MASS SPECTRA

M_N, M_W and M_Z were calculated according to equations 3-5:

$$\boldsymbol{M_N = \frac{\sum M_i n_i}{\sum n_i}} \quad \textbf{(3)}$$

$$\boldsymbol{M_W = \frac{\sum M_i^2 n_i}{\sum M_i n_i}} \quad \textbf{(4)}$$

$$\boldsymbol{M_Z = \frac{\sum M_i^3 n_i}{\sum M_i^2 n_i}} \quad \textbf{(5)}$$

$M_N \ldots\ldots Number - average\ molar\ mass\ \left[\frac{g}{mol}\right]$

$M_W \ldots\ldots Weight - average\ molar\ mass\ \left[\frac{g}{mol}\right]$

$M_Z \ldots\ldots z -\ average\ molar\ mass\ \left[\frac{g}{mol}\right]$

$n_i \ldots\ldots molar\ fraction\ of\ species\ i$

$M_i \ldots\ldots molar\ mass\ of\ species\ i\ \left[\frac{g}{mol}\right]$

The soluble polystyrenes could be detected in both dithranol and DCTB at different laser power, matrix concentrations and solvents used. The resin sample and the polystyrene particle size standard could not be detected using this set-up. Only impurities at very low intensities were detected. This led to the assumption of the resin consisting of one single or only a few macromolecules since no leachable small oligomers or fragments could be detected.

3.2.2 Comparison of different sample preparation methods: volume technique, thin layer technique and solvent-free technique

Figure 33 gives an overview of recorded mass spectra of the resin A400_h at different concentrations with dithranol dissolved in both THF and toluene as a matrix at a mass range of 1000 to 5000 Da. A pattern, similar to an oligomer pattern, is visible. (This could not be seen in Figure 30 since the range from 500 to 3000 Da was shown there and the much higher intensity of low mass impurities covers this low-intensity distribution.) Due to its much lower intensity this distribution only becomes visible when zooming in on the 1000 to 3000 Da range. At first this pattern seems like the pattern that would be expected when looking at the resin. Unfortunately, it could also be seen in the dithranol blank (treated exactly the same as the sample except for not adding the analyte). Also, there seems to be no concentration correlation. When comparing the different concentrations of resins in Figure 33 it is seen that the intensity does not vary much even when concentration differences of three orders of magnitude are looked at.

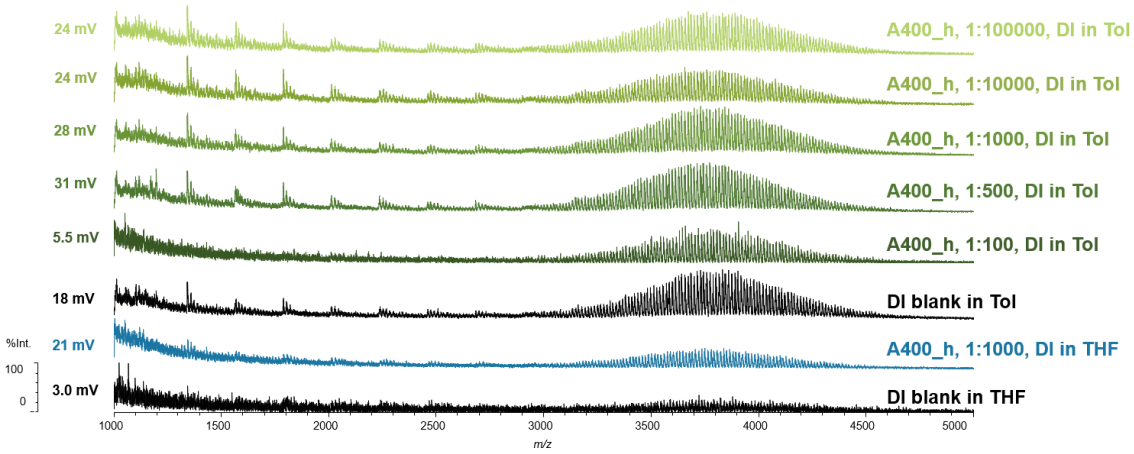

FIGURE 33: COMPARISON OF MASS SPECTRA OF A400_h RESIN AT DIFFERENT CONCENTRATIONS IN DITHRANOL. THE GREEN MASS SPECTRA SHOW DIFFERENT CONCENTRATIONS OF THE RESIN IN DITHRANOL DISSOLVED IN TOLUENE. THE BLUE MASS SPECTRA SHOWS THE RESIN SPECTRA IN DITHRANOL IN THF. THE BLACK MASS SPECTRA SHOW THE ACCORDING BLANK MASS SPECTRA.

When looking more closely at the distribution seen between 3500 and 4000 Da (compare Figure 34) it can be seen that the distance between two oligomer peaks is equal to about 14 Da which suggests a polyethylene-based polymer. A typical oligomer distance for a polystyrene-based polymer would be 104 Da. Polyethylene-based polymers are found in Eppendorf tubes and Eppendorf tips which is a plausible source for the impurity.

This led to the conclusion that polymers were “extracted” from containers, tubes and tips by the organic solvents toluene and THF. Henceforth, only glass vials were used for sample preparation and only Hamilton glass syringes for liquid dosage. Furthermore, two additional sample preparation techniques which use less to no organic solvents were tested.

Firstly, the thin layer technique which can be used if the sample is not soluble in organic solvents and simultaneously leads to a homogenous distribution of sample on the matrix.

Secondly, to avoid leaching completely and to make sure not to overlook any resin distributions underneath the polyethylene distribution a solvent free sample preparation method was tested as well.

Figure 35 compares the mass spectra of the soluble polystyrene of 2500 Da using different sample preparation techniques. Interestingly, the solvent free sample preparation lead to a shift of the distribution maximum to higher molecular masses. Another effect is the reduced resolution achieved with the solvent free sample preparation technique as shown in Figure 36. It can be seen that for the volume preparation technique single monoisotopic peaks are visible within an oligomer peak. On the other hand, for the solvent free preparation only the envelope of the distribution is visible. M_N, M_W and M_Z of all three preparation techniques shown in Figure 35 were calculated according to equations 3-5 and are compared in Table 11. The loss in resolution can be explained when considering that the sample was transferred to the target plate using a spatula and the crystals were crushed with the spatula tip. This led to an uneven surface thicker than the one obtained with the standard volume preparation technique. Therefore, the height of the sample was different at different sample positions which led to a broadening of the recorded peaks.

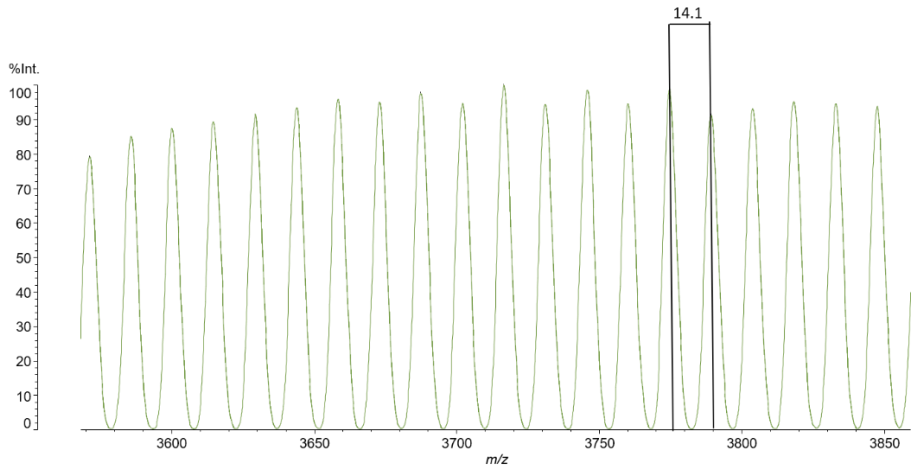

FIGURE 34: ZOOM IN ON THE MASS SPECTRUM OF A400_h IN DITHRANOL. A MASS DIFFERENCE OF 14.1 DA IS SEEN BETWEEN TWO MONOMER PEAKS WHICH SUGGESTS A POLYETHYLENE POLYMER DISTRIBUTION

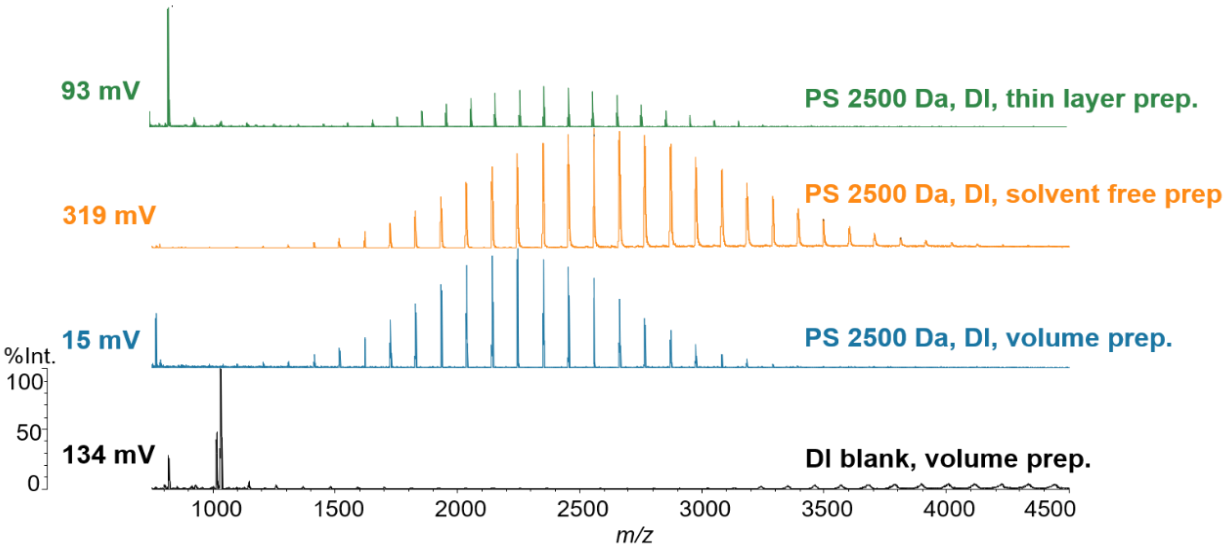

FIGURE 35: COMPARISON OF THE MASS SPECTRA OF THE 2500 DA POLYSTYRENE STANDARD USING DIFFERENT SAMPLE PREPARATION TECHNIQUES

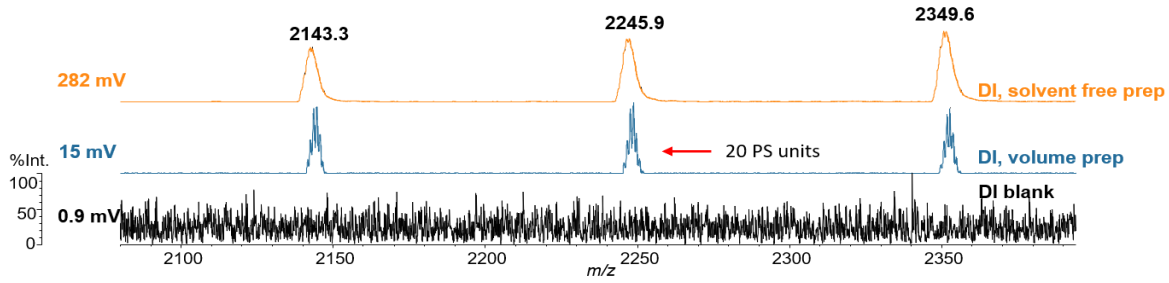

FIGURE 36: COMPARISON OF THE SPECTRA'S RESOLUTION OF THE 2500 DA POLYSTYRENE STANDARD USING DIFFERENT SAMPLE PREPARATION TECHNIQUES

TABLE 10: COMPARISON OF SPECIFIED AVERAGE MOLECULAR WEIGHT AND DIFFERENT MOLECULAR WEIGHT VALUES CALCULATED FROM MEASURED SPECTRA

Preparation technique	M_N	M_W	M_Z	*Polydispersity index D*
Volume prep.	2161	2201	2238	1.018
Thin layer prep.	2328	2401	2472	1.031
Solvent free prep.	2622	2720	2813	1.037

No characteristic peaks could be detected for both the A400_h resin and the polystyrene particle size standard of 40 nm with any of the tried sample preparation techniques. It was seen in the mass spectra for the soluble polystyrenes that the resolution was best for the volume technique and different sample preparation methods led to different spectra intensities and slight mass shifts.

3.2.3 COMPARISON OF DIFFERENT LASER POWER AND DIFFERENT MALDI MS MATRICES

The effect of different laser power and different MALDI matrices on the oligomer distribution and the resolution were tested for the soluble polystyrene standards. It is exemplarily demonstrated for the 2500 Da polymer in Figure 37-39. Furthermore, those two effects were also tested on the polystyrene particle standard and the resin A400_h. Both did not show any difference compared to Figure 30.

Figure 37 shows the spectra of the 2500 Da polystyrene at laser power 90-120 in dithranol and at laser power 80 in DCTB. It can be seen that the signal intensity greatly increases with increasing laser power used and also oligomer peaks at the distribution's border become visible. This also means an increase in sensitivity. Even though the lowest laser power of 80 is used for DCTB, the signal intensity is comparable to a much higher laser power used for dithranol. This is due to the fact, that DCTB has a much higher energy-transfer than dithranol. It is seen that DCTB also leads to a shift of the distribution maximum to higher masses. Since larger oligomers require more energy for desorption and ionization this finding is conclusive with the suggestion of DCTB transferring more energy to the analyte molecules.

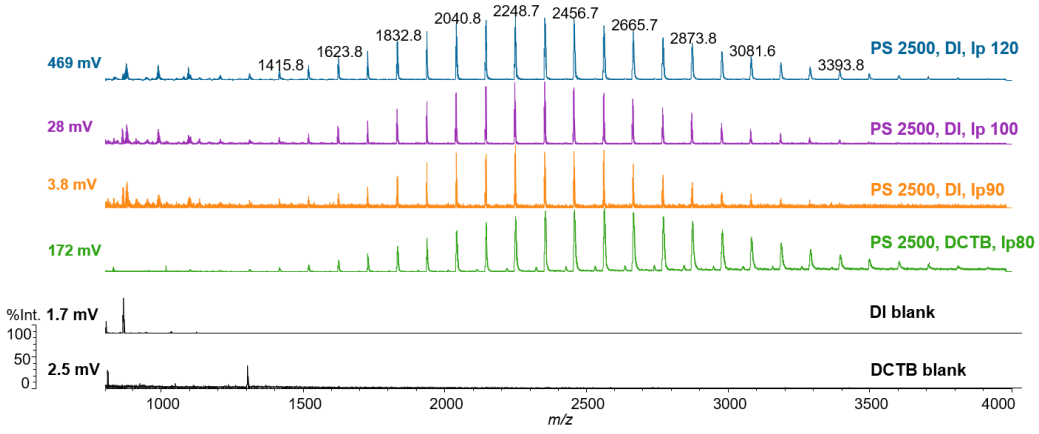

FIGURE 37: SPECTRA OF THE 2500 DA POLYSTYRENE RECORDED AT DIFFERENT LASER POWER

Table 11 compares the measured mean mass of the 2500 Da polystyrene (shown in Figure 37) and the calculated (theoretical) mass. One polystyrene oligomer was assumed to consist of x polystyrene units (of mass 104.15 Da), one Ag atom (of mass 105 Da) and one tert-butyl end group (of mass 58.12 Da). The measured mass deviated less than 0.1 % for all oligomer peaks labeled in Figure 37.

TABLE 11: MASS DIFFERENCE BETWEEN MEASURED AND CALCULATED (THEORETICAL) MASS

Measured (mean) mass [Da]:	*Number of polystyrene units*	*Calculated mass [Da]*	*Relative deviation [%]:*
1415.8	12	1414.9	0.062
1623.8	14	1623.2	0.036
1832.8	16	1831.5	0.070
2040.8	18	2039.8	0.048
2248.7	20	2248.1	0.026
2456.7	22	2456.4	0.011
2665.7	24	2664.8	0.037
2873.8	26	2873.0	0.027
3081.6	28	3081.3	0.009
3393.8	31	3393.8	0.001

Figure 38 shows the influence of laser power on the fine structure. For higher laser power the fine structure gets less visible. This is due to the higher initial energy spread within the produced ions which leads to a reduction of resolution. On the other hand, the sensitivity increases which leads to a tradeoff depending on the needed sensitivity versus resolution.

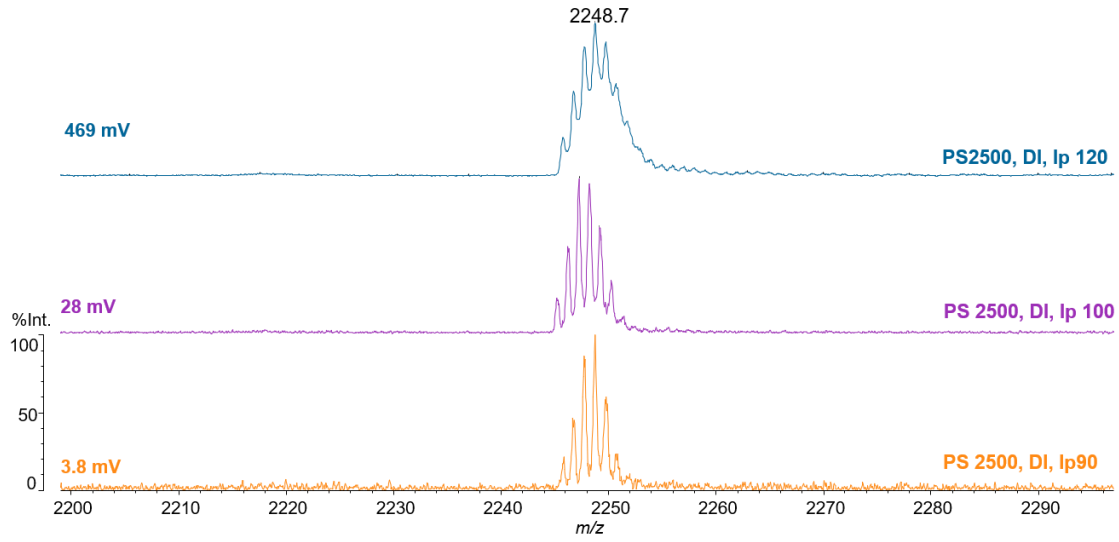

FIGURE 38: COMPARISON OF THE RESOLUTION OF ONE OLIGOMER PEAK OF THE 2500 DA DISTRIBUTION AT DIFFERENT LASER POWER FOR DITHRANOL AS MATRIX

Figure 39 compares one oligomer peak measured in two different matrices. It can be seen that for DCTB a lower laser power leads to a much higher intensity. On the other hand, the fine structure is not visible anymore. Dithranol leads to lower signal intensities but the fine structure can be seen nicely. Likewise, in this case the choice of matrix depends on whether greater sensitivity or resolution is wanted.

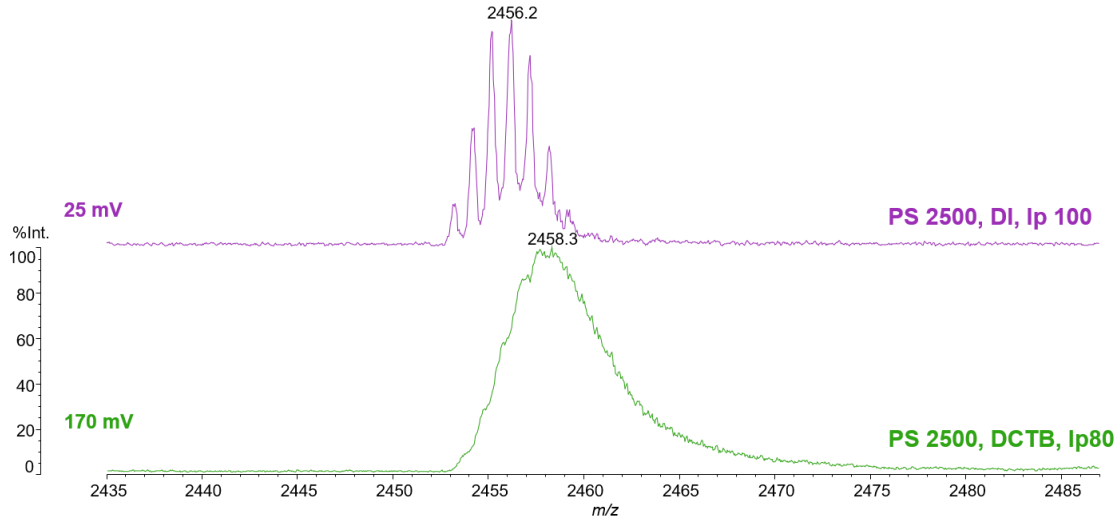

FIGURE 39: COMPARISON OF THE RESOLUTION OF ONE OLIGOMER PEAK OF THE 2500 DA DISTRIBUTION WITH DITHRANOL AND DCTB AS MATRIX

To conclude it can be said that MALDI MS spectra could be taken of different soluble polystyrene standards using different MALDI matrices, different solvents and different sample preparation techniques. It was not possible to record mass spectra for the polystyrene particle standard of 40 nm and the A400_h resin, even though many different set-ups were tested. This led to the conclusion that both particles are insoluble in the tested solvents and do not contain smaller leachable oligomers or fragments. Therefore, it was decided to test desorption/ionization methods with higher energy transfer rates to achieve (characteristic) fragmentation.

3.3 LDI MS EXPERIMENTS

Due to the laser beam's direct interaction with the sample without previous energy spread due to a MALDI matrix, a much higher energy transfer rate is to be expected in LDI experiments related to a thermal heating process. Furthermore, the same instrument used for MALDI MS can be used for LDI experiments. Therefore, in a next step the resin sample A400_h (as representative of its group) was analyzed using LDI MS. A 50 kDa soluble polystyrene standard and the 40 nm polystyrene size standard were analyzed as reference accordingly.

3.3.1 COMPARISON OF SOLUBLE POLYSTYRENES, POLYSTYRENE BEADS AND RESIN PARTICLES

Figure 40 shows a comparison of the mass spectra of the soluble polystyrene of 50 kDa, the polystyrene size standard of 40 nm and the resin A400_h as well as a spectrum of a blank Si target. For the soluble polystyrene, only peaks related to the added silver cation (107, 109 Ag^+ and 214, 216, 218 $2Ag^+$) are visible. The spectrum of the polystyrene size standard does not significantly differ compared to the Si target blank and the recorded intensities are really low. Only for the resin sample there are fragments of a high intensity visible (e.g. m/z = 58, 105, 117 and 131) which significantly differ from the ions found in the blank sample.

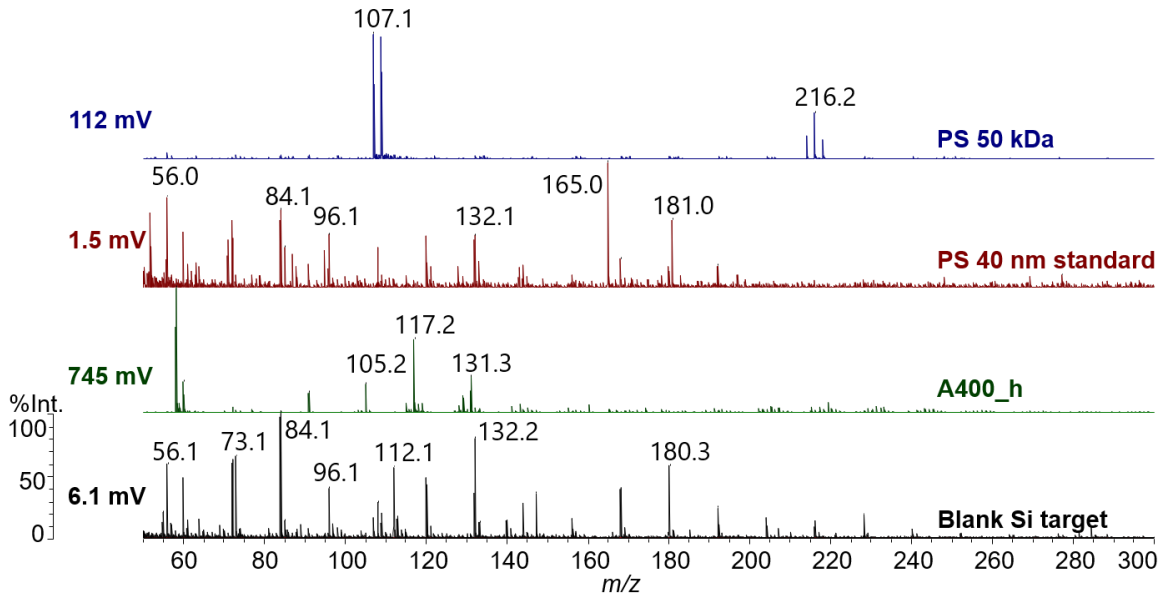

FIGURE 40: COMPARISON OF THE RECORDED MASS SPECTRA OF THE SOLUBLE POLYSTYRENE, THE POLYSTYRENE PARTICLE STANDARD AND THE RESIN A400_h

Figure 41 and 42 show the resin sample in a region of 40 to 200 Da as compared to a blank Si target. The main fragment ions can be attributed to fragments related to a polystyrene-based structure. The fragment at 58.0 Da can be attributed to a *tert*-methyl amine which is the fixed charge group used in the A400_h resin. Therefore, it can be concluded that the found fragments can be attributed to the investigated resin.

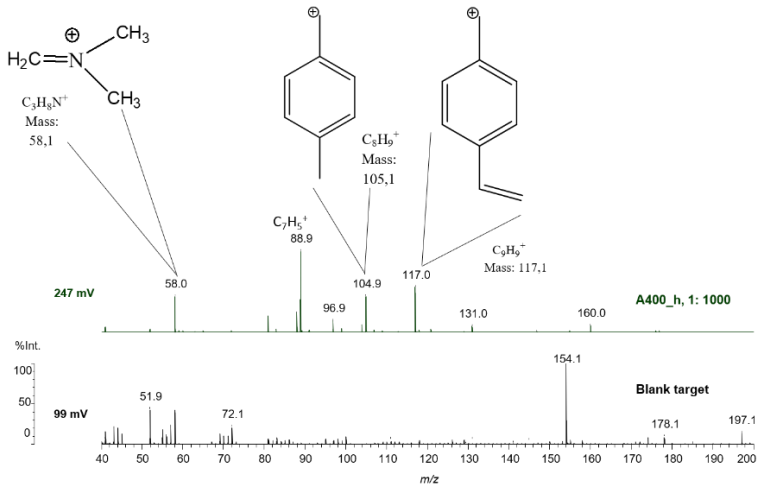

FIGURE 41: MASS SPECTRA OF THE RESIN SAMPLE A400_h AND SUGGESTED FRAGMENT STRUCTURE FOR LOWER-MASS FRAGMENTS

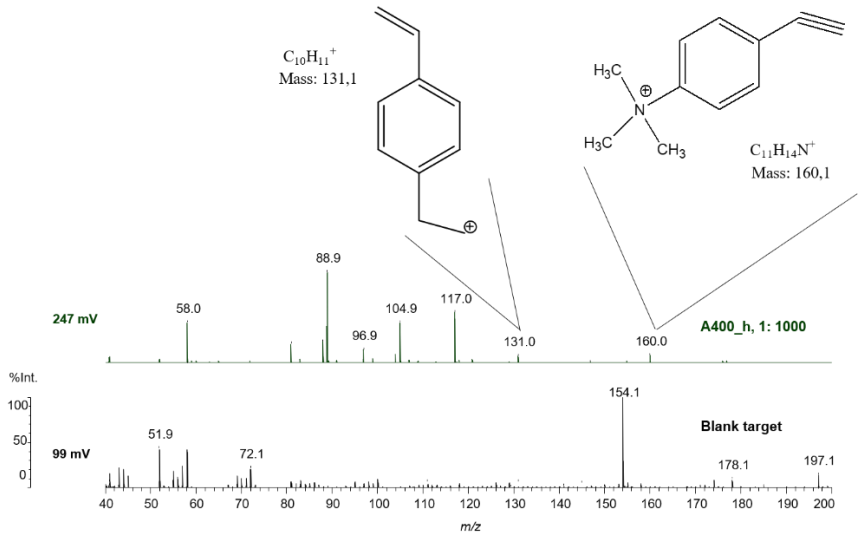

FIGURE 42: MASS SPECTRA OF THE RESIN SAMPLE A400_h AND SUGGESTED FRAGMENT STRUCTURE FOR HIGHER-MASS FRAGMENTS

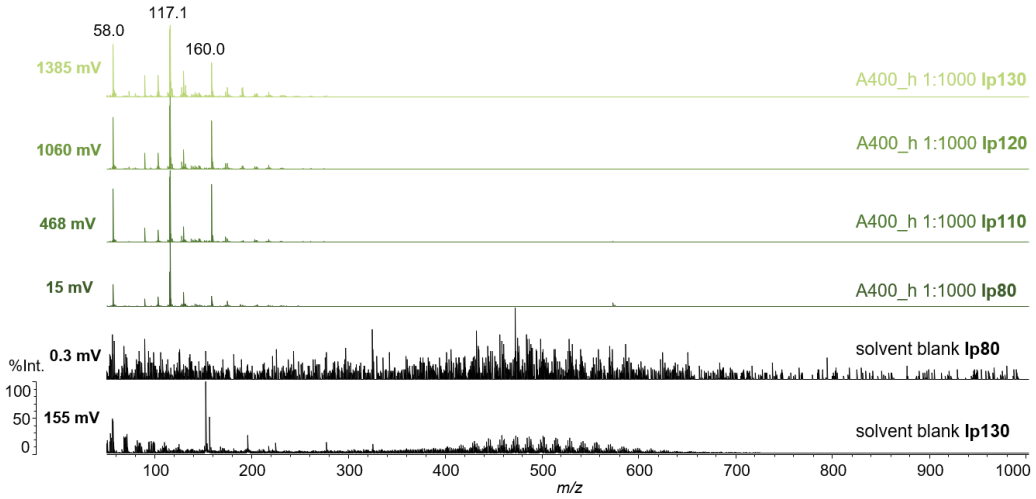

FIGURE 43: RESIN FRAGMENT SPECTRA AT DIFFERENT LASER POWER

The influence of the laser power on the fragmentation pattern and the intensity was tested and is shown in Figure 43. Even though the signal intensity is greatly increasing for higher laser power, the fragmentation patter does not alter significantly. Therefore, the sensitivity of the measurement can be increased by higher laser power without information loss.

To conclude it was possible to record a characteristic fragmentation pattern of the A400_h resin which showed a dependence on the used laser power utilizing LDI MS. A fragmentation pattern for the soluble polystyrene and the polystyrene particle standard was not detected.

3.3.2 Measurement of spiked cell extracts at different concentrations

In a next step the applicability of the used set-up for resin detection in a cell extract sample was tested. Figure 44 shows the recorded mass spectra of spiked cell extracts at different spike ratios as compared to a pure cell extract spectrum and a pure resin spectrum. Since the resin fragments are not detectable in the spiked samples even at spike ratios of 10:1 [v:v] (resin:cell extract, CE) it can be concluded that the cellular components lead to a suppression of the transferred laser energy which in turn prevents fragmentation. However, to verify this statement further experiments are necessary.

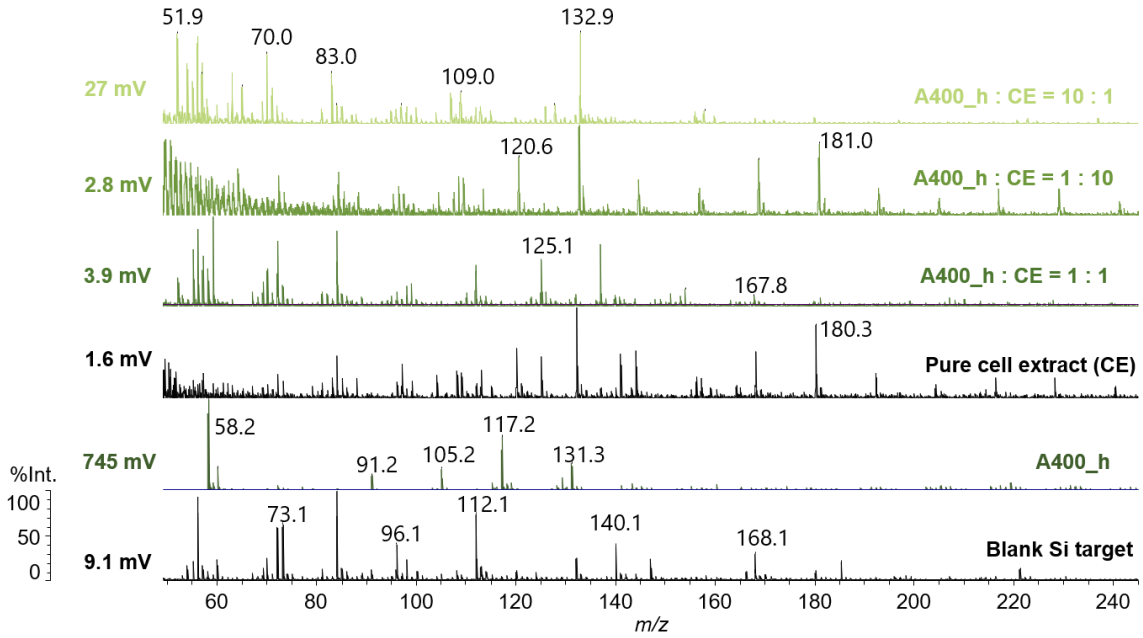

Figure 44: Spectra of cell extracts spiked with A400_h resin at different spike ratios as compared to blank cell extract, pure resin spectra and a Si target blank

Therefore, it was found that characteristic resin fragments could not be detected in a spiked cell extract.

3.4 SIMS experiments

Since it was shown in section 3.3.1 that higher energy transfer to the resin leads to a characteristic fragmentation patter, SIMS was tested for its usability in resin characterization due to its even higher energy transfer rate. A soluble polystyrene of 50 kDa and a polystyrene particle size standard of 40 nm were analyzed as reference accordingly. Finally, the resin's detectability in a cell extract was looked at.

3.4.1 Comparison of soluble polystyrenes, polystyrene beads and resin particles

The recorded spectra of the polystyrene particle standard, the soluble polystyrene of 50 kDa and the resin A400_h are shown in Figure 45. The fine structure of the recorded spectra is shown in

Figure 47. The spectra mostly overlap with some exceptions. The most prominent fragments are shown in detail in Figure 46. The fragment at 58.1. Da can be attributed to a trimethyl amine which is the fixed charge on the resin. It can be seen in Figure 46 that this fragment is only present in the resin spectrum. On the other hand, the fragment of 91.1 Da, which can be attributed to a polystyrene-related fragment, is seen in all three spectra but most prominently in the polystyrene particle standard spectrum. The fragment of mass 117.1 Da is another polystyrene-related fragment and found in all three spectra. Nevertheless, it is most prominently seen in the resin spectrum. The slight mass-shift within the different spectra can be attributed to the slightly different sample height of the different analytes.

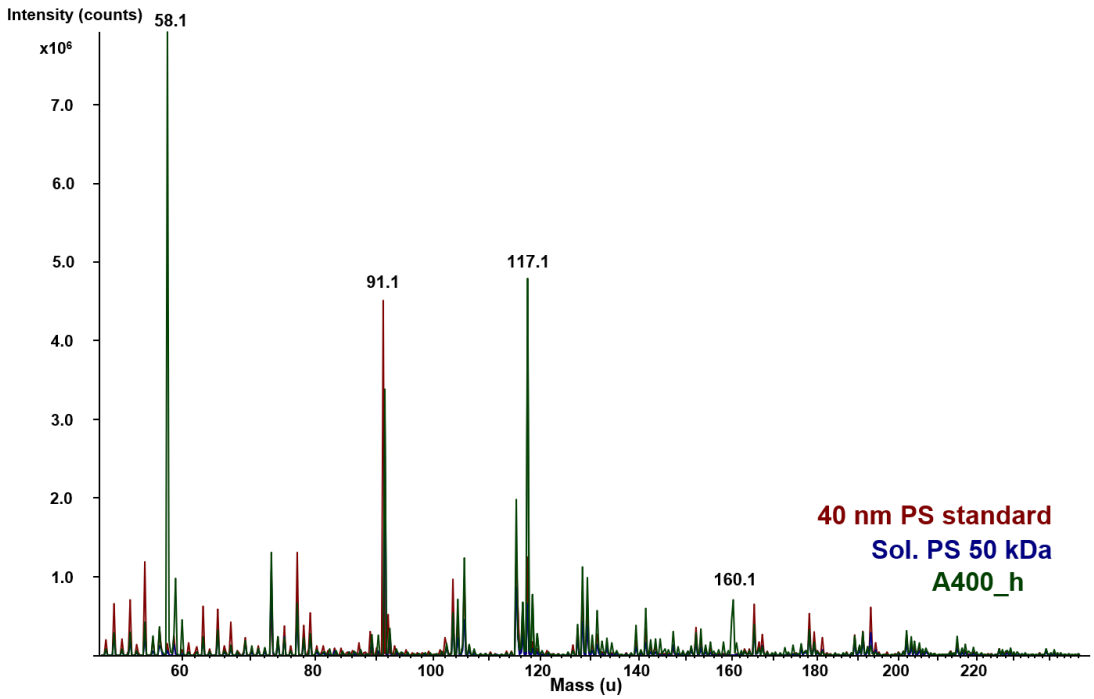

FIGURE 45: COMPARISON OF MASS SPECTRA OF POLYSTYRENE PARTICLE STANDARD, SOLUBLE POLYSTYRENE AND RESIN A400_h

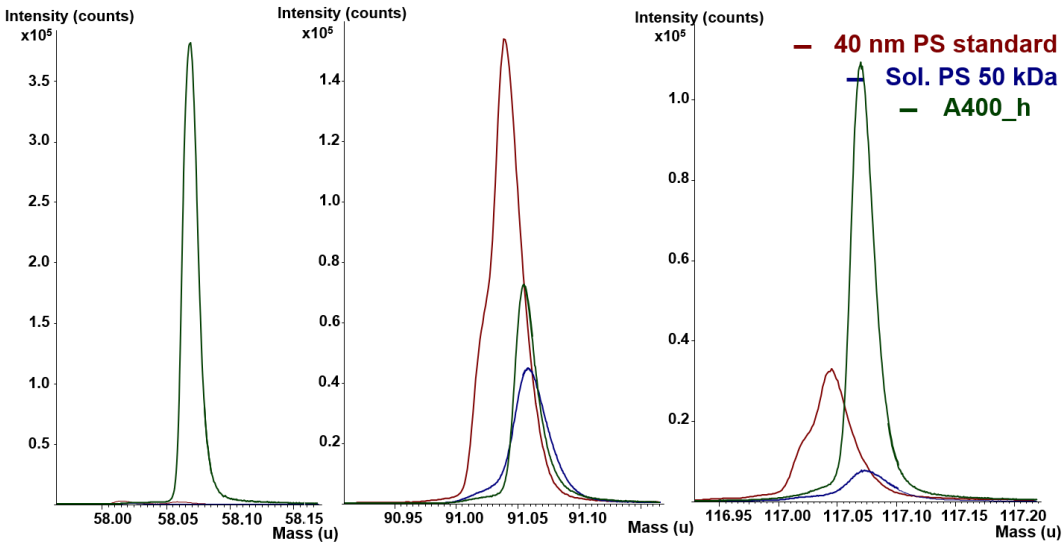

FIGURE 46: COMPARISON OF THE THREE MOST PROMINENT FRAGMENTS OF THE MASS SPECTRA OF THE POLYSTYRENE PARTICLE SIZE STANDARD, THE SOLUBLE POLYSTYRENE AND THE RESIN A400_h

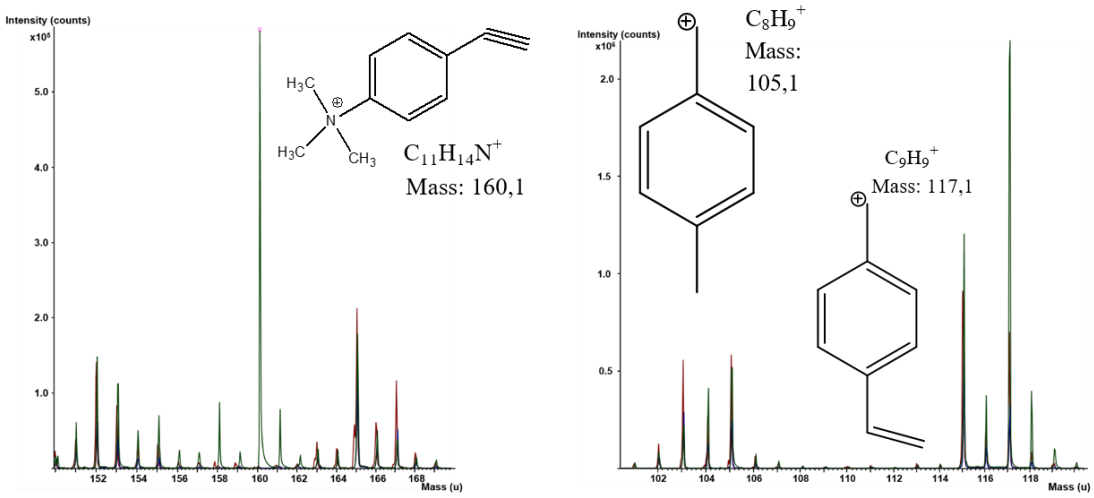

FIGURE 47: COMPARISON OF THE FINE STRUCTURE SPECTRA OF THE SOLUBLE POLYSTYRENE, THE POLYSTYRENE PARTICLE STANDARD AND THE RESIN A400_h INCLUDING A RESIN-SPECIFIC FRAGMENT (LEFT) AND POLYSTYRENE-SPECIFIC FRAGMENTS (RIGHT)

Spectra were also recorded after sputtering the sample with O_2^+ and thereby removing a few nm of material from the sample surface. This lead to identical spectra but yielded lower absolute intensities.

Overall it can be said that spectra for all three analyte groups could be recorded which is different to LDI MS where only the resin sample showed a characteristic fragment spectrum. This is probably due to the higher energy transfer to the sample of SIMS compared to LDI MS. The SIMS spectra of all three analyte groups mostly overlap, except for some resin-related fragments, containing an amine-group, which can only be found in the resin spectrum and are therefore characteristic. The fact that no polystyrene standard fragment-ions or soluble polystyrene fragment-ions were seen using LDI MS might also be explained by the lower energy transfer to the sample as well. Furthermore, “sweet-spots” are more visible in SIMS due to a better built-in camera and therefore easier to target. Especially in the case of the soluble polystyrenes suspended in water, which were distributed very unevenly, this might be a reason why no spectrum could be recorded utilizing LDI MS. This has to be investigated further.

3.4.2 MEASUREMENT OF SPIKED CELL EXTRACTS

In a next step the applicability of the resin detection in a cell extract sample was tested. Figure 48 shows the recorded spectra of pure cell extract as compared to spiked cell extract at a spike ratio of 1:1. Both spectra show clear differences. This is especially visible when looking at the fine structure as shown in Figure 49. The most prominent resin fragments 58.1, 91.1 and 117.1 are also visible in the spiked cell extract.

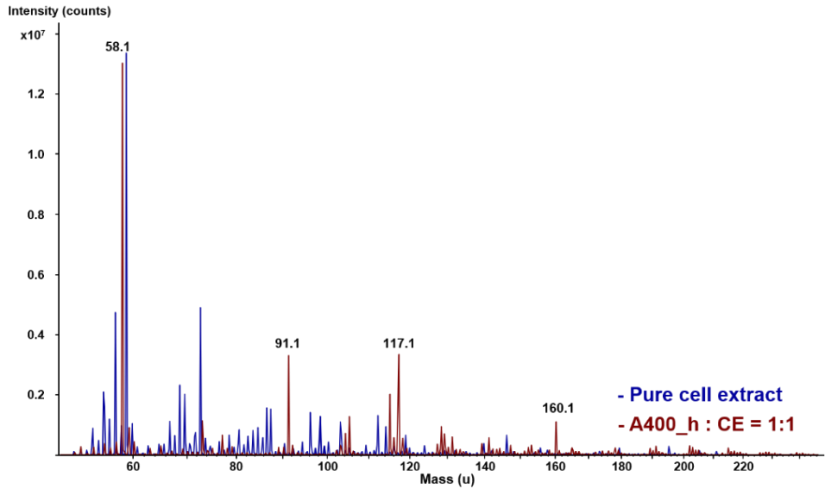

FIGURE 48: COMPARSION OF MASS SPECTRA OF PURE CELL EXTRACT AND A 1:1 MIXTURE OF CELL EXTRACT AND RESIN A400_h

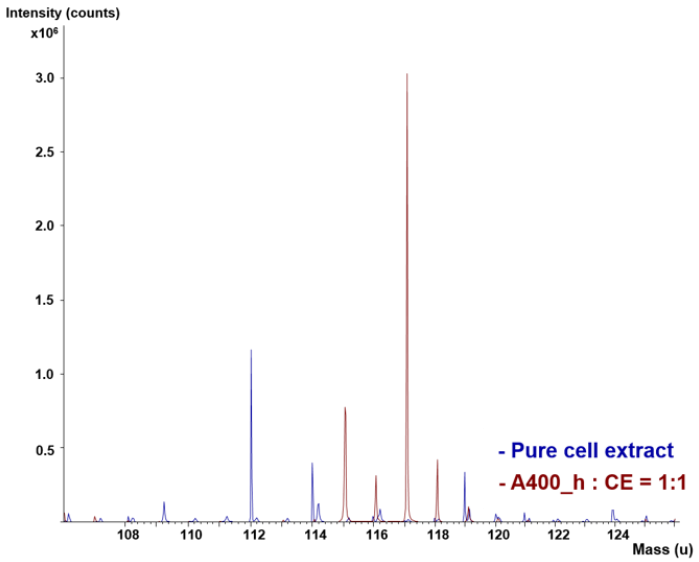

FIGURE 49: FINE STRUCTURE OF THE MASS SPECTRA OF PURE CELL EXTRACT AND A 1:1 MIXTURE OF CELL EXTRACT AND RESIN A400_h

Therefore, it can be concluded that the resin particles can be detected in a spiked cell extract. Since this was just a proof-of-concept experiment, further method development is needed. Since SIMS yielded the same resin fragment ions as LDI MS it seems likely that resin fragments could be seen in LDI MS as well, if higher energy was applied or sample preparation optimized in a way to remove more cell extract material, which leads to a dissipation of the applied energy.

3.5 PYROLYSIS GC MS EXPERIMENTS

Like SIMS, pyrolysis GC MS leads to a high energy transfer to the sample even though the type of energy used is of pure thermal origin. Therefore, it was of interest to see differences in fragmentation between those techniques. On top of that two different types of information, the gas chromatographic retention times and their mass spectra, can be obtained from the detected pyrolytic fragments. Thus, five different resin samples were analyzed by pyrolysis GC MS and compared.

3.5.1 COMPARISON OF DIFFERENT RESIN SAMPLES

Figure 50 shows a comparison of the pyrolysis chromatograms of the five different resin samples analyzed. Independent of the resin type or milling energy used the chromatograms look almost identical. Figure 51 shows the according mass spectra of three representative pyrolysis fragments. The fragment at 3.5 min seems to be the trimethylamine fragment consisting of a mass of 58 Da. When looking at the fragment ion mass spectra of the pyrolysis fragment at 15.25 and 39.50 min it can be seen that most fragments are of the same mass as the fragments seen in LDI and SIMS (e.g. 91, 117 and 160 Da). Therefore, it seems that electron ionization leads to a similar fragmentation pattern as laser- or secondary ion-induced fragmentation.

To conclude, five different resin samples were analyzed and no significant difference in their pyrolysis fragmentation pattern was seen. The EI mass spectra of the pyrolysis fragments showed a similar fragmentation pattern as the fragments generated by LDI and SIMS. Further method development is necessary to determine, whether resin samples could be detected in cell extracts and can be differentiated from plain polystyrene particles or soluble polystyrenes.

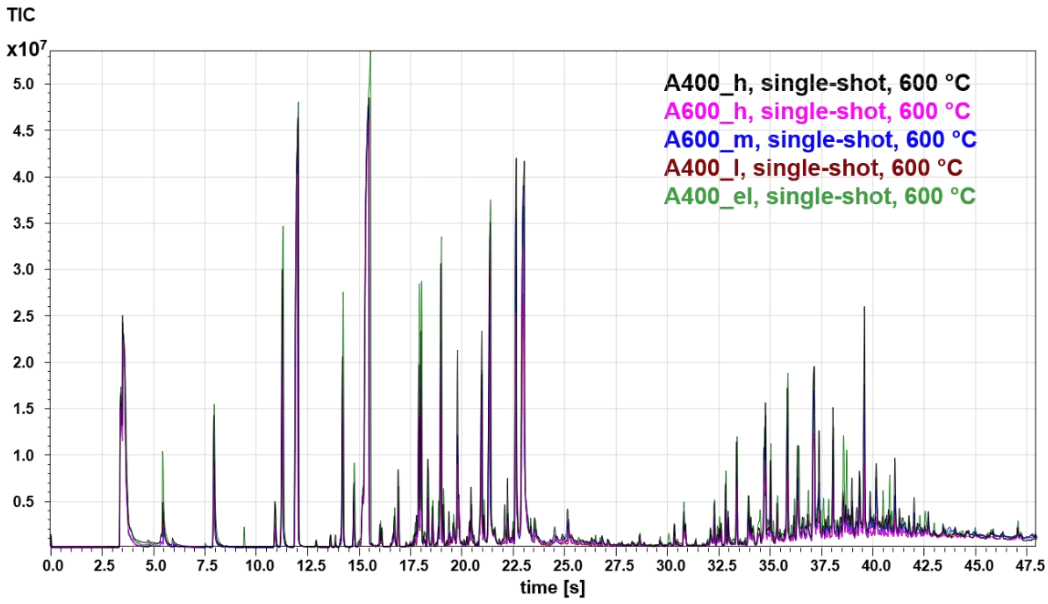

FIGURE 50: COMPARISON OF PYROLYSIS CHROMATOGRAMS OF FIVE DIFFERENT RESIN SAMPLES

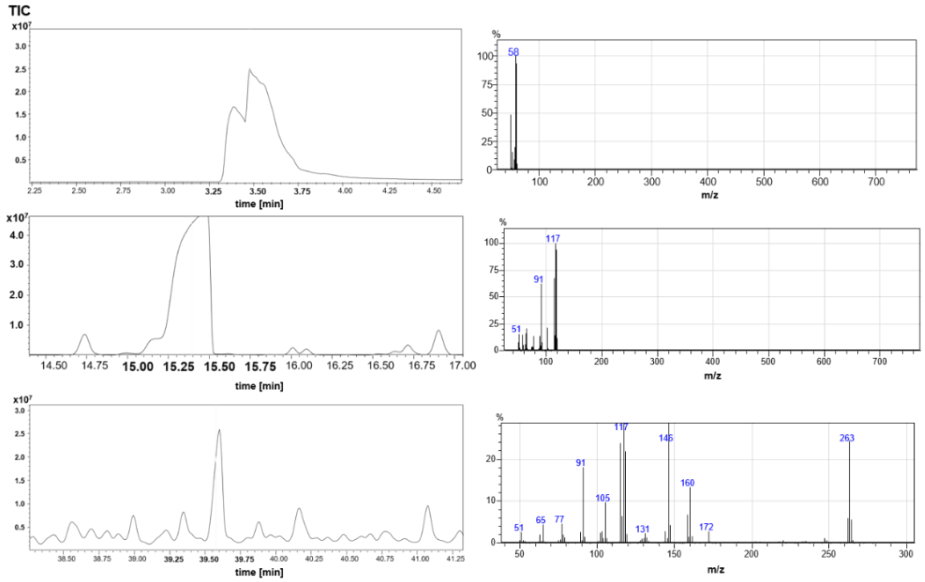

FIGURE 51: COMPARISON OF MASS SPECTRA OF THREE DIFFERENT PYROLYSIS FRAGMENTS OF THE A400_h RESIN. FRAGMENT ON THE LEFT SIDE AND ACCORDING MASS SPECTRUM ON THE RIGHT SIDE

3.6 SEM EXPERIMENTS

SEM pictures of the resin A400_h and A600_h were taken at different concentrations of aqueous suspension to get an overview of the particle structure and their size(-distribution). Furthermore, SEM pictures of the resin samples after "dissolution" in organic solvents were taken, to see the effect of the organic solvent on the resin sample.

3.6.1 MEASUREMENTS OF RESINS IN WATER AND THF

Figure 52Figure 56 show a selection of the SEM pictures of resin A400_h and A600_h at different dilutions in aqueous suspension and organic solution. Figure 57 shows the effect of filtration.

It is seen that the drying process leads to an agglomeration of particles with pores for a dilution of 1:100 and 1:1000. At a dilution of 1:10000 individual particles and smaller agglomerates are visible. Their size is about 100-200 nm. It cannot be excluded that those "particles" are formed due to individual particle agglomeration during the drying process. Therefore, further investigation of the sample is necessary.

In Figure 57 the effect of THF on the resin particles can be seen. The appearance seems more "fluid" compared to the aqueous suspensions. This might be due to a morphological change in the resin structure within the organic solvent.

Figure 54 and Figure 57 show the same concentration of particles in aqueous solution before and after filtration using a 0.2 µm syringe filter. When comparing those figures, it can be seen that filtration removes a big amount of the particles but not all of them.

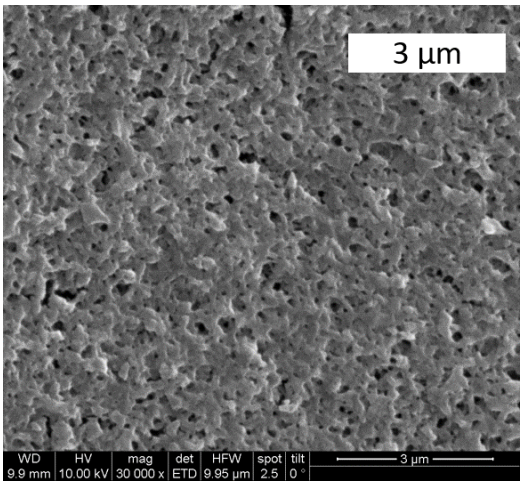

FIGURE 52: 1:100 DILUTION OF A400_h SOLUTION IN H_2O

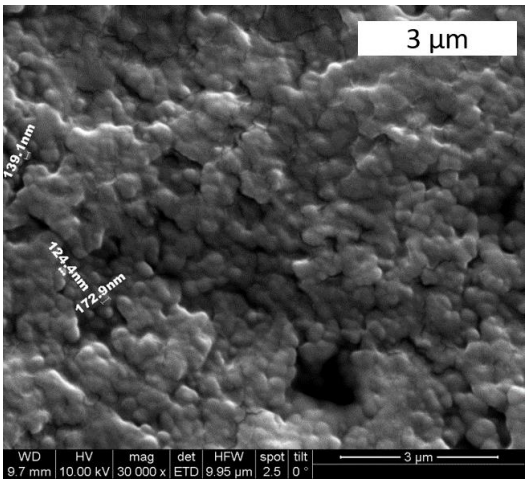

FIGURE 53: 1:1000 DILUTION OF A400_h SOLUTION IN H_2O

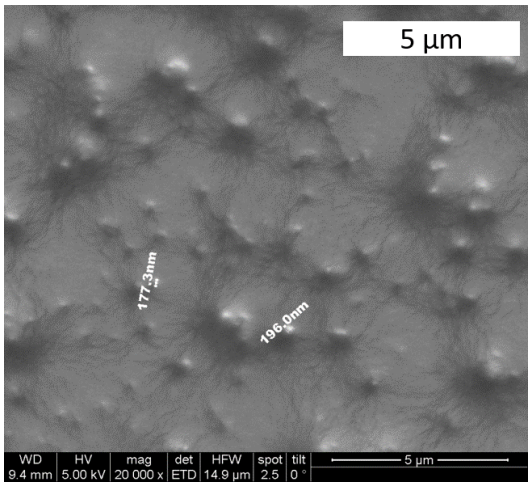

FIGURE 54: 1:10000 DILUTION OF A400_h SOLUTION IN H_2O

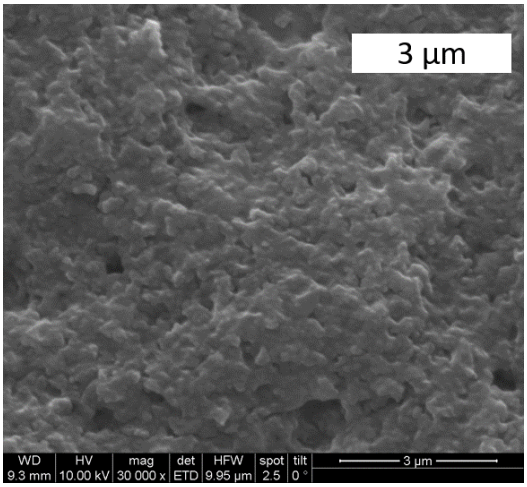

FIGURE 55: 1:1000 DILUTION OF A600_h SOLUTION IN H_2O

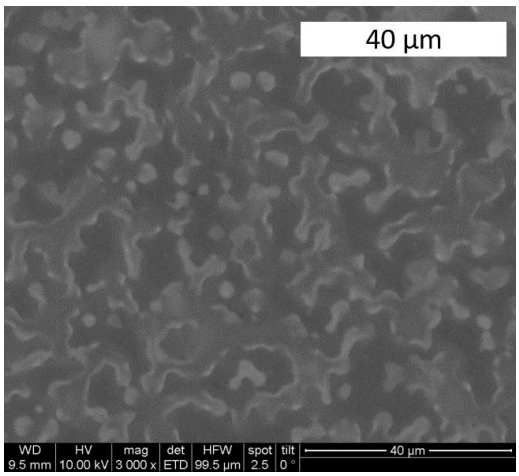

FIGURE 56: 1:1000 DILUTION OF A400_h SOLUTION IN THF

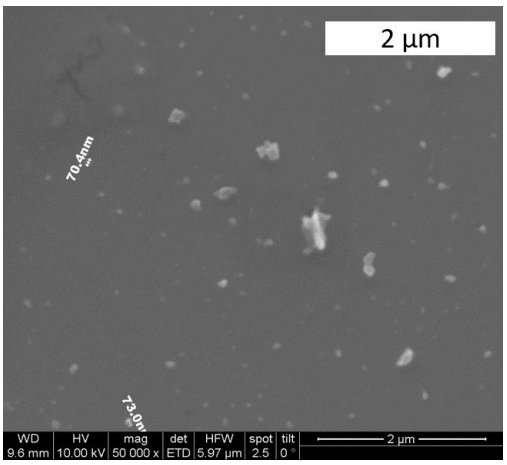

FIGURE 57: 1:10000 DILUTION OF A400_h SOLUTION IN H_2O AFTER FILTRATION

3.7 LASER DIFFRACTION EXPERIMENTS

In a next step all six received resin samples were analyzed using laser diffraction to get an overview of the particle size distribution in the > 100 nm range. LD was chosen since it is a well-established technique and easy to handle. Moreover, LD covers a broad size range which was favorable since the particle's expected size (-range) was unclear. Additionally, particle size standards of 40 nm, 80 nm, 100 nm and 200 nm were measured for comparison and to test the boundaries of the LD measurements. Finally, standard mixtures consisting of varying parts of the above-mentioned size standards were measured to evaluate the detectability of smaller sized particles in a mixture using LD.

3.7.1 MEASUREMENT OF POLYSTYRENE STANDARDS AND STANDARD MIXES

Figure 58 compares the size distribution of the 80 nm, the 100 nm and the 200 nm particle size standard. The 200 nm standard showed a broader distribution as compared to the other two which is shifted to a higher diameter, even though its maximum does not correspond to the specified 200 nm. The 80 nm and 100 nm standard show an almost identical maximum. They only differ in signal intensity with the 80 nm standard showing a lower intensity. To achieve the necessary laser attenuation for taking a measurement (which is about 10 %) 30 droplets of the 200 nm standard solution had to be added. For the 100 nm standard 170 and for the 80 nm standard 200 droplets had to be added. Nonetheless, the laser attenuation was lowest for the 80 nm standard (7.99 % as compared to 11.18 % for the 200 nm standard) which might explain the lower signal intensity. A measurement of the 40 nm standard was attempted but abandoned after adding more than 300 droplets and only achieving a laser attenuation of 1.46 %.

Figure 59 shows the size distribution of three different polystyrene size standard mixtures each containing 40 nm, 60 nm, 80 nm and 100 nm standard as prepared according to section 2.9.1. The PS mix 1:1 contains the same weight content of all four standards. The PS mix same number conc. contains the same particle number concentration and the PS mix various contains the same weight concentration of all standards except for the 40 nm standard which was added at half the weight concentration as the others. It is seen that even though the measured intensity for the standard mixtures varies, the maximum is the same suggesting that LD is not able to distinguish those three very different mixtures.

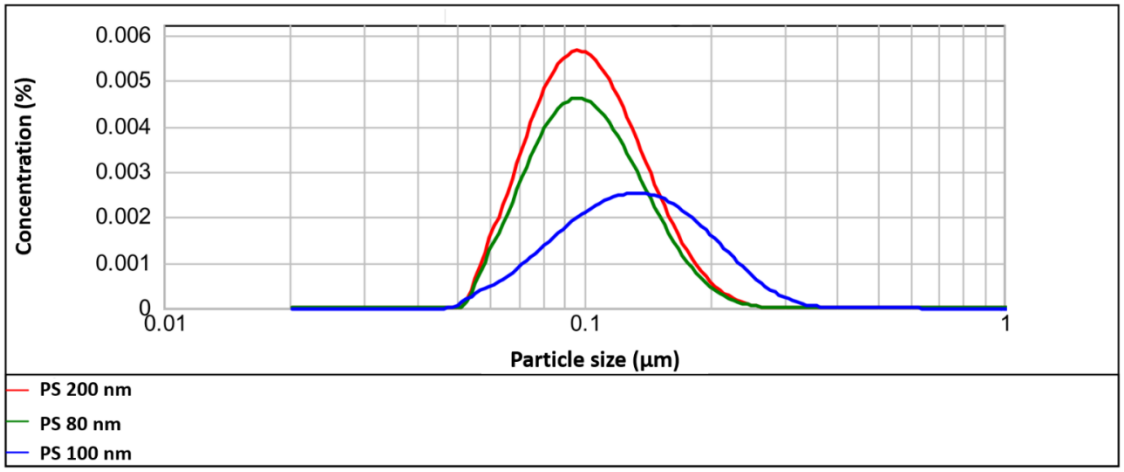

FIGURE 58: SIZE DISTRIBUTION OF THREE DIFFERENT POLYSTYRENE BASED PARTICLE SIZE STANDARDS

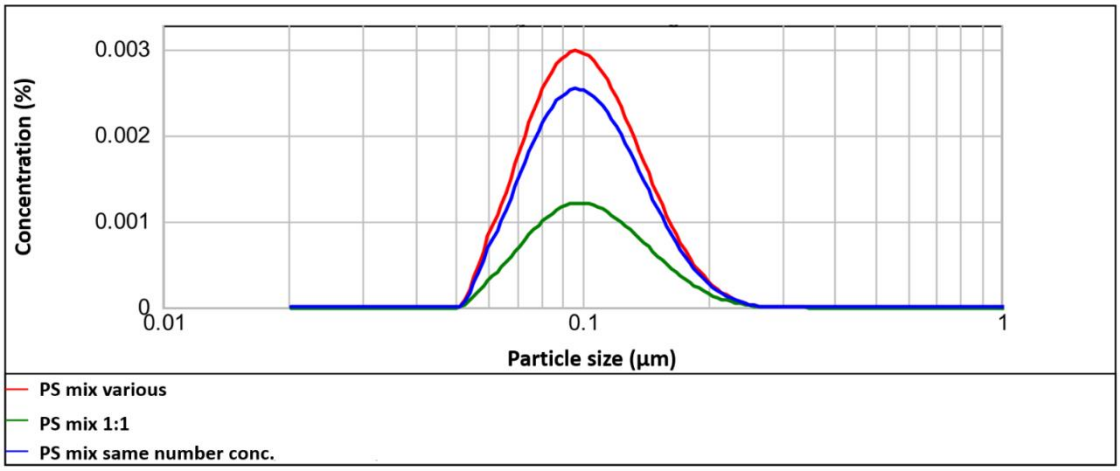

FIGURE 59: SIZE DISTRIBUTION OF THREE DIFFERENT POLYSTYRENE STANDARD MIXES EACH CONTAINING 40 nm, 60 nm, 80 nm AND 100 nm STANDARD AS DESCRIBED IN SECTION 2.9.1

It can be concluded that LD is not a suitable method to distinguish and characterize particles with diameters lower than a few hundred nm.

3.7.2 MEASUREMENT OF RESIN PARTICLES

Figure 60 compares the size distributions of all six received resin samples. A400_0 is a sample after pre-milling (before the fine-milling step). It consists of mainly larger particles with a maximum around 100 µm. Still a certain amount of smaller particles cannot be excluded since it was shown previously that LD overestimated the bigger particle contents. A400_el only contains a low amount of milling energy content and therefore, still mainly consists of particles of about 3-4 µm diameter. On the other hands the resins of higher milling energy content show a maximum around about 100 nm. It has to be kept in mind that LD does not discriminate lower diameter ranges as shown in the previous section. Therefore, the “true” maximum of the resin distributions might be lower.

Figure 61 shows the resins of higher milling energy content in more detail. It can be seen that the intensity of the maximum and therefore the relative amount of smaller particles decreases for lower milling energy content whereas the second maximum at around 1 µm increases. For low milling energy there even appears a third maximum at around 3-4 µm particle size, which is identical to the maximum seen for the resin A400_el.

Figure 62 compares the size distribution of the resins with highest milling energy content to distribution of the PS mix various. It can be seen that the maximum of the PS mix various is shifted slightly to lower particle size and the distribution is narrower. The resins seem to contain a higher amount of finer particles. Still, those conclusions have to be verified using another method, since LD is not capable to resolve differences in the particle size range of approx. 100 nm and below.

Therefore, it was possible to detect particle size standards down to 80 nm using LD even though no distinction between the 80 nm and 100 nm standard was possible anymore. Likewise, for particle standard mixes no differentiation was possible. All received resin sample were analyzed and an increase of smaller particles as well as loss of larger resin material was seen for higher milling energy content.

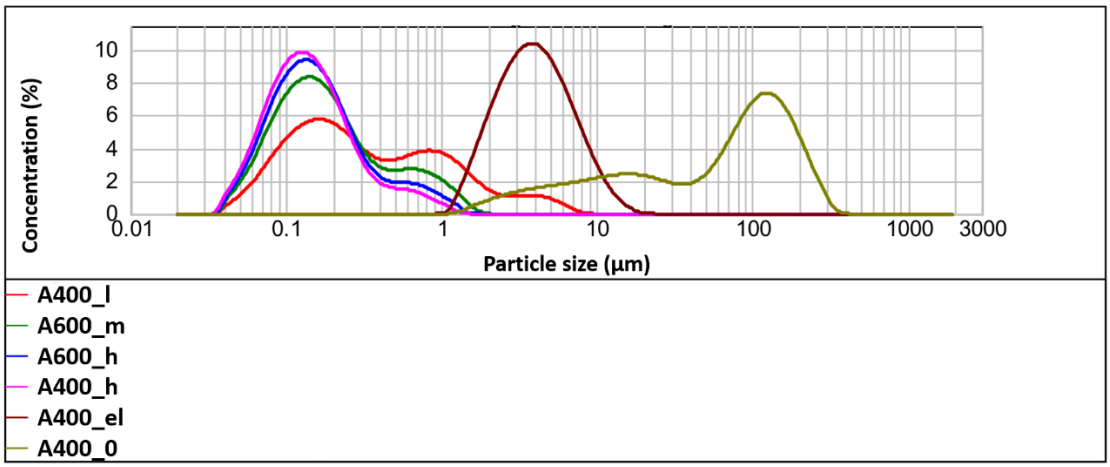

FIGURE 60: COMPARISON OF THE SIZE DISTRIBUTIONS OF ALL SIX RECEIVED RESIN SAMPLES

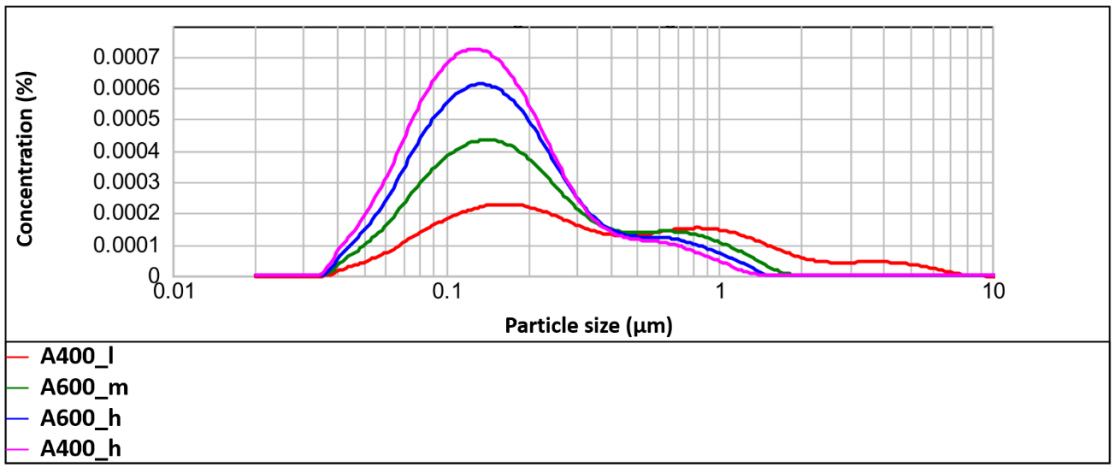

FIGURE 61: COMPARISON OF THE SIZE DISTRIBUTION SOF THE FOUR RESIN SAMPLES WITH HIGHEST CONTENT OF NANO PARTICLES

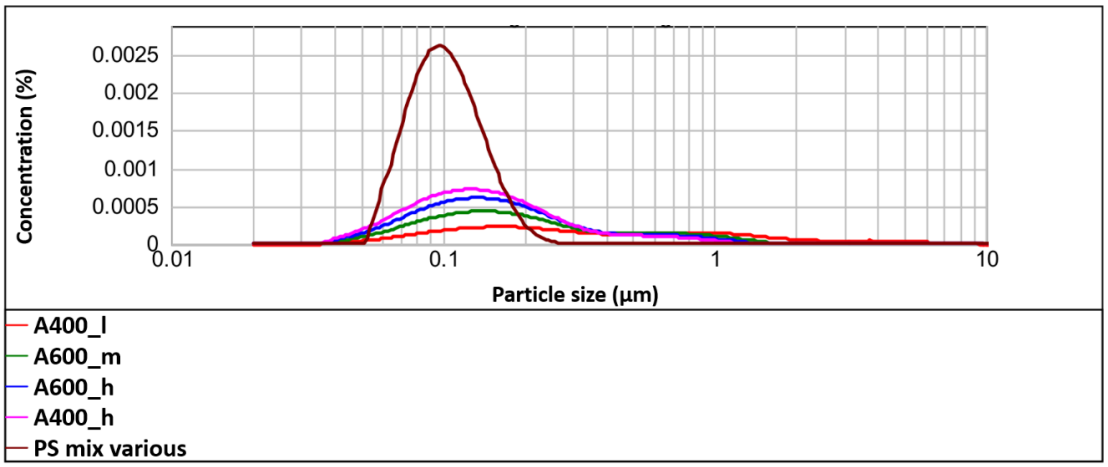

FIGURE 62: COMPARISON OF THE SIZE DISTRIBUTION SOF THE FOUR RESIN SAMPLES WITH HIGHEST CONTENT OF NANO PARTICLES AND THE PS MIX VARIOUS

3.8 GEMMA EXPERIMENTS

Since nES GEMMA covers a size range of a few nanometer up to several hundred nanometer it was chosen as a suitable technique to characterize the lower size range of the resin particles not accessible using LD. In addition, nES GEMMA offers the possibility of particle number-based detection and surface-dry particle diameters are obtained. All resin particle samples (except for the sample A400_0) were analyzed. In addition, particle size standards of the sizes 20 nm, 40 nm, 60 nm, 80 nm and 100 nm were measured individually as well as in mixtures. Furthermore, the retention of the resin nanoparticles using a 0.2 µm filter and a 300 kDa filter was investigated.

3.8.1 POLYSTYRENE SIZE STANDARD MEASUREMENTS, RESIN MEASUREMENTS AND SIZE STANDARD MIXTURES MEASUREMENTS

Figure 63 and Figure 67 show the GEMMA measurements of particle size standards with different mean diameter. All measurements were done at two different concentrations. The absolute signal intensity is shown on the left. The higher concentrated standards also show higher absolute particle counts. On the right the relative particle counts are shown as well as a Gaussian fit of the measured curve and the determined maximum. It is seen that the relative curves are almost identical for relative particle counts. The DMA hereby separates according to the electrophoretic mobility diameter (EMD) of the particles, which depends on a number of features (e.g. the charge state, the mass and the shape of the measured object). In case of spherical objects, the EMD is equivalent to the diameter of the solvent free particle (surface).

At lower diameter high particle counts are seen. This is due to an agglomeration of smaller molecules, non-volatile salts and detergents during the spray-process. Since there is a high amount of salt and detergents in the particle standards solution (to prevent an agglomeration of the particles in solution) this background signal is also very high. It can be seen when looking closely at Figure 63Figure 67 that this curve (henceforth called background signal) is steeper for smaller dia-meters at higher particle concentrations. This is because at higher concentrations more impurities are present in the solution and therefore, bigger agglomerates can form.

Table 12 compares the maxima derived from the GEMMA measurements with the specified values from the standard certificates. For the 40 nm standard and the 100 nm standard three measurements were done on three different days to derive a standard deviation of the mean diameter. The standard deviation is also stated in Table 12. All other mean diameters are the result of a single measurement. All determined mean diameters are within the specified size range except for the 20 nm and 60 nm standard. This is because a different method was used to determine the mean diameter.

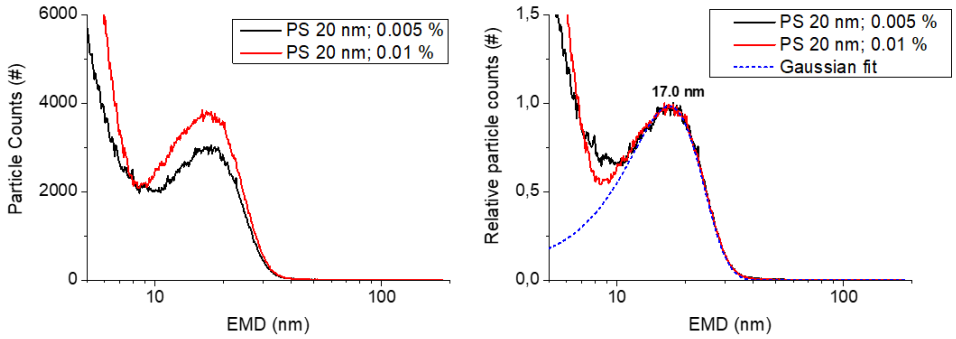

FIGURE 63: 20 nm PARTICLE STANDARD GEMMA MEASUREMENTS AT TWO DIFFERENT CONCENTRATIONS. ON THE LEFT THE ABSOLUTE PARTICLE COUNTS ARE GIVEN, ON THE RIGHT THE RELATIVE COUNTS ARE SHOWN. FURTHERMORE, A GAUSSIAN FIT WAS APPLIED TO THE MEASURED CURVES TO DETERMINE THE MAXIMUM

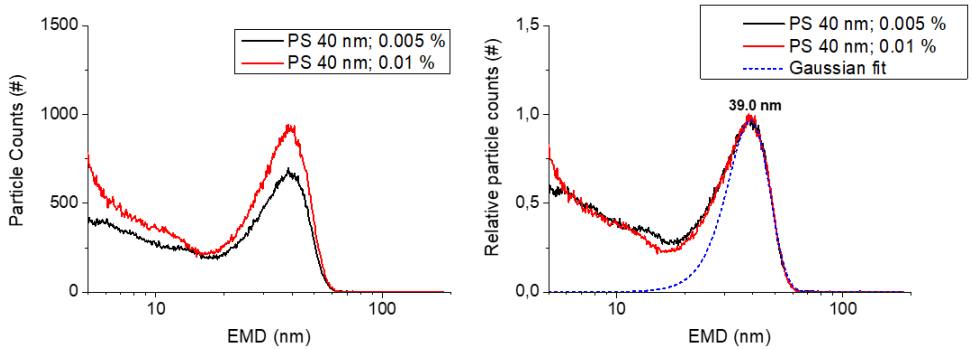

FIGURE 64: 40 nm PARTICLE STANDARD GEMMA MEASUREMENTS AT TWO DIFFERENT CONCENTRATIONS. ON THE LEFT THE ABSOLUTE PARTICLE COUNTS ARE GIVEN, ON THE RIGHT THE RELATIVE COUNTS ARE SHOWN. FURTHERMORE, A GAUSSIAN FIT WAS APPLIED TO THE MEASURED CURVES TO DETERMINE THE MAXIMUM

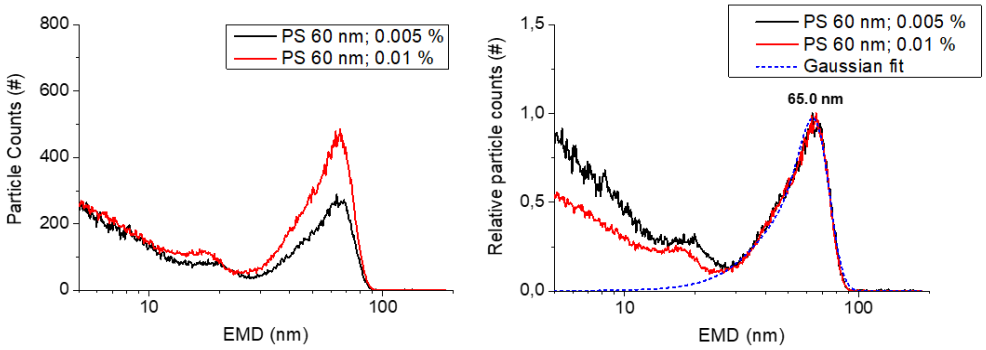

FIGURE 65: 60 NM PARTICLE STANDARD GEMMA MEASUREMENTS AT TWO DIFFERENT CONCENTRATIONS. ON THE LEFT THE ABSOLUTE PARTICLE COUNTS ARE GIVEN, ON THE RIGHT THE RELATIVE COUNTS ARE SHOWN. FURTHERMORE, A GAUSSIAN FIT WAS APPLIED TO THE MEASURED CURVES TO DETERMINE THE MAXIMUM

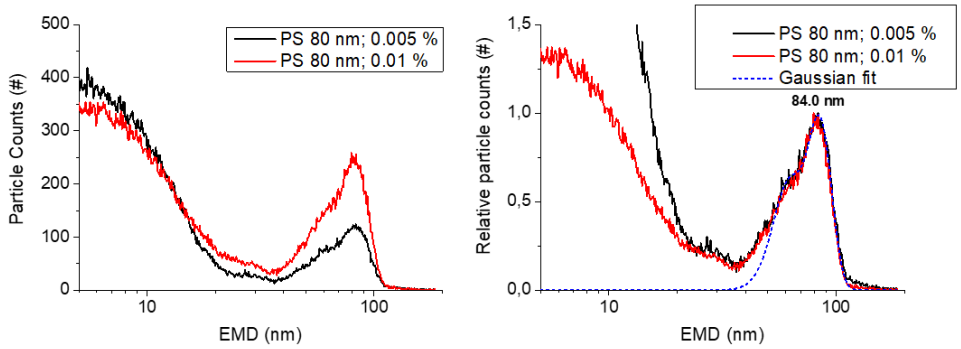

FIGURE 66: 80 NM PARTICLE STANDARD GEMMA MEASUREMENTS AT TWO DIFFERENT CONCENTRATIONS. ON THE LEFT THE ABSOLUTE PARTICLE COUNTS ARE GIVEN, ON THE RIGHT THE RELATIVE COUNTS ARE SHOWN. FURTHERMORE, A GAUSSIAN FIT WAS APPLIED TO THE MEASURED CURVES TO DETERMINE THE MAXIMUM

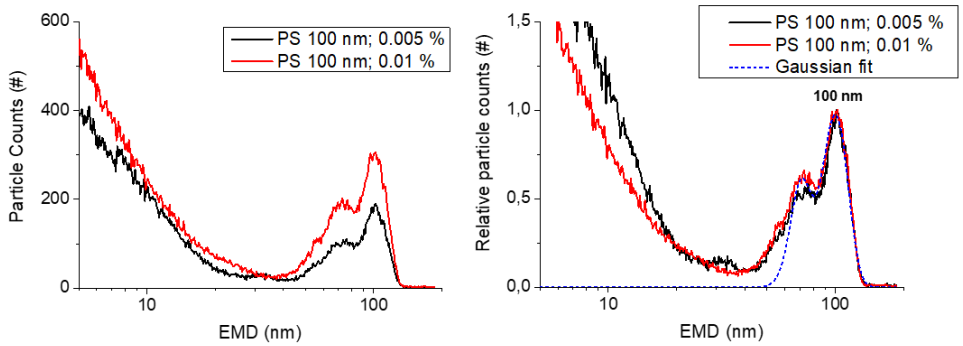

FIGURE 67: 100 NM PARTICLE STANDARD GEMMA MEASUREMENTS AT TWO DIFFERENT CONCENTRATIONS. ON THE LEFT THE ABSOLUTE PARTICLE COUNTS ARE GIVEN, ON THE RIGHT THE RELATIVE COUNTS ARE SHOWN. FURTHERMORE, A GAUSSIAN FIT WAS APPLIED TO THE MEASURED CURVES TO DETERMINE THE MAXIMUM

TABLE 12: COMPARISON OF MEAN DIAMETER OF THE PARTICLE STANDARDS DETERMINED BY GEMMA AND GIVEN IN THE CERTIFICATE. FOR THE 40 NM STANDARD AND THE 100 NM STANDARD THREE MEASUREMENTS ON THREE DIFFERENT DAYS WERE DONE AND THE STANDARD DEVIATION OF THE MEASURED MEAN DIAMETER IS GIVEN. ALL OTHER MEAN DIAMETERS DETERMINED BY GEMMA ARE THE RESULT OF A SINGLE MEASUREMENT

Product name	Certified mean diameter	Size determination method for certification	Measured diameter with GEMMA
Nanosphere Size Standards 3020A	22 ± 2 nm	Photon correlation microscopy	17.0 nm
Nanosphere Size Standards 3040A	41 ± 4 nm	Photon correlation microscopy	38.8 ± 0.3 nm
Nanosphere Size Standards 3060A	60 ± 4 nm	Transmission electron microscopy	65.0 nm
Nanosphere Size Standards 3080A	81 ± 3 nm	Transmission electron microscopy	84.0 nm
Microparticle size Standard based on polystyrene monodisperse	102 ± 3 nm	Disc centrifugation	101 ± 1 nm

Interestingly, for bigger diameters a second distribution of smaller diameter becomes visible within a “pure” standard solution. If this additional peaks correspond to multiple charged PS particles or indeed correspond to an additional sample compound needs to be further investigated.

Three particle standard mixtures were prepared. The first containing the same number concentration of all received particle standards and the second containing the same weight concentration of all received particle standards except the 20 nm standard (since the sample has not been received at the time of the measurement). The third mixture was adapted to mimic the determined resin distribution and consisted of all particle standards of the same weight concentration except for the 40 nm standard, which was added at half the weight concentration of the other standards and the 20 nm standard which was not added.

The mixture of same number concentration was measured at two different concentrations and is shown in Figure 70. Due to the lack of a 30 nm standard the curve does not show a plateau throughout the whole covered diameter range. The distribution shows a maximum around 80 nm and lower particle counts for the smaller and the bigger diameter range. This indicates a size-selectivity of the method, which is by far not as prominent as seen in laser diffraction measurements.

All three particle standard mixtures are compared in Figure 71. For the mixture of same weight-concentration the smallest standard of 40 nm is most prominent, since the absolute number of particles exceeds that of the other standards.

Figure 69 compares the resin distribution with the standard mixture distribution. The standard mixture distribution is not as smooth as the resin distribution due to the discreet diameter sizes of the particle standards, but it can be estimated that the resin contains particles of a similar size range.

Due to the high amount of total particle content leading to repeated capillary clogging throughout the measurements those measurements were hard to perform. Therefore, the shown curves should be regarded as estimates. The measurements were performed at pH 4. For further measurements a higher pH should be considered.

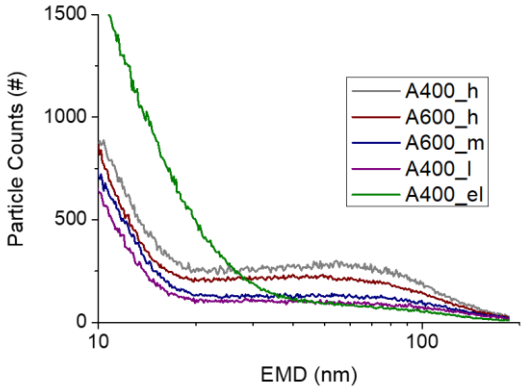

FIGURE 68: COMPARISON OF GEMMA MEASUREMENTS OF FIVE RECEIVED RESIN SAMPLES

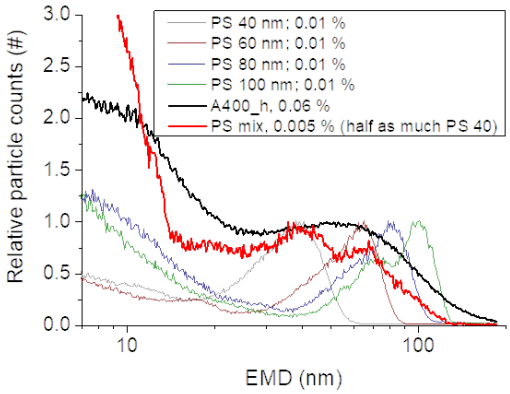

FIGURE 69: COMPARISON OF GEMMA MEASUREMENT OF A RESIN SAMPLE TO A PARTICLE STANDARD MIXTURE. THE INDIVIDUAL STANDARDS USED IN THE MIXTURE ARE ALSO SHOWN IN THE GRAPH.

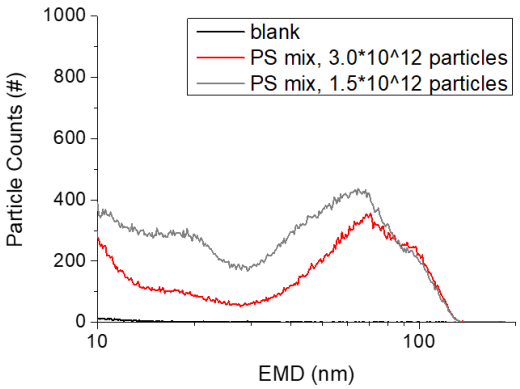

FIGURE 70: COMPARSION OF THE SAME STANDARD PARTICLE MIXTURE AT DIFFERENT NUMBER CONCENTRATIONS

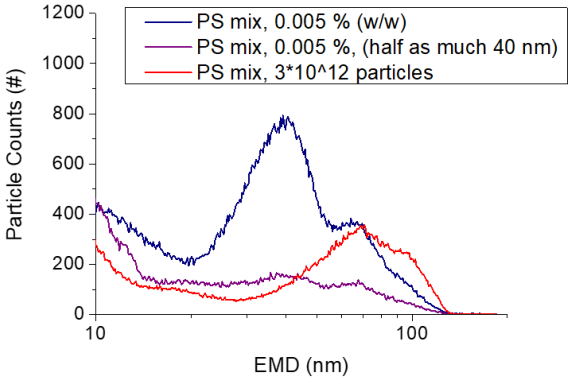

FIGURE 71: COMPARISON OF PARTICLE STANDARD MIXTURES OF DIFFERENT PARTICLE STANDARD CONTENT

All received particle size standards except for the 200 nm could be measured at the GEMMA instrument at two different concentrations and the peak of the distribution was determined and compared with the specified mean. It was not possible to measure the 200 nm standard due to the size limitation of the utilized DMA. By application of an advanced, different DMA the size range can be increased up to 800 nm. Due to the different distribution determination method small variations in determined mean diameter as compared to the specified diameter were seen. Three different standard mixtures were measured as well as all received resin samples and the determined distributions compared to the resin distribution. The particles standard mix with most similar distribution consisted of all sizes at same weight concentration except for the 40 nm standard which was added at half the weight concentration of the others and the 20 nm standard which was not added.

3.8.2 Influence of several method parameters on the recorded resin distribution

To estimate the robustness of the method and their impact on the resin distribution a few validation parameters were tested for resin A400_h. This included the influence of the resin concentration, the influence of the time the capillary was flushed with sample before recording a distribution (flushing time), the sheath flow rate, the inter-day variability and the effect of a fresh capillary on the background signal.

Figure 72 shows the distribution of resin A400_h at concentrations ranging from 0.15 % to 0.001 %. At 0.15 % resin content, no stable spray could be achieved and the capillary clogged up very quickly. Therefore, the shown distribution is an estimate of only two measurements. It is seen in Figure 72 that the maximum of the background signal is shifting to lower masses for lower concentrated samples. This consolidates the assumption that it is caused by agglomerates of smaller molecules. Figure 73 shows the resin A400_h distribution at a concentration of 0.001 % and 0.0005 %. Both are clearly distinguishable from the measured blank, which does not show any particle counts in the according size range. 0.0005 % was determined as the lowest detectable concentration of the method.

Figure 74 shows the resin A400_h distribution measured on two different days. On the left the absolute counts are shown, on the right the relative counts are visualized. There is a slight variation of the distribution intensity when looking at the absolute counts which might be due to a little differently shaped capillary, slightly different capillary position or voltage applied. When looking at the relative signals the resin distributions of both days are comparable. Only the background signal varies marginally. It can also be seen in Figure 74 that the resin distribution shows a flat maximum at 50 nm. Figure 75 shows the absolute particle counts of the 40 nm particle standard distribution recorded on different days. Also in this case there are only slight deviations in the particle distribution visible and only the background signal varies more strongly.

Figure 76 shows the resin A400_h distribution recorded at different sheath flow rates of the DMA. At lower sheath flow rates smaller diameter ranges are recordable.

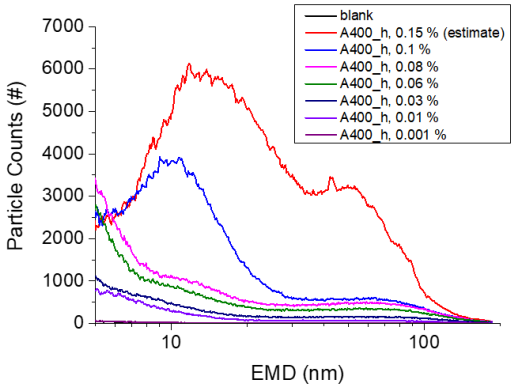

FIGURE 72: RESIN A400_h MEASURED AT DIFFERENT CONCENTRATIONS. AT 0.15 % RESIN CONTENT THE SPRAY WAS ALREADY VERY UNSTABLE FOR WHICH REASON THE MEASURED DISTIRBUTION IS ONLY AN ESTIMATE

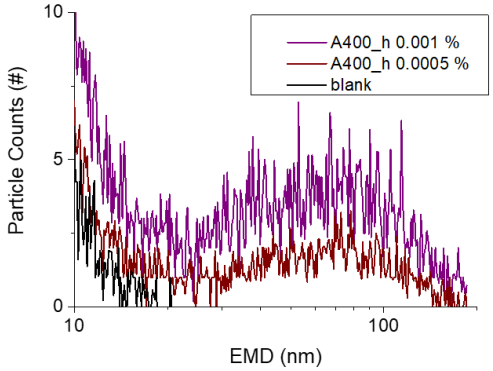

FIGURE 73: LOW CONCENTRATIONS OF RESIN A400_h.

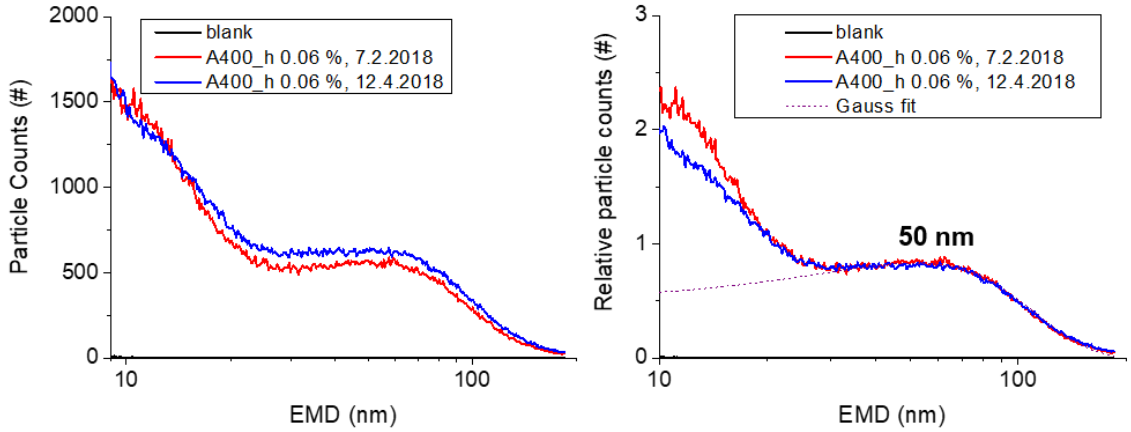

FIGURE 74: RESIN A400_h AT 0.06 % MEASURED AT TWO DIFFERENT DAYS. ON THE LEFT THE ABSOLUTE PARTICLE COUNTS, ON THE RIGHT THE RELATIVE COUNTS AND A GAUSS FIT WITH A MAXIMUM AT 50 NM ARE SHOWN

In Figure 77 the development of the blank signal after using a new capillary, flushing the capillary for approximately 2 h and after several measurements is shown. It is seen that the high background signal can be significantly reduced by extensive capillary flushing.

Figure 78 shows the development of the recorded resin distribution for resin A400_h over time. The background signal reduces over time and only stays stable after approximately 70 min. Nevertheless, the resin distribution between 30 and 100 nm is immediately visible and remains constant over the whole recorded time range.

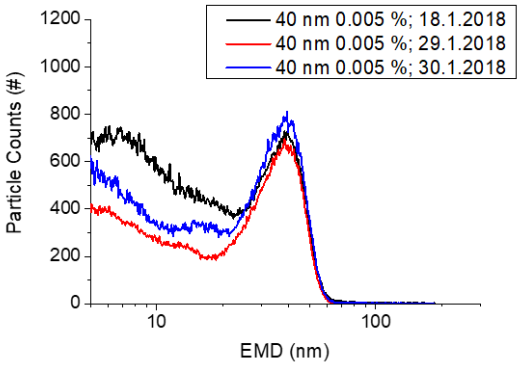

FIGURE 75: PARTICLE STANDARD OF 40 nm DIAMETER 0.005 % MEASURED ON DIFFERENT DAYS

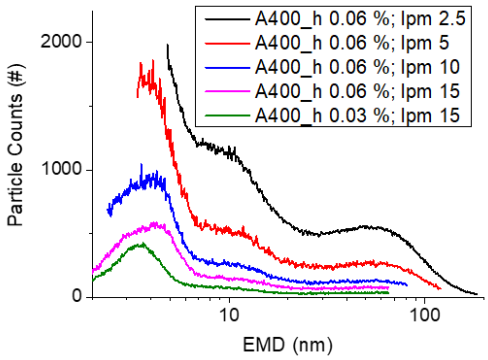

FIGURE 76: RESIN A400_h 0.06 % MEASURED WITH DIFFERENT SHEATH FLOW RATES OF THE DMA, RESULTING IN DIFFERENT COVERED DIAMETER RANGES

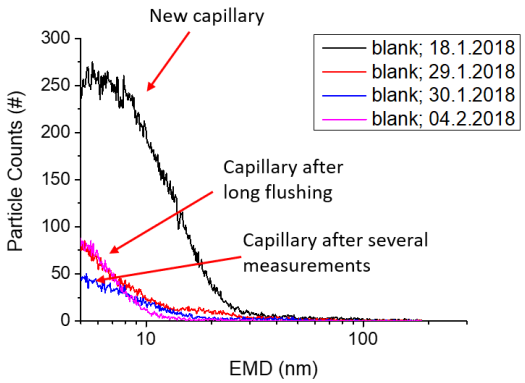

FIGURE 77: DEVELOPMENT OF BLANK SIGNAL AFTER INSERTING A NEW CAPILLARY (BLACK), FLUSHING FOR 2 h ON TWO DIFFERENT DAYS (RED AND PINK) AND AFTER SEVERAL MEASUREMENTS (BLUE)

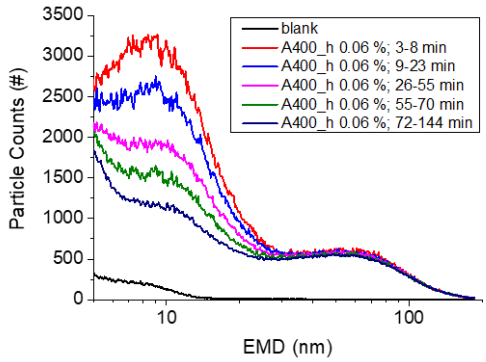

FIGURE 78: DEVELOPMENT OF BACKGROUNDSIGNAL OF RESIN DISTRIBUTION IN RELATION TO FLUSHING TIME OF SAMPLE

It was therefore seen that the recorded resin distribution does not depend strongly on the used capillary, capillary set-up (expressed in measurements on different days), resin concentration or flushing time. These variabilities greatly influence the intensity and the maximum of the agglomerate-peak though (in the range of 10 – 20 nm EMD). Only a change in sheath-flow-rate and therefore a change in the recorded diameter range leads to a change in the recorded resin distribution. Therefore, the method can be considered as robust to characterize the provided resin samples.

3.8.3 FILTRATION USING A 0.2 µm FILTER

In early experiments it was seen that the resin particles seemed to be removed by using a 0.2 µm syringe filter. This was investigated in more detail for three different resin types. Resin A400_h containing the highest fraction of nano particles, resin A400_l containing fewer and resin A400_el containing the least number of nano particles. Due to blockage of the syringe filter the filtered resin concentrations could not be too high.

Figure 79 shows the distribution of resin A400_h at two different concentrations before and after filtration. At both concentrations the distribution recorded after filtration does not differ from the blank signal which suggests removal of nanoparticles in large parts. Figure 80 shows the distribution of resin A400_el at two different concentrations before and after filtration. Since resin A400_el contains a lower amount of nanoparticles, a higher mass concentration of the resin could be used for filtration experiments. At a mass concentration of 0.005 % the resin distribution is already identical to the blank. Here the filtered resin's distributions are likewise identical to the blank. Figure 81 shows the distribution of resin A400_l at two different concentrations before and after filtration. This resin contains a nanoparticle amount between resin A400_h and resin A400_el. On the left the whole range of particle counts is shown. On the right the distribution is zoomed in to a lower particle counts to make the difference between filtered and unfiltered resin distributions visible.

Interestingly, the 0.2 µm filter seems to remove the resin particles in the below 100 nm range in large parts. This is probably due to the fact, that the cellulose acetate filter membrane carries a negative surface charge in aqueous solution, whereas the resins contain positive charges at the selected pH of 4.

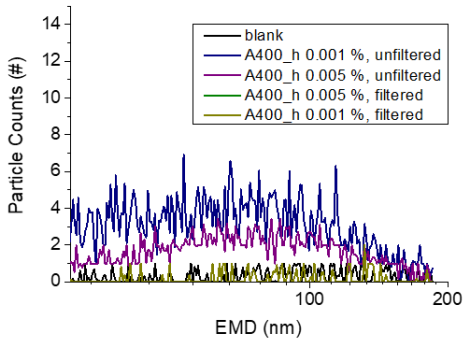

FIGURE 79: RESIN A400_h AT TWO DIFFERENT CONCENTRATIONS BEFORE AND AFTER FILTRATION WITH A 0.2 µm FILTER

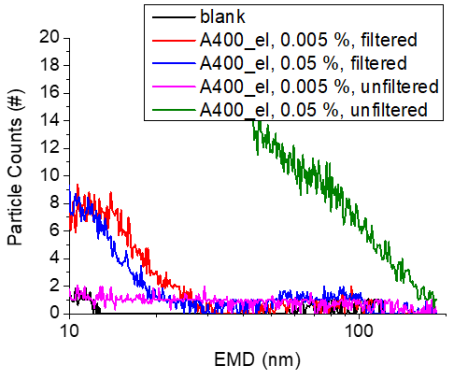

FIGURE 80: RESIN A400_el AT TWO DIFFERENT CONCENTRATIONS BEFORE AND AFTER FILTRATION WITH A 0.2 µm FILTER

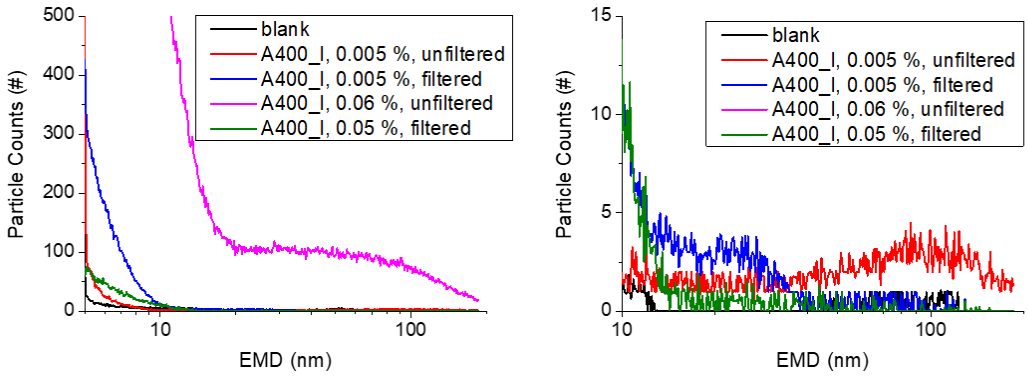

FIGURE 81: RESIN A400_l AT TWO DIFFERENT CONCENTRATIONS BEFORE AND AFTER FILTRATION WITH A 0.2 µm FILTER. LEFT THE WHOLE RECORDED RANGE AND ON THE RIGHT A ZOOM FOR LOWER PARTICLE COUNTS TO VISUALIZE THE DISTRIBUTIONS AT LOWER CONCENTRATIONS

3.8.4 FILTRATION USING A 300 kDa FILTER

For measurements of cell extracts the amount of salt and small organic molecules present in the cell extract had to be reduced as much as possible to avoid agglomerates. This was done using a 300 kDa centrifugal device consisting of an Eppendorf tube with a filter separating the upper and the lower part. Prior to measuring the cell extracts the effect of filtration was tested on plain resin samples. The retentate after the second filtration step as well as the filtrate after the first and the second filtration step were measured and are shown in Figure 82 as compared to an unfiltered resin sample of the same concentration.

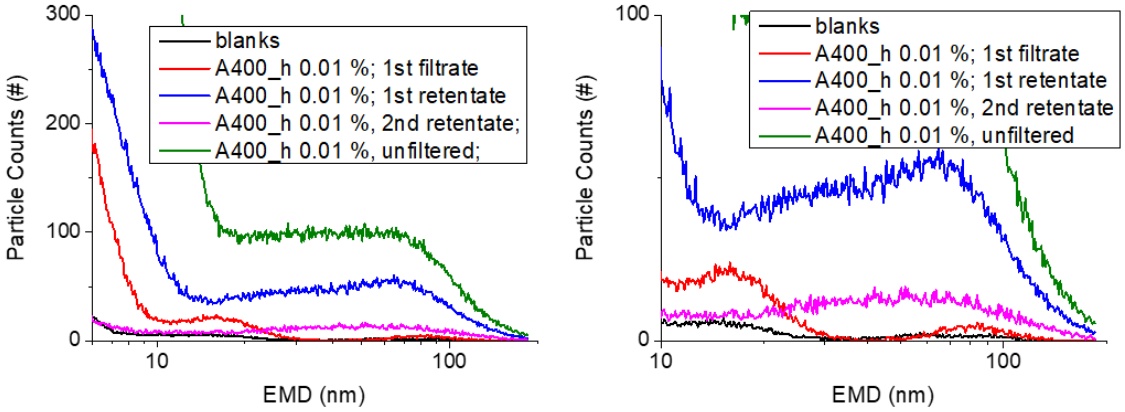

FIGURE 82: FILTRATE AND RETENTATE AFTER FIRST AND SECOND FILTRATION OF A400_h WITH A 300 kDa FILTER. ON THE LEFT THE WHOLE RECORDED RANGE IS SHOWN, ON THE RIGHT THE DISTRIBUTION WAS ZOOMED IN AT LOWER PARTICLE COUNTS TO VISUALIZE THE LOWER CONCENTRATION RANGE

It can be seen in Figure 82 that filtration significantly reduces the amount of nanoparticles in the retentate which is most likely due to adsorption effects onto the filter membrane. The filtrate shows an increased signal intensity at round 10-20 nm whereas the retentate shows a decrease in this range compared with the unfiltered resin sample.

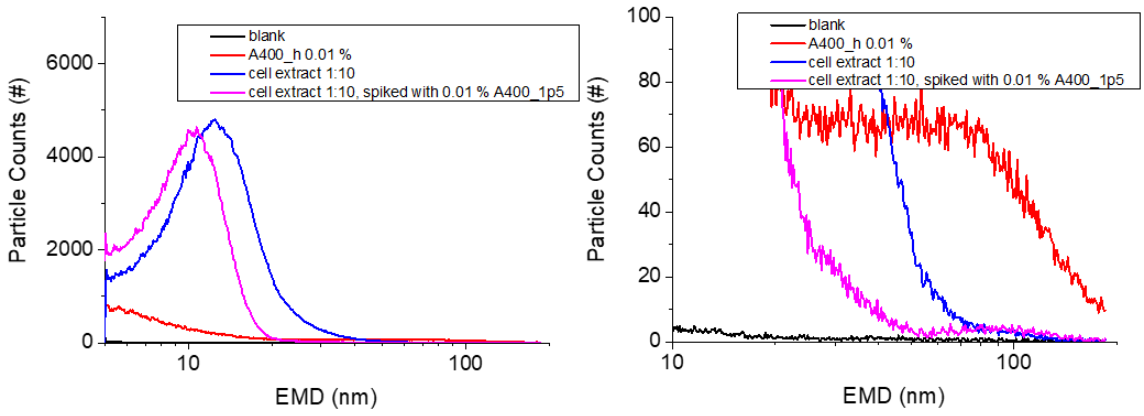

FIGURE 83: CELL EXTRACT AND SPIKED CELL EXTRACT MEASUREMENTS AS COMPARED TO PURE RESIN A400_h. ON THE LEFT THE WHOLE RECORDED RANGE IS SHOWN, ON THE RIGHT THE LOWER PARTICLE COUNTS RANGE WAS ZOOMED IN TO VISUALIZE THE LOWER CONCENTRATIONS

Figure 83 shows the distribution of a spiked cell extract (with resin A400_h) as compared to an unspiked cell extract and a pure resin sample. On the left the whole range is shown and, on the right, only the size range around 100 nm is shown. The cell extract was diluted 1:10 with MQ water. Both cell extract samples show a prominent agglomeration peak between 10 and 20 nm. The added resin sample leads to a shift of the agglomeration peak towards a smaller size range, which might be due to the dilution effect. When looking more closely at the 100 nm range (where the resin distribution is to be expected) a small peak can be seen in the spiked cell extract. This indicates the detectability of resin particles in cell extract samples. Since the agglomeration peak overlaps the signal of a potential peak at 100 nm for the pure cell extract this assumption cannot be verified and an additional investigation with more diluted cell extract samples must be done.

Therefore, it was seen that repeated filtration leads to a significant loss of resin particles and should be avoided. Furthermore, cell extracts containing resin particles were successfully measured and a strong hint of the detectability of the resin within the cell extract sample was found.

CONCLUSION

Six polystyrene-divinylbenzene (cross-linked) based anionic exchange material samples (called resin) of different nanoparticle content (based on different applied milling energy) were characterized according to their mass spectrometric behavior, their size distribution and their detectability in aqueous solution and cell extract samples.

Four different mass spectrometric techniques were compared with respect to the detectability of a representative resin sample. For comparison a poly-styrene-based particle standard of 40 nm and soluble polystyrenes of different average molecular weight were analyzed.

For MALDI MS, different sample preparation methods, matrices and solvents were tested. The mass spectra of soluble polystyrenes of three different average molecular weights could be recorded using these set-ups but the polystyrene-based particle standard and the resin samples could not be detected. This was probably due to their too high mass, the strong cross-linkages, the absence of leachable oligomers and smaller fragments and the insufficient energy transfer of the MALDI process for fragmentation of the particles.

For LDI MS, SIMS and pyrolysis GC MS, a characteristic (pyrolysis-)fragment pattern of the resin samples could be detected. Utilizing SIMS, characteristic fragmentation patterns for the polystyrene-based particle standard and a soluble polystyrene sample could also be recorded. On the other hand, LDI MS did not yield a reproducible fragmentation pattern for the polystyrene-based particle standard or the soluble polystyrene. These two standards were not tested using pyrolysis GC MS but five different resin samples were analyzed (instead of only one representative sample). The five different samples did not show any difference in pyrolysis GC MS (chromatographic pattern and mass spectrometric pattern).

Out of the four tested methods, SIMS showed the highest potential for successful direct detection of resin particles in different matrices and at lower concentrations. Also, the resin mass spectra could be distinguished from other chemically similar compounds (represented by the polystyrene-based particle standards and soluble polystyrenes tested as well).

Though LDI MS and pyrolysis GC MS seem to be able to detect resin particles in aqueous solution, they could not be detected in cell extracts by the former and no cell extract samples were tested by the latter method so far. Therefore, further tests and method development are necessary to estimate the potential of those two methods and it is not possible to draw a conclusion which of the above three MS methods (SIMS, LDI and pyrolysis GC EI-MS) is most suitable to detect resin samples in aqueous solution or cell extract samples at this point.

Contrary to the MS techniques used in this thesis, which all utilize similar principles and thus cover a similar size-range and range of chemical properties, the three different particle sizing techniques applied utilize very different physical principles and can therefore not be compared directly.

SEM revealed the actual shape of the particles but since it can only be done in the dry state a certain amount of agglomeration could not be prevented. Nevertheless, it gave a particle size estimate and showed the significant effect of different solvents on the resin structure during preparation.

While GEMMA covered the lower nanometer range up to a few hundred nanometers, LD measurements range up to a few thousand micrometers but do not allow the measurement of particles smaller than approx. 100 nanometers. In addition, a high number of particles is

necessary to obtain results with high statistical significance, which was not obtained in the lower nanometer range. Therefore, it gave insight on the particle size distribution for the resin samples containing more particles of larger diameter (lower milling energy applied). For samples with higher milling energy application barely any particles larger than 200 nm were visible and therefore, GEMMA is the preferable method to determine their particle size distribution. Also, for samples containing bigger sized particles, GEMMA can reveal the distribution of the particles of smaller diameter which might not even be seen using only LD since there is a strong method-inherent over-estimation of larger particles.

GEMMA was shown to be a powerful tool for detection of smaller sized particles due to its high reproducibility of measurements and low detection limits. Furthermore, it was shown that filtration lead to a removal of resin particles in the nanometer range and that it was possible to measure cell extract samples using GEMMA. The trueness of the determined size range was verified by measuring certified size standards.

OUTLOOK

Four different mass spectrometric methods were tested for their applicability in this thesis. Thereby, focusing on the detectability and the ability to distinguish between different types of polystyrene-based structures.

The usability of MALDI MS for resin detection can be excluded. All other MS (LDI MS, SIMS and pyrolysis GC EI-MS) methods show a potential to detect the polystyrene-based (cross-linked) resins in aqueous samples or even in cell extract samples. Nonetheless, all three methods have to be developed further in the following.

The LDI MS method has to be optimized in terms of ideal sample preparation and laser power as well as laser wavelength used as well as in reducing the amount of matrix within the cell extract samples to reduce the energy loss due to dissipation. In a next step the method's limit of detection should be determined in aqueous solution and cell extract samples. Furthermore, a con-centration / response curve should be recorded to determine the linearity of the method.

The SIMS method was tested furthest within this thesis. Nevertheless, its limit of detection still has to be determined in aqueous solution and cell extract samples. Furthermore, a concentration/response curve should be recorded as with LDI MS to determine the linearity of the method.

The same holds true for the pyrolysis GC EI-MS method. Additionally, measurements of spiked cell extracts and the polystyrene-based particle standard as well as the soluble polystyrenes have to be done.

When looking at the results, it might seem like the SIMS method is most suitable for resin detection. This is only because most experiments were done for this method. Therefore, none of the three MS methods can be preferred for further method development at this point and tests should be done for all three.

Furthermore, the reproducibility and the robustness of the measurements of all three tested MS techniques should be investigated in more detail.

The SEM and the LD method were both used to characterize the resin samples in terms of shape of the particles and size distribution. The LD method is not suitable for nanoparticles below 100 nm diameter and samples exhibiting multimodality. Further measurements are not necessary on that part since the limits of detection can be expected to be far too high for the latter method to be usable.

The GEMMA method was developed furthest in aqueous solution, including tests of some validation parameters like intra-day variability, some robustness parameters and an estimation of the limit of detection. Further experiments have to be done to verify the detectability of resin particles in cell extract samples and optimize the according measurement parameters.

REFERENCES

(1) Harland, C. E. *Ion Exchange: Theory and Practice*, 2nd ed.; Royal Society of Chemistry, **1994**.

(2) Taylor, P.; Ali, M. A.; Rahman, M. A.; Alam, A. M. S. Use of EDTA-Grafted Anion-Exchange Resin for the Separation of Selective Heavy Metal Ions. *Anal. Chem. Lett.* **2013**, No. October, 37–41.

(3) Babick, F.; Mielke, J.; Wohlleben, W.; Weigel, S.; Hodoroaba, V. D. *How Reliably Can a Material Be Classified as a Nanomaterial? Available Particle-Sizing Techniques at Work*; Springer Netherlands, **2016**; Vol. 18.

(4) European Commission, environment http://ec.europa.eu/environment/chemicals/nanotech/faq/definition_en.htm (accessed Jul 27, **2018**).

(5) Hug, H. *Instrumelle Analytik: Theorie und Praxis*, 1st ed.; Europa-Lehrmittel: Nourney, **2015**.

(6) Budzikiewicz, H.; Schöfer, M. *Massenspektrometrie: Eine Einführung*, 6th ed.; WILEY-VCH, **2005**.

(7) Montaudo, G. *Mass Spectrometry of Polymers*; CRC Press: Boca Raton, FL, USA, **2002**.

(8) Premier Biosoft http://www.premierbiosoft.com/tech_notes/mass-spectrometry.html (accessed Oct 10, **2018**).

(9) Pasch, H.; Schrepp, W. *MALDI-TOF Mass Spectrometry of Synthetic Polymers*; Springer laboratory; Springer: Berlin, Germany, **2003**.

(10) Karas, M.; Bachmann, D.; Hillenkamp, F. Influence of the Wavelength in High-Irradiance Ultraviolet Laser Desorption Mass Spectrometry of Organic Molecules. *Anal. Chem.* **1985**, *57* (14), 2935–2939.

(11) Creative Proteomics https://www.creative-proteomics.com/technology/maldi-tof-mass-spectrometry.htm (accessed Oct 20, **2018**).

(12) Perera, I. K.; Perkins, J.; Kantartzoglou, S. Spin-Coated Samples for High Resolution Matrix-Assisted Laser Desorption/Ionization Time-of-Flight Mass Spectrometry of Large Proteins. *Rapid Commun. Mass Spectrom.* **1995**, *9* (2), 180–187.

(13) Holzlechner, M.; Reitschmidt, S.; Gruber, S.; Zeilinger, S.; Marchetti-Deschmann, M. Visualizing Fungal Metabolites during Mycoparasitic Interaction by MALDI Mass Spectrometry Imaging. *Proteomics* **2016**, *16* (11–12), 1742–1746.

(14) Axelsson, J.; Hoberg, A.-M.; Waterson, C.; Myatt, P.; Shield, G.; Varney, J.; Haddleton, D. M.; Derrick, P. J. Improved Reproducibility and Increased Signal Intensity in Matrix-Assisted Laser Desorption/Ionization as a Result of Electrospray Sample Preparation. *Rapid Commun. Mass Spectrom.* **1998**, *11* (2), 209–213.

(15) Pittenauer, E.; Allmaier, G. High-Energy Collision Induced Dissociation of Biomolecules: MALDI-TOF/RTOF Mass Spectrometry in Comparison to Tandem Sector Mass Spectrometry. *Comb. Chem. High Throughput Screen.* **2009**, *12* (2), 137–155.

(16) Martin, K.; Spickermann, J.; Räder, J.; Müllen, K. Why Does Matrix-Assisted Laser

Desorption/Ionization Time-of-Flight Mass Spectrometry Give Incorrect Results for Broad Polymer Distributions? *Rapid Commun. Mass Spectrom.* **1996**, *10* (12), 1471–1474.

(17) Jackson, C.; Larsen, B.; McEwen, C. Comparison of Most Probable Peak Values As Measured for Polymer Distributions by MALDI Mass Spectrometry and by Size Exclusion Chromatography. *Anal. Chem.* **1996**, *68* (8), 1303–1308.

(18) McEwen, C. N.; Jackson, C.; Larsen, B. S. Instrumental Effects in the Analysis of Polymers of Wide Polydispersity by MALDI Mass Spectrometry. *Int. J. Mass Spectrom. Ion Process.* **1997**, *160* (1), 387–394.

(19) Cox, F. J.; Johnston, M. V.; Dasgupta, A. Characterization and Relative Ionization Efficiencies of End-Functionalized Polystyrenes by Matrix-Assisted Laser Desorption/Ionization Mass Spectrometry. *J. Am. Soc. Mass Spectrom.* **2003**, *14* (6), 648–657.

(20) Brown, R. S.; Weil, D. A.; Wilkins, C. L. Laser Desorption-Fourier Transform Mass Spectrometry for the Characterization of Polymers. *Macromolecules* **1986**, *19* (4), 1255–1260.

(21) Chen, R.; Yalcin, T.; Wallace, W. E.; Guttman, C. M.; Li, L. Laser Desorption Ionization and MALDI Time-of-Flight Mass Spectrometry for Low Molecular Mass Polyethylene Analysis. *J. Am. Soc. Mass Spectrom.* **2001**, *12* (11), 1186–1192.

(22) Salzer, R. Probeaufgabetechniken in der Gaschromatographie http://www.chemgapedia.de/vsengine/vlu/vsc/de/ch/3/anc/croma/gc_probenaufgabe.vlu/Page/vsc/de/ch/3/anc/croma/gc/komb/pyrolyse/pyrolysem66ht0600.vscml.html (accessed Jul 16, **2018**).

(23) Schrattenecker, J. D. Pyrolyse-Gaschromatographie/Massenspektrometrie Zur Identifizierung von Pechen Auf Historischen Keramikfunden, TU Wien: Wien, **2015**.

(24) Lichtenstein, N. Curie-Punkt-Pyrolyse Mit GC/MS-Kopplung Als Methode Zur Analyse von Polymeren, Bochum University: Altendorf, **1979**.

(25) Montaudo, G.; Samperi, F.; Montaudo, M. S. Characterization of Synthetic Polymers by MALDI-MS. *Prog. Polym. Sci.* **2006**, *31* (3), 277–357.

(26) Ma, X. M.; Lu, R.; Miyakoshi, T. Application of Pyrolysis Gas Chromatography/Mass Spectrometry in Lacquer Research: A Review. *Polymers (Basel).* **2014**, *6* (1), 132–144.

(27) Chromatography online http://www.chromatographyonline.com/comparing-capabilities-time-flight-and-quadrupole-mass-spectrometers-0 (accessed Oct 20, **2018**).

(28) Wikipedia Gas Chromatography https://en.wikipedia.org/wiki/Gas_chromatography#/media/File:Gas_chromatograph-vector.svg (accessed Oct 20, **2018**).

(29) Babick, F.; Ullmann, C. Error Propagation at the Conversion of Particle Size Distributions. *Powder Technol.* **2016**, *301*, 503–510.

(30) Allmaier, G.; Blaas, D.; Bliem, C.; Dechat, T.; Fedosyuk, S.; Gösler, I.; Kowalski, H.; Weiss, V. U. Monolithic Anion-Exchange Chromatography Yields Rhinovirus of High Purity. *J. Virol. Methods* **2018**, *251*, 15–21.

(31) Bereszczak, J. Z.; Havlik, M.; Weiss, V. U.; Marchetti-Deschmann, M.; Van Duijn, E.; Watts, N. R.; Wingfield, P. T.; Allmaier, G.; Steven, A. C.; Heck, A. J. R. Sizing up Large Protein

Complexes by Electrospray Ionisation-Based Electrophoretic Mobility and Native Mass Spectrometry: Morphology Selective Binding of Fabs to Hepatitis B Virus Capsids. *Anal. Bioanal. Chem.* **2014**, *406* (5), 1437–1446.

(32) Subirats, X.; Weiss, V. U.; Gösler, I.; Puls, C.; Limbeck, A.; Allmaier, G.; Kenndler, E. Characterization of Rhinovirus Subviral A Particles via Capillary Electrophoresis, Electron Microscopy and Gas Phase Electrophoretic Mobility Molecular Analysis: Part II. *Electrophoresis* **2013**, *34* (11), 1600–1609.

(33) Weiss, V. U.; Bereszczazk, J. Z.; Havlik, M.; Kallinger, P.; Gösler, I.; Kumar, M.; Blaas, D.; Marchetti-Deschmann, M.; Heck, A. J. R.; Szymanski, W. W.; et al. Analysis of a Common Cold Virus and Its Subviral Particles by Gas-Phase Electrophoretic Mobility Molecular Analysis and Native Mass Spectrometry. *Anal. Chem.* **2015**, *87* (17), 8709–8717.

(34) Lee, H.; Chen, S.-C.; Kim, C.; Westenburg, E.; Moon, S. I.; Pui, D. Y. H. Evaluation of Concentration Measurement Techniques of Colloidal Nanoparticles for Microfiltration and Ultrafiltration Applications: Inductively Coupled Plasma-Mass Spectrometry, Nanoparticle Tracking Analysis and Electrospray-Scanning Mobility Particle Sizer. *Sep. Purif. Technol.* **2017**, *184*, 34–42.

(35) Kaufman, S. L. Analysis of Biomolecules Using Electrospray and Nanoparticle Methods: The Gas-Phase Electrophoretic Mobility Molecular Analyzer (GEMMA). *J. Aerosol Sci.* **1998**, *29* (5–6), 537–552.

(36) Kaufman, S. L.; Skogen, J. W.; Dorman, F. D.; Zarrin, F.; Lewis, K. C. Macromolecule Analysis Based on Electrophoretic Mobility in Air: Globular Proteins. *Anal. Chem.* **1996**, *68* (11), 1895–1904.

(37) Kallinger, P.; Weiss, V. U.; Lehner, A.; Allmaier, G.; Szymanski, W. W. Analysis and Handling of Bio-Nanoparticles and Environmental Nanoparticles Using Electrostatic Aerosol Mobility. *Particuology* **2013**, *11* (1), 14–19.

(38) Hinterwirth, H.; Lindner, W.; Lämmerhofer, M. Bioconjugation of Trypsin onto Gold Nanoparticles: Effect of Surface Chemistry on Bioactivity. *Anal. Chim. Acta* **2012**, *733*, 90–97.

(39) Wikipedia - Scanning electron microscope https://en.wikipedia.org/wiki/Scanning_electron_microscope (accessed Sep 29, **2018**).

(40) Hayat, M. A. *Principles and Techniques of Electron Microscopy*; Van Nostrand Reinhold: New York, USA, **1970**.

(41) Flegler, S. L.; Heckman, J. W.; Klomparens, K. L. *Elektronenmikroskopie*; Spektrum Akad. Verl.: Heidelberg, Germany, **1995**.

(42) Skoog, D. A.; Holler, F. J.; Crouch, S. R. *Instrumentelle Analytik*, 6., vollst.; Lehrbuch; Springer Spektrum: Berlin, Germany, **2013**.

(43) Bacher, G.; Szymanski, W. W.; Kaufman, S. L.; Zllner, P.; Blaas, D.; Allmaier, G. Charge-Reduced Nano Electrospray Ionization Combined with Differential Mobility Analysis of Peptides, Proteins, Glycoproteins, Noncovalent Protein Complexes and Viruses. *J. Mass Spectrom.* **2001**, *36* (9), 1038–1052.

(44) Tycova, A.; Prikryl, J.; Foret, F. Reproducible Preparation of Nanospray Tips for Capillary Electrophoresis Coupled to Mass Spectrometry Using 3D Printed Grinding Device.

Electrophoresis **2016**, *37* (7–8), 924–930.

(45) Quirk, R. P.; Pickel, J. M.; Arnould, M. A.; Wollyung, K. M.; Wesdemiotis, C. Efficient Synthesis of ω-(p-Vinylbenzyl)Polystyrene by Direct Functionalization of Poly(Styryl)Lithium with p-Vinylbenzyl Chloride in Hydrocarbon Solvent with Lithium 2,3-Dimethyl-3-Pentoxide. *Macromolecules* **2006**, *39* (5), 1681–1692.

(46) Bahr, U.; Deppe, A.; Karas, M.; Hillenkamp, F.; Giessmann, U. Mass Spectrometry of Synthetic Polymers by UV-Matrix-Assisted Laser Desorption/Ionization. *Anal. Chem.* **1992**, *64* (22), 2866–2869.

(47) Hanton, S. D.; Parees, D. M. Extending the Solvent-Free MALDI Sample Preparation Method. *J. Am. Soc. Mass Spectrom.* **2005**, *16* (1), 90–93.

(48) Pei, L.; Lucy, C. A. Insight into the Stability of Poly(Diallydimethylammoniumchloride) and Polybrene Poly Cationic Coatings in Capillary Electrophoresis. *J. Chromatogr. A* **2014**, *1365*, 226–233.

(49) Harland, C. E. *Ion Exchange: Theory and Practice*, 2nd ed.; Royal Society of Chemistry: Cambridge, **1994**.

(50) Willemse, R. X. E.; Staal, B. B. P.; van Herk, A. M.; Pierik, S. C. J.; Klumperman, B. Application of Matrix-Assisted Laser Desorption Ionization Time-of-Flight Mass Spectrometry in Pulsed Laser Polymerization. Chain-Length-Dependent Propagation Rate Coefficients at High Molecular Weight: An Artifact Caused by Band Broadening in Size Exclu. *Macromolecules* **2003**, *36* (26), 9797–9803.

(51) Hanton, S. D.; Hyder, I. Z.; Stets, J. R.; Owens, K. G.; Blair, W. R.; Guttman, C. M.; Giuseppetti, A. A. Investigations of Electrospray Sample Deposition for Polymer MALDI Mass Spectrometry. *J. Am. Soc. Mass Spectrom.* **2004**, *15* (2), 168–179.

(52) Danis, P. O.; Karr, D. E.; Mayer, F.; Holle, A.; Watson, C. H. The Analysis of Water-soluble Polymers by Matrix-assisted Laser Desorption Time-of-flight Mass Spectrometry. *Org. Mass Spectrom.* **1992**, *27* (7), 843–846.